Chapter 5

Model analysis of CO and H_2 uptake by soil

5.1 Introduction

This Chapter presents model analysis to CO and H_2 uptake by soil. No approach by model analysis has been done to CO and H_2 uptake by soil so far, and therefore, our understanding of the soil CO and H_2 uptake processes has remained poor.

H_2 has a higher molecular diffusivity than CO due to smaller molecular weight. Knowledge of the difference in molecular diffusivity between CO and H_2 would be useful for understanding the soil uptake processes of these gases. This Chapter clarifies how the surface fluxes (net deposition velocity) are controlled by in-situ biological uptake rate and soil gas diffusivity calculated from the 3-phase system (solid, liquid, gas) in the soil (Yonemura et al., 2000c; 2000d).

5.2 Model to soil uptake of CO and H_2

5.2.1 Diffusion model

To understand the diffusion aspects of CO and H_2 uptake by soil, a diffusion equation with production and uptake terms was employed on the assumption that mainly the molecular diffusion process drives the transport of CO and H_2 in soil. Fick's Law and the mass balance of gas per unit volume of soil are expressed as follows:

$$F = D_S \frac{\partial C_M}{\partial z} \tag{5.1}$$

$$\frac{\partial C_M}{\partial t} = \frac{\partial}{\partial z}\left(D_S \frac{\partial C_M}{\partial z} \right) + \rho P_{in-situ} - u_{in-situ} C_M \tag{5.2}$$

where F is the flux of the gas (g cm^{-2} s^{-1}), ρ is the density of the pure gas (g cm^{-3}), C_M is the concentration as mass per unit volume of soil (g cm^{-3}), z is the soil depth (cm), D_s is soil gas diffusivity (cm^2 s^{-1}), $P_{in\text{-}situ}$ (s^{-1}) is the in-situ production rate on the spatial base, and $u_{in\text{-}situ}$ (s^{-1}) is the in-situ uptake rate on the spatial base. Note that z increases downwards whereas F is positive for upward fluxes. C_M is related to the concentration of air in the soil, C (ppbv), as follows:

$$C_M = V_a C \tag{5.3}$$

where V_a (dimensionless) is the ratio of gas on a volume basis (air-filled porosity; volumetric content of gas phase). We assume vertical uniformity of D_s, ρ, and V_a. Fick's law and the mass balance equation are then rewritten using C as follows:

$$F = \rho V_a D_S \frac{\partial C}{\partial z}; \tag{5.4}$$

$$\frac{\partial C}{\partial t} = \frac{D_S}{V_a}\frac{\partial^2 C}{\partial z^2} + \frac{P_{in-situ}}{V_a} - u_{in-situ} C. \tag{5.5}$$

The uptake term ($u_{in\text{-}situ}C$) reflects bacterial or enzymatic uptake and is first order; the production term ($\frac{P_{in\text{-}situ}}{V_a}$) reflects abiological production of CO and is zero order, which is supported by previous studies (e.g., Conrad and Seiler, 1985a, b). Please note that by the balance of uptake and production terms in eq. (5.5), eq. (1.17) is obtained. The $u_{in\text{-}situ}$ and $P_{in\text{-}situ}$ are given by:

$$1 = V_s + V_a + V_b \tag{5.6}$$

$$u_{in\text{-}situ}=d_P V_s u_s; \tag{5.7}$$

$$P_{in\text{-}situ}=d_P V_s P_s, \tag{5.8}$$

where d_p is the particle density of the soil (set at 2.67 g cm^{-3}), V_s (dimensionless) is the ratio of solids on a volume basis, V_l (dimensionless) is the ratio of liquids (water) on a volume basis, u_s (cm^3 g^{-1} s^{-1}), and P_s (cm^3 g^{-1} s^{-1}) are the in-situ uptake rate and the in-situ production rate, respectively, on the basis of mass of dry soil.

Soil gas diffusivity, D_s, was treated in terms of the 3-phase system (solid, liquid, and gas) of soil in view of previous gas diffusion studies (Millington and Quirk, 1961; Sallam et al., 1984).

$$D_s = D_A V_a^{\gamma} (V_a + V_l)^{\gamma}; \tag{5.9}$$

$$D_A = D_0 \frac{1013.25}{P_{atmos}} \left(\frac{T + 273.15}{273.15} \right)^{\gamma}, \tag{5.10}$$

where D_A is molecular diffusivity (cm^2 s^{-1}), P_{atmos} is the atmospheric pressure, set at 1013.25 hPa, and T is soil temperature (°C). Equation (5.9) shows that decreases in air-filled porosity by water decrease diffusion more than do decreases in air-filled porosity by solids (Rust et al., 1957). CO and H_2 molecular diffusion constants, D_0 and γ (Table 5.1), were fitted from the data of Marrero and Mason (1972).

Surface net deposition velocity, v_{nd}, , and gross deposition velocity, v_{gd}, are obtained by

$$v_{nd} = -\frac{F_0}{\rho C_{atm}}; \tag{5.11}$$

$$v_{gd} = -\frac{F_0}{\rho(C_{atm} - C_{eq})}, \tag{5.12}$$

where F_0 (ng cm^{-2} s^{-1}) is the flux at the soil surface, C_{atm} (dimensionless) is atmospheric concentration and C_{eq} (dimensionless) is the compensation (equilibrium) concentration of the gas in the soil.

Based on eq. (5.5), the present study made a differential equation for numerical simulation with the assumption of vertical uniformity of soil properties. Although Ball et al. (1997a) reported that D_s and V_a have the tendency to be smaller with soil depth, this assumption is enough to describe the essential understanding of CO and H_2 uptake process by soil using a simulation model. The soil layer was divided in 1-mm units to 1000 mm depth. The time step was set at 0.01 sec. The ratio of solids on a volume basis, V_s, was set at 0.2, which corresponds to the case of a well-cultivated field and reflects a state of near surface soil. Atmospheric concentrations of CO and H_2 in the top layer of soil, as the upper boundary condition, were set to be 200 and 550 ppbv, respectively, throughout this study. These concentrations are in the typical range of the boundary layer in the northern hemisphere. It was assumed that there would be no transport to soil deeper than the bottom (1000 mm). Iterative calculations were conducted until the soil concentration profile converged to a steady state.

We made a two-layer model for the simple description of CO and H_2 uptake profiles that reflected the distribution of in-situ uptake rates (Fig. 5.1). The upper layer cannot absorb CO or H_2, but can produce CO because CO production is an abiological process; the present study hereinafter call this upper layer the inactive layer. The lower layer can uptake CO and H_2 and produce CO; the present study call this the active layer. The present study define d_i (cm) as the depth of the inactive layer.

We summarized abbreviations for some variables in Appendix.

5.2.2 Analytical solutions for a mono-layered model

To understand the basic difference between the uptake and emission processes by soil, the steady state of eq. (5.5) was considered, assuming vertical uniformity of soil properties. If the gas concentrations are controlled only by diffusion and production processes, eq. (5.5) can be written as:

$$\frac{D_S}{V_a}\frac{\partial^2 C}{\partial z^2} + \frac{P_{in-situ}}{V_a} = 0 \ . \tag{5.13}$$

and eq. (5.13) can be solved analytically. The thickness of the production layer is defined as d (cm):

$$C = C_{atm} + \frac{2P_{in-situ}}{D_s d} z - \frac{P_{in-situ}}{D_s} z^2 \ ; \tag{5.14}$$

$$F = \rho P_{in\text{-}situ} d \ . \tag{5.15}$$

This formulation shows that the flux values cannot be changed by physical properties of soil such as the soil gas diffusivity D_s or air-filled porosity V_a, although the gas concentration increases with soil depth (from the surface) and is high when soil gas diffusivity is low.

If the gas is absorbed by soil, eq. (5.5) can be written as:

$$\frac{D_S}{V_a}\frac{\partial^2 C}{\partial z^2} - u_{in-situ} C + \frac{P_{in-situ}}{V_a} = 0 \ . \tag{5.16}$$

This can be also solved analytically as:

$$C = (C_{atm} - C_s)\exp\left(-\sqrt{\frac{V_a u_{in\text{-}situ}}{D_s}}z\right) + C_s \; ; \tag{5.17}$$

$$F = -(C_{atm} - C_s)\sqrt{V_a D_s u_{in\text{-}situ}} \; ; \tag{5.18}$$

$$v_{nd} = \frac{C_{atm} - C_s}{C_{atm}}\sqrt{V_a D_s u_{in\text{-}situ}} \; ; \tag{5.19}$$

$$v_{gd} = \sqrt{V_a D_s u_{in\text{-}situ}} \; . \tag{5.20}$$

Gas concentration decreases exponentially with soil depth from the surface, and deposition velocities increase with the square root of air-filled porosity V_a, soil gas diffusivity D_s, and in-situ soil uptake rate $u_{in\text{-}situ}$.

5.3 Experiment to obtain model parameters, $u_{in\text{-}situ}$ and $P_{in\text{-}situ}$ in regard to soil temperature

CO and H_2 in-situ uptake and production rates and their dependence on soil temperature used for the simulations were determined by experiments. Soil samples were taken from the mixture of top soil in the plowed layer of the arable field in the National Institute of Agro-Environmental Sciences The soil samples were placed in a box for one week in laboratory conditions at temperatures of 15 to 25°C.

The closed-chamber technique was applied to determine in-situ soil uptake rates of CO and H_2 (Fig. 5.2). To obtain these rates with no loss from diffusional resistance in the soil, a small amount of wet soil (about 10 g) was thinly spread on the bottom of the chamber. The experiments were found to be free from loss in in-situ uptake rates due to the molecular diffusion resistance in soil sample when sample soil of less than 50 g was used (Fig. 5.3). Gas samples were taken every 3 min for more than 12 min after enclosure. The temperature dependence of uptake rates was measured in triplicate with raising and lowering temperature.

To obtain in-situ CO production rates of soil, compensation CO concentrations equilibrated in the sample field were measured. The surface of the soil was covered with a closed chamber continuously and the gas concentration in the chamber was measured. The measurements were made during 3 to 6 March and 19 to 22 July 1996. Based on the compensation concentrations and the in-situ uptake rates, the dependence of the in-situ production rates on temperature was obtained using eq. (1.17).

The difference in CO and H_2 uptake between the inactive layer and deeper soil was investigated using the stored soil samples. The water content was measured gravimetrically at the same time. The depth of the inactive layer was less than 1 cm.

CO concentrations in the soil were measured at 0, 1, and 2 cm soil depth by slowly (>1 min) extracting soil gas samples not to disturb the concentration profile using a gas-tight syringe fixed to a pole by a clamp. This extraction of soil gas samples is possible because CO and H_2 reaction is rapid.

5.4 Results

5.4.1 $u_{in\text{-}situ}$ and $P_{in\text{-}situ}$

In the laboratory experiments, CO concentrations measured at 0, 1, and 2 cm depth were >150, <50, and <15 ppbv, respectively (Fig. 5.4). The CO and H_2 concentrations in soil decreased exponentially with soil depth. H_2 can permeate into soil more than CO. Surface soil (Case A) had smaller uptake rates than deeper dark soils (Case B) (Table 5.2). Soils in the shallower layer (Case B) had higher uptake rates than did the deeper layer (Case C) (Table 5.2), although there was little difference in water content between 1.5-cm (Case B) and 5-cm deep soil (Case C).

The dependence of in-situ uptake and production rate on soil temperature, obtained by laboratory experiments, is shown in Fig. 5.5. Gross in-situ uptake rates in function with temperature were obtained by linear regression from the net in-situ uptake rates in the lower temperature range ($\leq$ 20°C for CO and $\leq$ 30°C for H_2) because relatively low production rates were expected at these temperatures (Fig. 5.5a). The calculated activation energies based on the Ahhrenius equation were -6.78 and -6.95 kJ mol^{-1} for CO ($\leq$ 20°C) and H_2 ($\leq$ 30°C), respectively. These values were in reasonable accordance with those of Conrad and Seiler

(1985a). The CO in-situ production rate (Fig. 5.5b) was given by the combination of the gross CO in-situ uptake rate and the equivalent CO concentration value obtained from the closed chamber, using eq. (1.17). The activation energy of CO production was 65.3 kJ mol^{-1}, also in reasonable accordance with those of Conrad and Seiler (1985a, b) and Conrad (1988), taking into account the pH value.

CH_4 in-situ uptake rates which were simultaneously obtained (Fig. 5.5c), showed no dependence on temperature.

5.4.2 Calculations using experimental in-situ uptake and production rates

Figure 5.6 shows the changes in deposition velocities, with changes in air-filled porosity V_a (i.e. soil gas diffusivity) and depth in the inactive layer, using in-situ uptake and production rates obtained experimentally. The increase in deposition velocity due to the increase in air-filled porosity is more exponential than linear because the thickness of the uptake layer extended to deeper soil. In Fig. 5.6, when d_i = 0.2 cm and V_a = 0.6, the deposition velocity was lowered by about 14%, and when d_i = 0.5 cm and V_a = 0.6, the decrease was 29%. The effect of the inactive layer was stronger for CO than for H_2.

The relationship between observed and calculated deposition velocities in the forest (Fig. 5.7) show similar results. By setting d_i=1.0cm, the ratio of CO to H_2 deposition velocities were properly realized in the calculation. This shows that diffusion resistance of gas through dead leaves could be expressed by the depth of d_i. It should be noted that the variation in real observational data is larger than calculated ones. This is probably because variation in the measured soil moisture by TDR was less than the top soil moisture (TSM) responsible for the uptake of CO and H_2 as explained in Chapter 4. The difference of observational and calculated was also observed during periods from June to September 1997. This is probably because in summer d_i should be thick due to drought of surface soil.

The relationship between observed and calculated deposition velocities (Figs. 5.6 and 5.7) at least confirms the availability of the present model's application to CO and H_2 uptake by soil although further improvement is necessary.

The response of deposition velocities to temperature at intervals of 5°C was investigated using the in-situ uptake and production rates obtained experimentally (Fig. 5.8). The increase in D_s is shown by the solid line in Fig. 5.8. The combination of the uptake rates and

production rates leads to a maximum v_{nd} for CO because CO uptake and production are first and zero-order reactions, respectively. With increasing d_i, the optimum temperature for CO uptake decreased. Without the inactive layer (d_i = 0.0 cm), the temperature that maximized the v_{nd} was about 32°C; when d_i = 0.5 cm, the optimum temperature was about 26°C.

The difference between the presence and absence of production in the inactive layer is shown in Fig. 5.9. In the absence of CO production in the inactive layer, the soil always showed CO uptake. However, at temperatures > 20°C and assuming 5 cm of d_i, the soil was a net source of CO, and when $d_i \geq 2.0$ cm, as temperature increased, the v_{nd} decreased. The maximum CO concentration was shown when CO was emitted from the soil surface (Fig. 5.10). Under this condition, CO produced in the inactive layer was transported upward to the atmosphere and downward to the lower active soil layer.

5.4.3 Calculations incorporating changes in in-situ uptake rates

The v_d was calculated without a production term by changing uptake rates of the active layer and with d_i at fixed diffusivity at 20°C (Fig. 5.11). The calculated v_d values were identical with gross deposition velocities. However, the v_d did not increase in proportion to the in-situ uptake rates, $u_{in\text{-}situ}$, because soil uptake was restricted to the shallower zone when the $u_{in\text{-}situ}$ was high (Fig. 5.12). In the active layer, gas concentration decreased exponentially with soil depth; in the inactive layer, concentration decreased linearly with soil depth. Under the same $u_{in\text{-}situ}$, H_2 permeated deeper than CO due to the higher molecular diffusivity of H_2.

When d_i = 0.0 cm, the slope in Fig. 5.11 was 0.5, which means that v_d was increasing proportionally with the square root of $u_{in\text{-}situ}$ as shown by eq. (5.20).

The d_i reduced v_d at higher $u_{in\text{-}situ}$, when the curve approached a convergence value depending on the value of d_i.

When $u_{in\text{-}situ}$ of CO was doubled from 0.1 s^{-1} to 0.2 s^{-1}, the increases in deposition velocities v_d were 41.4 and 22.9% for d_i = 0.0 and 0.5 cm, respectively; when $u_{in\text{-}situ}$ of H_2 was doubled from 0.1 s^{-1} to 0.2 s^{-1}, the increases were 41.4 and 28.7% for d_i = 0.0 and 0.5 cm, respectively. The resistance to diffusion from the atmosphere to the active layer through the inactive layer was stronger for CO than for H_2, because H_2 has greater soil gas diffusivity, 0.126 $cm^2 s^{-1}$, than does CO, 0.0382 $cm^2 s^{-1}$.

5.4.4 Analysis of the contribution of the various factors affecting CO and H_2 uptake by soil

The effects of such factors as soil temperature, air-filled porosity V_a, and the depth of the inactive layer d_i, on deposition velocities, are summarized in Table 5.3. When the temperature changed from 0 to 40°C, the in-situ bacterial uptake rate of CO ranged from 0.8 to 0.18 $cm^3\ g^{-1}\ s^{-1}$ and the surface deposition velocity of CO increased by 47%. In the absence of production in soil, and within the range of controlling factors, their relative impact on deposition velocities was in the order of air-filled porosity $V_a > d_i > u_{in\text{-}situ}$ change due to temperature change > molecular diffusivity change due to temperature change; the value of the contribution of each factor was obtained around the point where the ratio of solids in volume $V_s = 0.2$, $V_a = 0.4$, and $u_{in\text{-}situ} = 0.2\ s^{-1}$. When there was no CO production in the soil, the controlling factors acted in a similar manner on both CO and H_2. In the presence of CO production in the soil, the coupling effect of d_i and temperature-induced high production caused a large decrease in v_{nd}.

The strength of deposition velocity dependence on each factor, within their ranges assumed in Table 5.3, was strongest in V_a. These trends are consistent with results in Chapter 4.

5.5 Discussion

5.5.1 Diffusion control of CO and H_2 uptake by soil

The analytical solutions (eqs. 5.18-5.20) show that physical properties of soil such as air-filled porosity V_a and soil gas diffusivity D_s are intrinsically more important for the uptake process than for the emission process. The numerical results show that the inactive layer causes resistance to diffusion from the atmosphere to the active layer and thus limits CO and H_2 uptake by soil in the higher range of $u_{in\text{-}situ}$ (Fig. 5.11). The vertical distribution of uptake rates in near-surface (mm scale) soil is very important in controlling CO and H_2 deposition onto soil.

Simulation results of this study (Figs. 5.11 and 5.12) show that soil gas diffusivity is very important in controlling the deposition velocities; properties of the soil in the top few

millimeters below the surface are very important. Simulation results of this study (Table 5.3) also show that gas diffusion is the major factor controlling CO and H_2 uptake in the arable field, consistent with the field measurements (Chapter 4). Both CO and H_2 deposition velocities increased as air-filled porosity and soil gas diffusivity became larger because the soil became drier. However, this increase could be suppressed by the inactive layer, which is thought to deepen due to water stress under dry conditions. Thus, diffusion is the rate-determining process for CO and H_2 uptake by soil when $u_{in\text{-}situ}$ are large.

Estimation of the range of $u_{in\text{-}situ}$ is needed to determine which factor controls deposition velocities: D_s or $u_{in\text{-}situ}$. Moxley and Smith (1998a) measured the initial CO utilization rates of samples of Scottish soils. If the initial utilization rates in Table 2 of Moxley and Smith (1998a) are regarded as being the same as $u_{in\text{-}situ}$, the range of their data corresponds to approximately 0.0036 to 0.038 s^{-1} for 41 sites, apart from the lowest rates of 2 sites. These $u_{in\text{-}situ}$ are lower than those of experiments in this study. If this range of values from Moxley and Smith (1998a) is applied to Fig. 5.11, the uptake rates are roughly proportional to the square-root of deposition velocities (eqs. 5.19 and 5.20), and the deposition velocity varied by a factor of 3.3 or less. This range of deposition velocities at various sites is roughly comparable to the changes expected due to the variation in air-filled porosity (Table 5.3).

The presence of inactive layer is analogous to diffusion resistance of the leaf layer in temperate forests, where net CO deposition is accelerated by clearing this layer (Chapter 4; Sanhueza et al., 1998). It can be consequential that leaf-layer resistance might compensate in-situ uptake, which might otherwise be higher in forest soils, resulting in similar deposition velocities in the arable field and forest. The H_2 deposition velocity may have been larger in the forest than in the arable field because the high molecular diffusivity of H_2 makes the leaf layer less of a diffusion barrier.

5.5.2 Factors affecting CO and H_2 uptake by soil

In-situ uptake reflects the activity of bacteria/enzymes in oxidizing CO/H_2, a process that is influenced in a complex manner by various environmental factors such as soil moisture, soil temperature, carbon and nitrogen content, oxygen concentration, and CO concentration.

Among the environmental factors, Moxley and Smith (1998a) found good correlation between deposition velocities and total organic carbon in Scottish soils. However, high

carbon content, as in forest floor soils, not only enhances in-situ CO uptake rate, it also results in exponentially increasing production of CO with increasing soil temperature. Correlation of in-situ CO uptake rate with carbon content is often masked by production, especially at higher temperatures.

Soil temperature is a basic and very important factor that influences all other factors that affect deposition velocity. Simulation results of this study (Figs. 5.8 and 5.9) showed that the optimum temperature to maximize v_{nd} depended not only on the quantitative balance between uptake and production functions but also on d_i. Thus, the optimum temperature for soil uptake of CO cannot be determined only by the optimum temperature of in-situ soil CO uptake by bacteria, but also by the distribution of oxidizing activity as denoted by d_i.

Atmospheric concentrations of CO and H_2 influence the v_{nd} and the temperatures that maximize them. Under high atmospheric concentration of CO, eq. (5.19) shows that the contribution of C_{eq}, which increases with temperature (Fig. 5.5b), is lessened and v_{nd} increases toward v_{gd}. As the atmospheric CO concentration increases, the apparent optimum temperature for v_{nd} is lowered because production is a zero-order reaction.

Further, CO enhances CO in-situ uptake itself (Smith et al., 1973; Spratt and Hubbard, 1981; Bender and Conrad, 1994a), which the present study call as "fertilization effect". This was observed in the difference not only in CO but also in H_2 uptake rate between cases B and C in Table 5.2, although the soil moisture content was similar. This effect may cause higher uptake rates in surface soil. Because the response time of this fertilization effect may be as fast as a week, under conditions of high soil gas diffusivity accompanied by low soil moisture, the deposition velocities could be enhanced by this effect. The fertilization effect could also lead to a more sensitive diffusional control of CO and H_2 uptake by soil.

Heichel (1973) and Moxley and Smith (1998a) reported that there is an optimum water content for CO oxidation. Both higher and lower moisture may reduce the in-situ uptake rates. Soil moisture is very important for controlling in-situ uptake rates because water is essential for bacterial growth. Under low soil moisture as in desert or arid soils, the presence of the inactive layer was considered to be crucially important, as is also shown in case A in Table 5.2. When soil temperature in arid soils during daytime was high, net emission was observed (e.g., Conrad and Seiler, 1985a; Sanhueza et al., 1994a, b). In these soils, the inactive layer is possibly thick due to the decrease in bacterial activity resulting

from water and thermal stresses. Furthermore, Moxley and Smith (1998b) showed that CO production is enhanced under very dry conditions. Previous studies (Conrad and Seiler, 1985a; Scharffe et al., 1990) mentioned that moisture supply activated CO uptake in arid soil, which suggests the presence of a thick d_i. The combination of a thick d_i and high temperature could crucially reduce net CO deposition onto soil (Fig. 5.10).

5.5.3 Relationship between deposition velocities of various gas species

Trace gases known to be absorbed by soil in addition to CO and H_2 are sulfur dioxide, nitrous oxide, nitrogen oxide, ammonia, and methane. Unlike CO, H_2, and methane, which are utilized biologically, the sulfur and nitrogen compounds have higher deposition velocities than 0.1 cm s^{-1} onto soil due to the physical process of dry deposition (McMahon and Denison, 1979). Biological deposition of gases other than CO and H_2 on soil might be limited, i.e. less than 0.1 cm s^{-1} (Fig. 5.11), if d_i is less than 0.2 cm.

In the case of methane, Dörr et al. (1993) and Ball et al. (1997a, b) concluded, from records of the methane uptake by differently aerated soils in Europe, that methane consumption in aerated soils is mainly influenced by the gas transport properties of sub-surface soil. Long-term CO- and H_2-uptake measurements and mechanical core studies at various sites are needed in order to determine the applicability of this finding to the process of CO and H_2 uptake by soil.

Experimental results of this study show that CO in-situ uptake rates were similar to those of H_2 (Fig. 5.5, Table 5.2), which may be attributed to their solubility in a matrix of bacteria or enzymes as mentioned by Conrad (1988); water solubility of CO and H_2 is 0.023 and 0.018 on a volumetric basis at 20°C, respectively (National Astronomical Observatory, 1994). The ratio of H_2 deposition velocities to those of CO is in the range 1.54 to 3.5 for both the present simulation when d_i = 0.0 cm and measurements in soils near Mainz (Liebl and Seiler, 1976). In view of the similarity in CO and H_2 uptake rates, the difference in their deposition velocities may be attributable to the difference in their molecular diffusivity.

5.6 Summary

In this Chapter, based on the understanding of previous Chapter 4 and previous measurement studies, the CO and H_2 soil uptake processes, which is connected with in-situ soil uptake and deposition onto soil, was investigated with a diffusion model. This is the first study of modeling of CO and H_2 uptake by soil.

The calculation results showed that top-soil physical properties such as soil gas diffusivity and air-filled porosity are very important controlling factors of deposition velocities. Namely, gas diffusion from the atmosphere to soil is rate-determining process for CO and H_2 uptake by soil, which is consistent with measurements. The difference in deposition velocity between CO and H_2 was attributed to the difference in their molecular diffusivity because similar uptake rates in soil were observed. The depth of the biologically inactive layer as well as the in-situ bacterial/enzymatic uptake rate of CO and H_2, are important factors in CO and H_2 consumption by soil, especially by arid soils. The presence of an inactive layer results in limited soil uptake of CO and H_2. The proposed two-layered model was useful to depict the features of CO and H_2 deposition onto soil that have been observed in Chapter 4 and previous studies.

Table 5.1 Molecular diffusion coefficients of CO and H_2. The coefficients were fitted using an exponential relationship; the data are from Marrero and Mason (1972).

Molecule	D_0 $cm^2 s^{-1}$	γ
CO	0.186	1.70
H_2	0.611	1.75

Table 5.2 CO and H_2 in-situ uptake rates at different depths in the experimental soil. In A, there was a low net uptake rate due to water stress. In B, there was a higher net uptake rate for both CO and H_2 than in C. This may be due to the CO (and H_2) fertilization effect (Smith et al., 1973; Spratt and Hubbard, 1981; Bender and Conrad, 1994a).

Case	Net CO uptake rate $cm^3 s^{-1} g^{-1}$	Net H_2 uptake rate $cm^3 s^{-1} g^{-1}$	Water content mass basis
A, Surface soil (0-1cm)			
1	0.028	0.12	0.17
2	0.021	0.09	0.21
3	0.003	0.01	0.17
Average	0.017	0.07	0.18
B, Soil just below A (about1.5cm)			
1	0.143	0.16	0.42
2	0.194	0.19	0.40
3	0.180	0.20	0.40
Average	0.172	0.18	0.41
C, Soil at about 5cm depth			
1	0.042	0.11	0.46
2	0.087	0.11	0.44
3	0.094	0.12	0.45
Average	0.074	0.11	0.45

Table 5.3
Effects of soil temperature, air-filled porosity Va, and the depth of inactive layer di on vd. The calculations were based on the experimental soil at T = 20°C, Va = 0.4, and di = 0.0 cm.

Condition	Control factor	Range		Intermediate control factor	Changes in v_d min-max (cm s^{-1})	Ratio of max/min in v_d
No CO production in soil	Temperature	0-40° C		$u_{in\text{-}situ}$ ($cm^3\ g^{-1}\ s^{-1}$)		
			CO	0.8-0.18	0.0160-0.0234	1.47
			H_2	0.5-0.13	0.0247-0.0380	1.54
				D_s ($cm^2\ s^{-1}$)		
			CO	0.0170-0.0214	0.0189-0.0212	1.12
			H_2	0.0558-0.0708	0.0301-0.0340	1.13
	V_a (Air-filled porosity)	0.2-0.6		D_s ($cm^2\ s^{-1}$)		
			CO	0.00223-0.0673	0.0069-0.0376	5.46
			H_2	0.00736-0.222	0.0110-0.0601	5.49
	d_i (the inactive layer)	0.0-1.0cm	CO		0.0201-0.0098	0.49
			H_2		0.0321-0.0213	0.66
CO production in soil	Coupling of temperature & d_i					v_{nd}
	d_i=0.0cm	0-40° C	CO		0.0172-0.0212	1.23
	d_i=1.0cm	0-40° C	CO		0.0084-0.0020	0.24

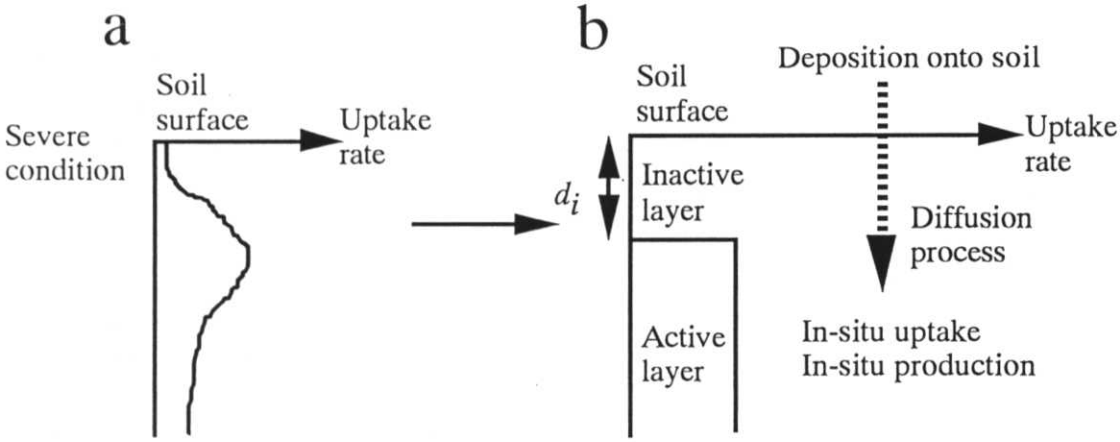

Figure 5.1
Simplification of the uptake profile in soil from (a) a real image to (b) the two-layer model. The variable d_i is the depth of the inactive layer and is considered to be an index of the distribution of in-situ uptake rates.

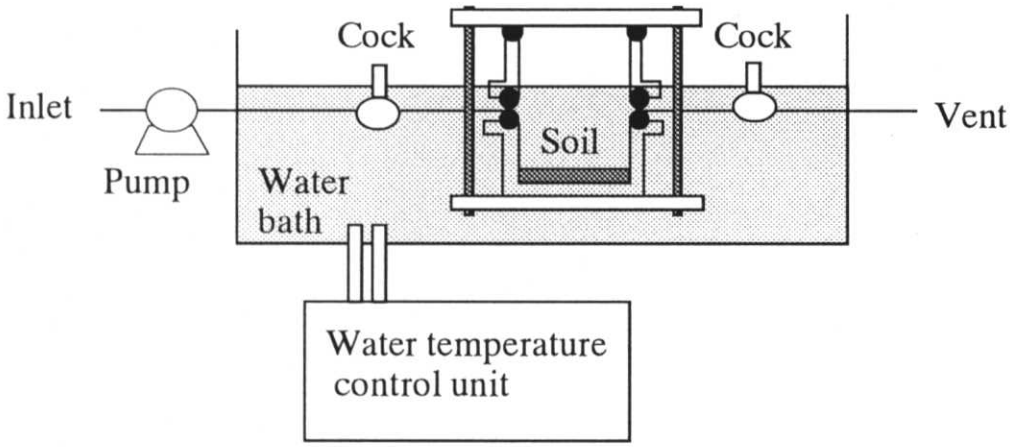

Figure 5.2
Schematic diagram of the laboratory experiments. The chamber, of inner volume 695 cm^3, was made of Pyrex® glass and was gas-tight. The gaskets used for the chamber were made of Viton® rings. About 10 g of wet soil were spread on the bottom of the chamber, which was immersed in a temperature-controlled water bath. After the air in the chamber was flushed, soil net uptake rate was measured.

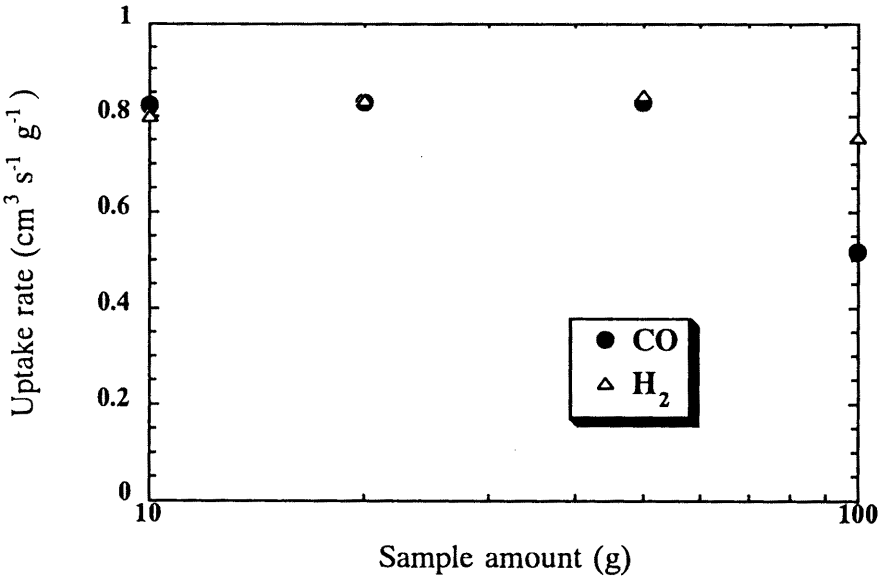

Figure 5.3 Dependence of observed uptake rate on sample amount in the chamber.

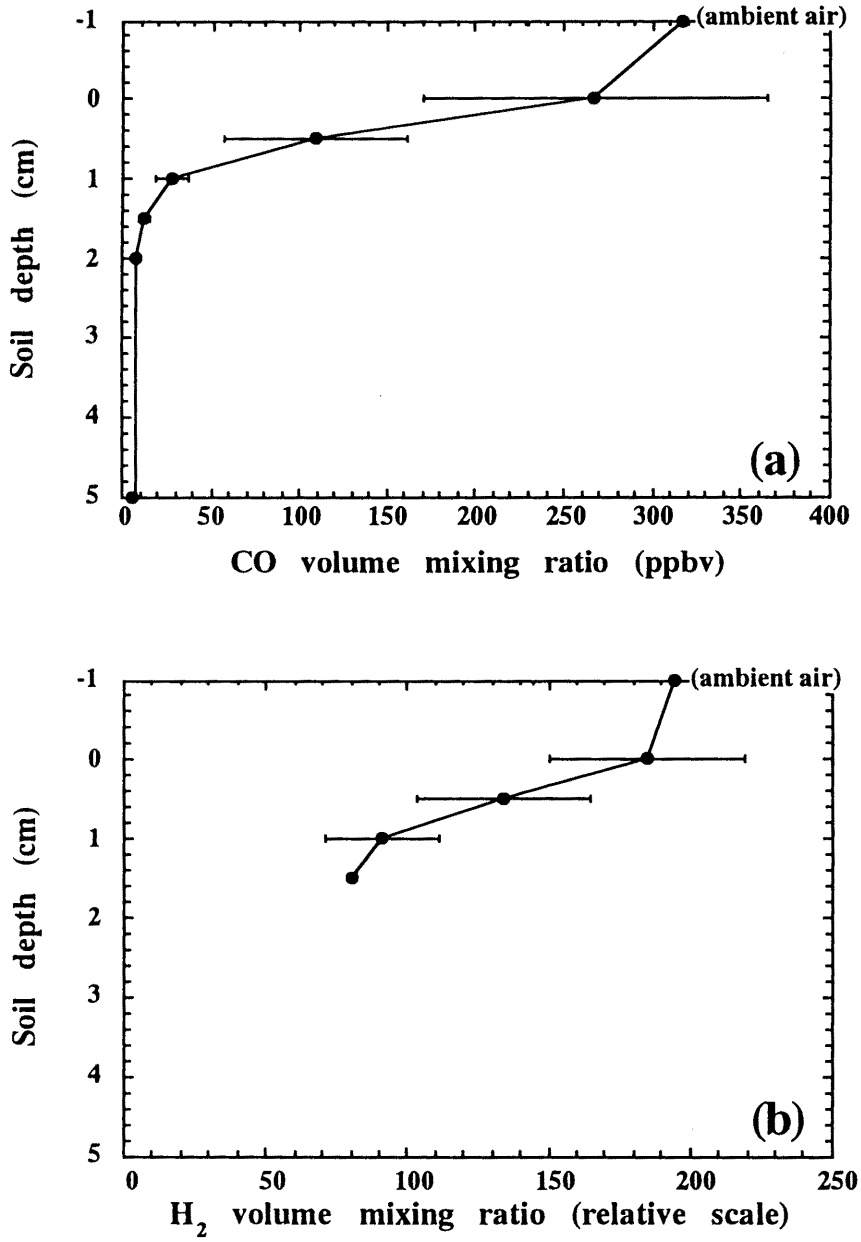

Figure 5.4 (a) CO and (b) H_2 concentration profiles in laboratory experiments. Teflon® tubes were inserted to soil to extract soil air because Teflon® is free from contamination. Error bars are standard deviations of 7 profiles.

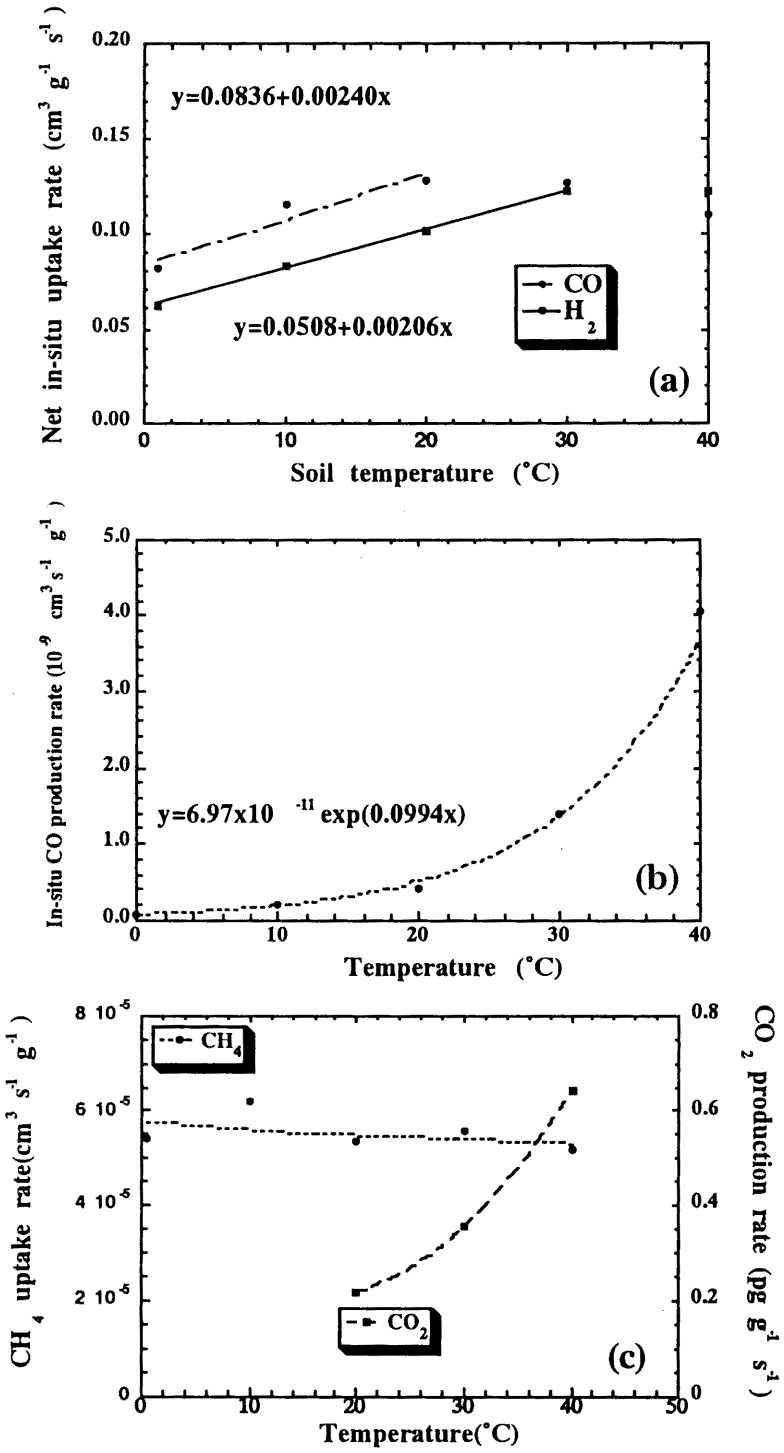

Figure 5.5

Temperature dependence of (a) net in-situ uptake rates of CO and H_2 of mixed soil (0-5cm) from laboratory experiments, (b) in-situ CO production rates calculated using (a) and the CO equilibrium concentration measured by field experiments, and (c) CH_4 in-situ uptake rates and CO_2 in-situ production rates. The data points in (a) were averages of 3 temperature-dependent curves. The regressions in the lower temperature range were regarded as approximating gross uptake rate curves. The data points in (b) were representative values of continuous measurements at 3-min intervals over several days in two different seasons.

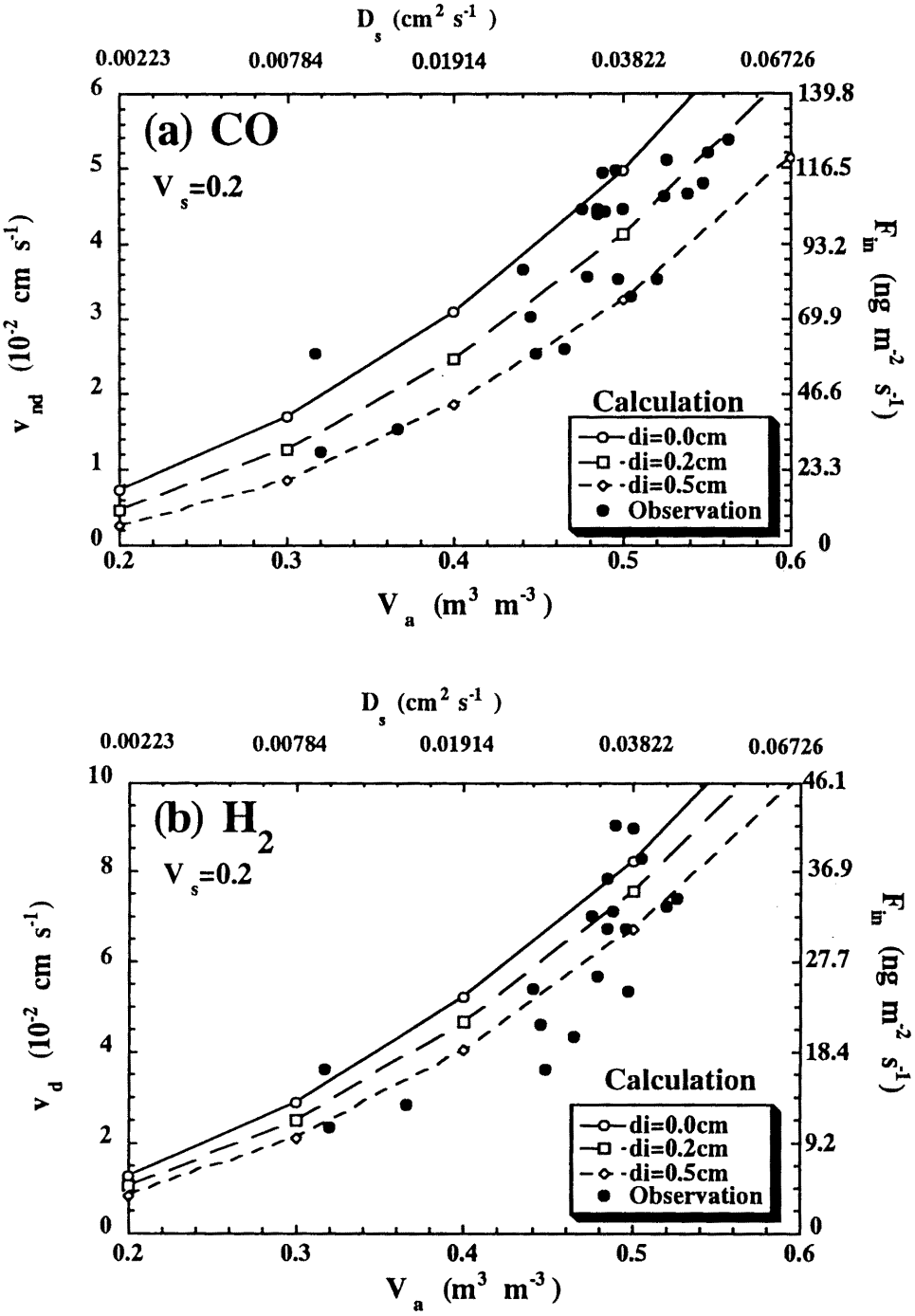

Figure 5.6

Observe and calculated (a) CO and (b) H_2 deposition velocities as a function of air-filled porosity, V_a . Calculations were made under conditions of V_s = 0.2, T = 20°C, and 2 times larger uptake rates than an the arable soil (0-5cm) (Fig.5.5a) to reflect top soil uptake (Table 5.2). Right Y-axis means net uptake by soils (ng m^{-2} s^{-1}), defined by F_{in}=-10000F_0.

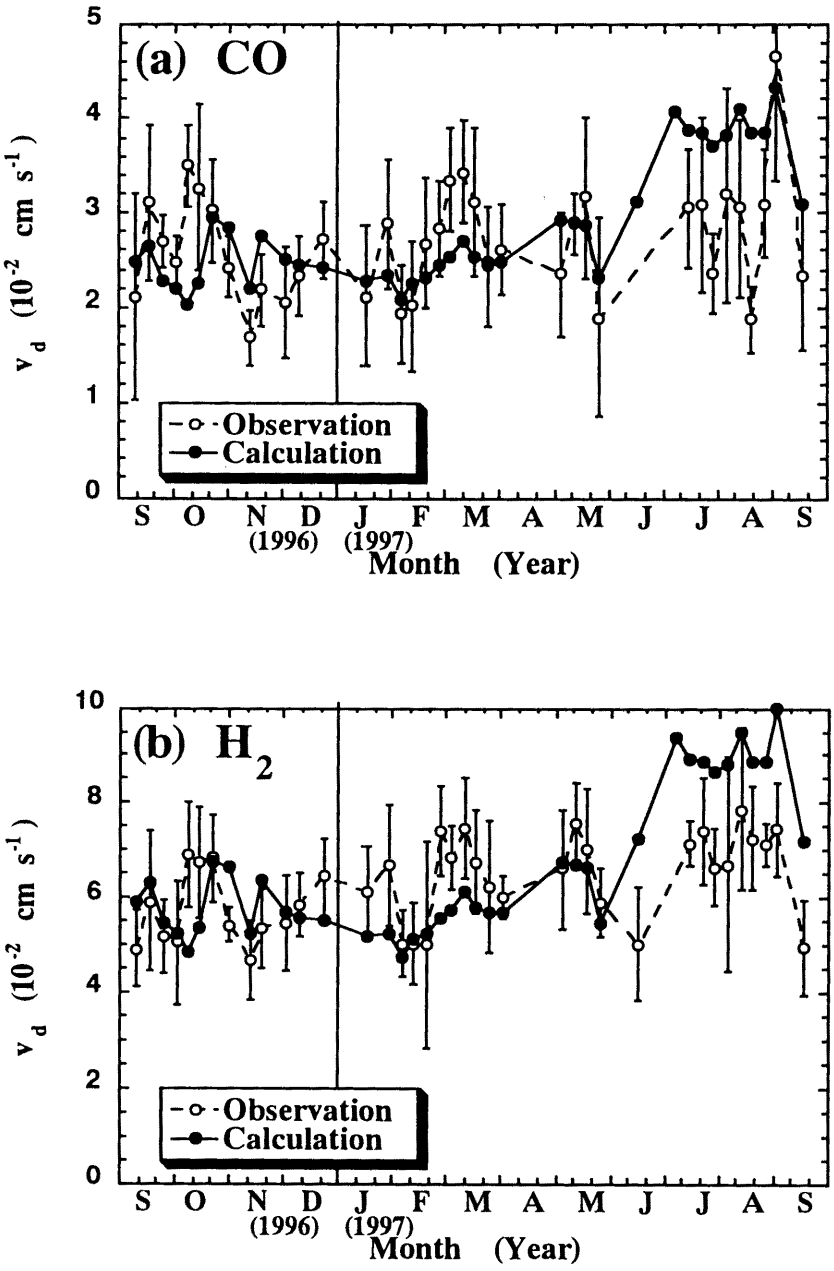

Figure 5.7
Observed and calculated (a) CO and (b) H_2 deposition velocities in the forest. Calculations were made under conditions of V_a, V_s in the forest, 5 times larger uptake rates than an the arable soil (Fig.5.5a) and d_i=1.0cm.

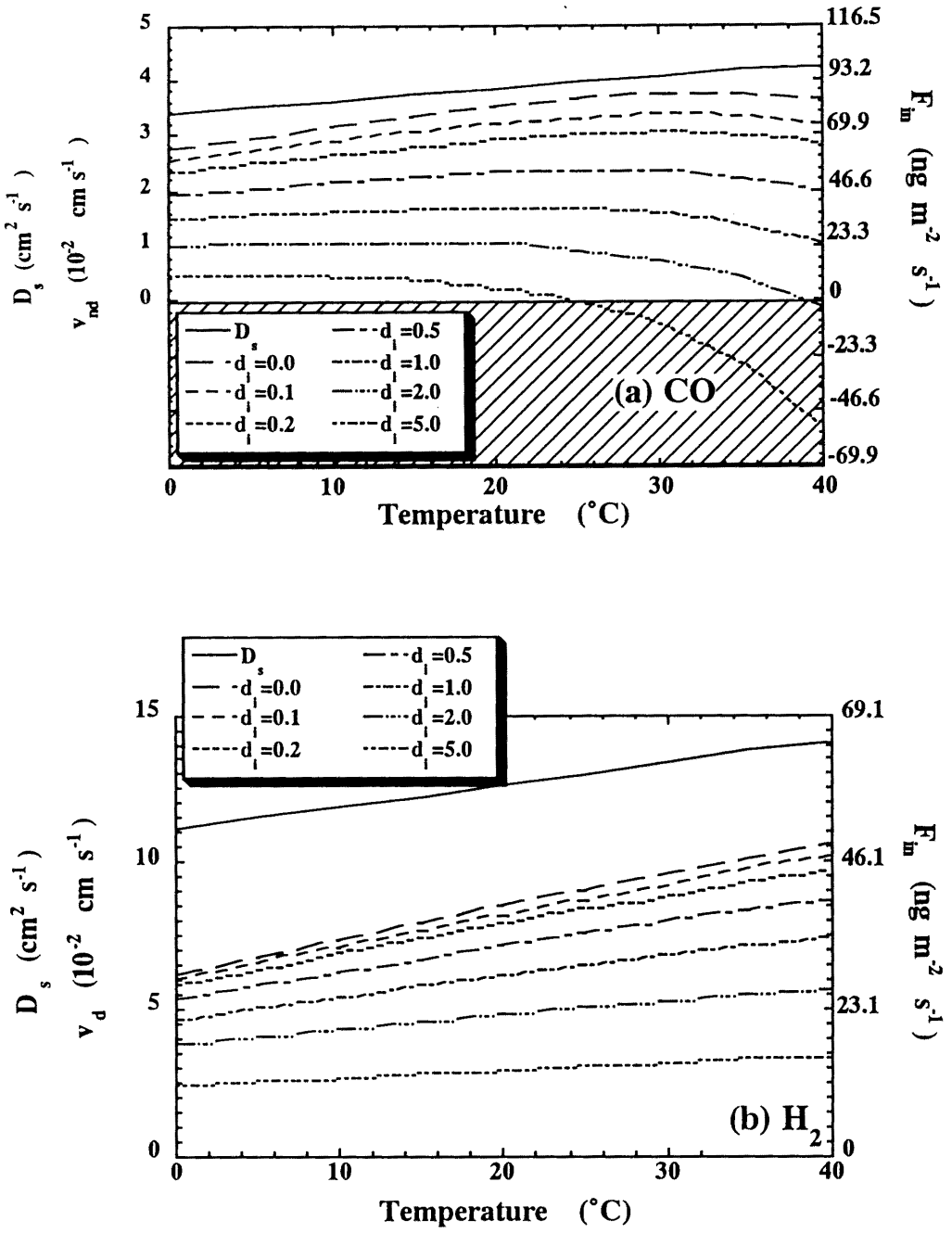

Figure 5.8
Calculated temperature dependence of deposition velocities for (a) CO and (b) H_2. Solid lines are curves of soil gas diffusivity. CO is emitted from soil in the shaded area. Calculations were made under conditions of V_s = 0.2 and V_a = 0.5. For CO, the optimum temperature to maximize the vd varied with d_i.

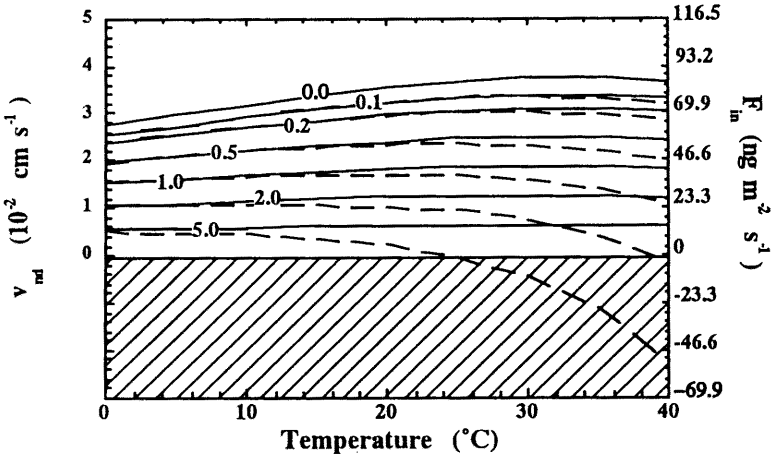

Figure 5.9 Calculated impact of the CO source in the inactive layer on v_{nd}. Numerals on lines are depths of the inactive layer d_i. Solid lines represent calculations assuming no production in the inactive layer; wavy lines show production taking into account the inactive layer. CO is emitted from soil in the shaded area. Calculations were made under the conditions of V_s = 0.2 and V_a = 0.6.

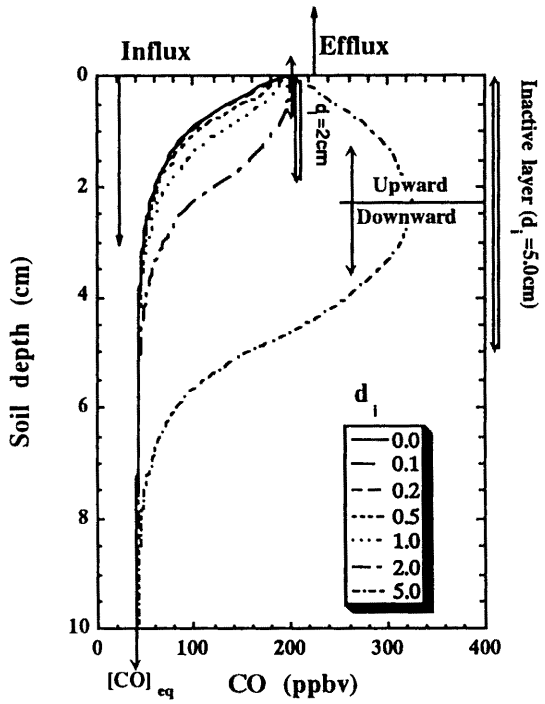

Figure 5.10 Calculated CO concentration profiles calculated for the experimental soil at 40°C under the conditions of V_s = 0.2 and V_a = 0.5. When d_i = 2.0 and 5.0 cm, CO is transported to the atmosphere and to deeper soil layers from the inactive layer. In conditions of high soil temperature together with a thick d_i, the deposition velocity of CO is markedly lowered or CO is emitted from soil.

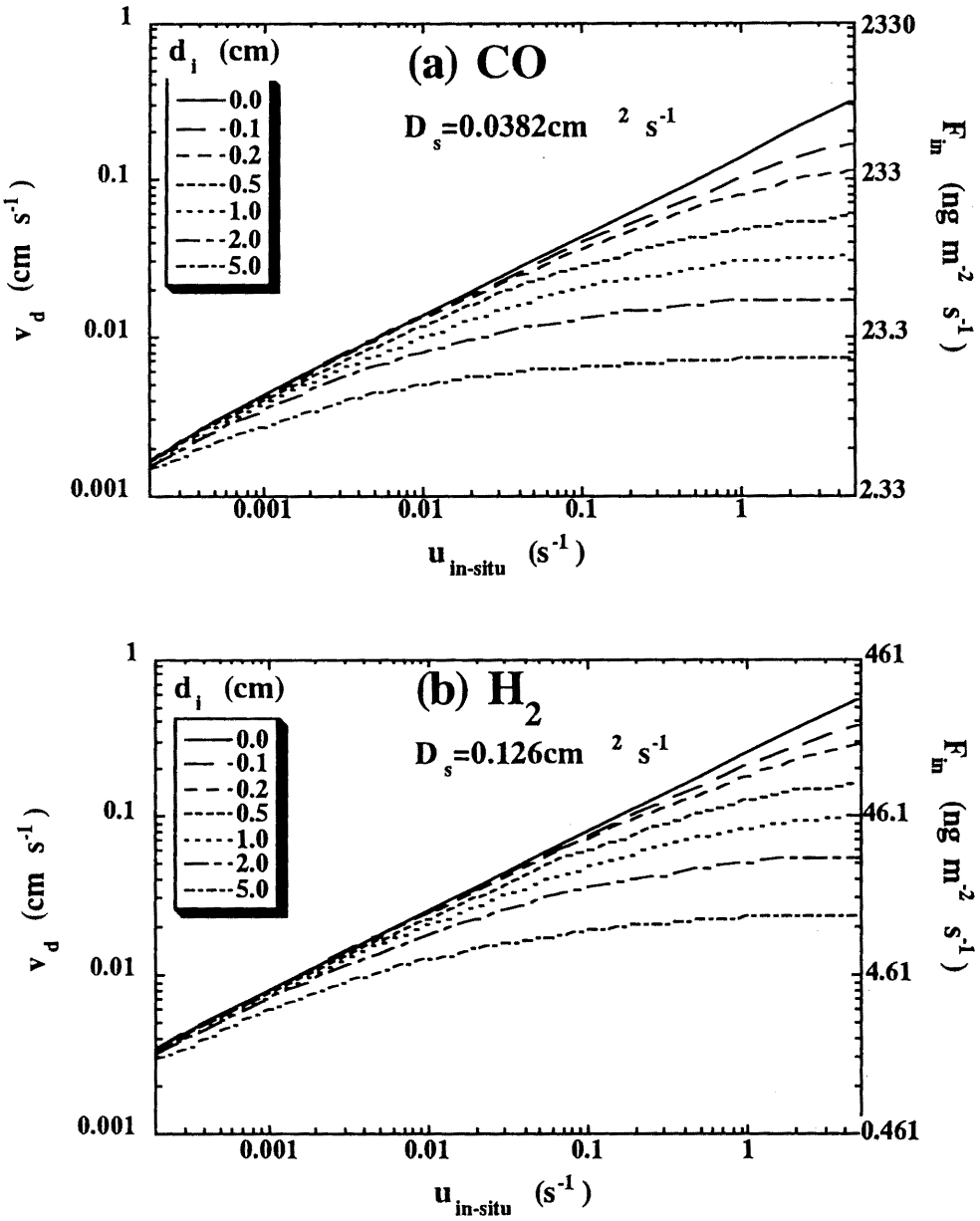

Figure 5.11 Calculated relationship between in-situ uptake rate $u_{in\text{-}situ}$, and v_d for (a) CO and (b) H_2 under the conditions of T = 20°C, V_s = 0.2, V_a = 0.5, and with no CO production in the soil. Flux values to the right of the graph were those at STP and T = 20°C. D_s is the soil gas diffusivity.

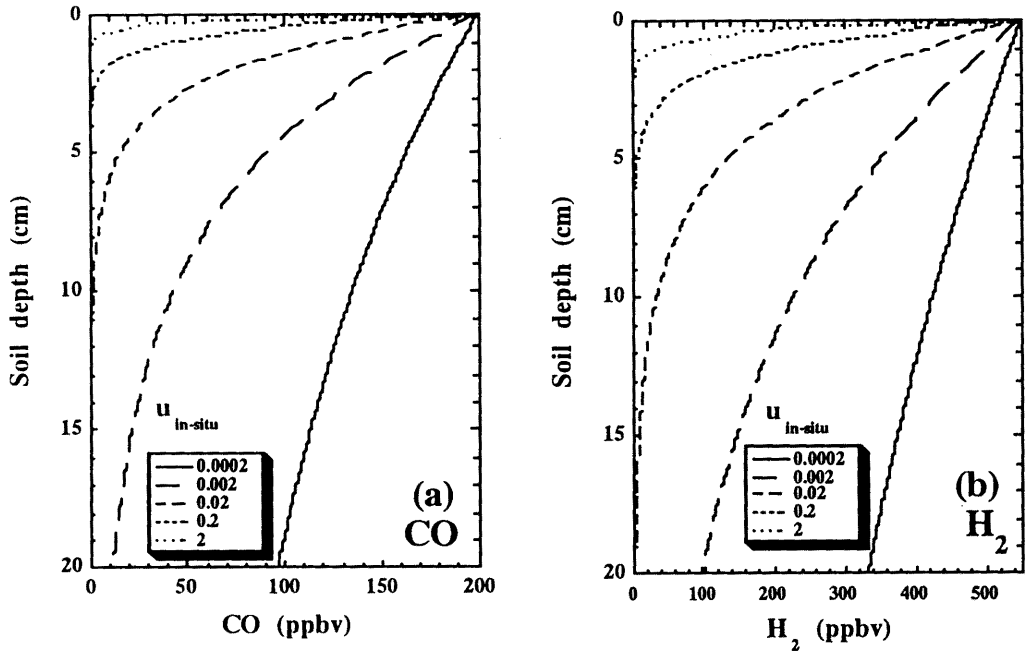

Figure 5.12 Concentration profiles of (a) CO and (b) H_2 from Fig. 5.11. Values in the insets are in-situ uptake rates. As the in-situ uptake rate increases, the depth of the oxidation layer becomes shallower. H_2 can permeate deeper than CO due to its larger molecular diffusivity.

Chapter 6

A process-based model to estimate global CO-, H_2-, and CH_4- uptake strengths by soils

6.1 Introduction

This Chapter propose a process-based model that explicitly incorporates biological uptake processes as well as the physical diffusion process to investigate the characteristics and distribution of the global uptake strengths of CO, H_2, and CH_4 (Yonemura and Yokozawa, 1999). The mechanisms revealed in previous Chapters 4 and 5 are incorporated into the model. CH_4 global uptake was also considered because the differences in mechanism is useful to understand the CO and H_2 global uptake by soils. There have been several studies on the global estimation of CH_4 uptake by soils. Seiler and Conrad (1987) estimate it to be (32±16) Tg yr^{-1}. Born et al. (1990) and Dörr et al. (1993) estimate it to be between 9 and 56 Tg yr^{-1} with a best value of 28.7 Tg yr^{-1}, which corresponds to about 7% of the total global destruction rate by OH radicals. Potter et al. (1996b) estimate it to be 17 to 23 Tg yr^{-1}, using global grid data and incorporating the soil-texture-class criteria of the FAO (EPA, 1992) and estimating soil-moisture content from the water balance with a bucket model. Ridgwell et al. (1999) estimate it to be 38 Tg yr^{-1} (20 to 51 Tg yr^{-1}) using a similar but more process-based model than Potter et al. (1996b) used.

6.2 Data and model

The formulation of the influx, F (molecules cm^{-2} s^{-1}), obeyed those in Chapter 5. The dimension of ρ was taken as number density (molecules cm^{-3}). When the temperature was below 0°C, uptake was set at zero because the diffusion from the atmosphere into the soil cannot occur because of snow cover, as is shown by previous data (e.g., Crill, 1991).

6.2.1 In-situ uptake and production rates of CO, H_2, and CH_4

In-situ uptake and production rates (Fig. 6.1) are influenced by various environmental factors because the processes directly reflect microbial activities that utilize CO, H_2, and CH_4. We therefore considered that the in-situ uptake processes of gas in soil should be modeled by incorporating these mechanisms rather than flux values observed at the soil surface. We assumed that the in-situ uptake and production rates depend on both temperature and soil-water content as follows:

$$u_{in\text{-}situ} = f_{uT} \times f_{uW} \times u_{max}; \tag{6.1}$$

$$P_{in\text{-}situ} = f_{PW} \times OC \times P_T, \tag{6.2}$$

where f_{uT} is the temperature-dependence factor of $u_{in\text{-}situ}$ (dimensionless), f_{uW} is the soil-moisture-dependence factor (dimensionless), u_{max} is the maximum in-situ uptake rate (s^{-1}), f_{PW} is the soil-water-dependence factor of $P_{in\text{-}situ}$ (dimensionless), OC is volumetric organic carbon (g m^{-3}), and P_T is the temperature-dependence factor of $P_{in\text{-}situ}$ (molecules g^{-1}organic carbon s^{-1}).

The in-situ uptake rates of CO, H_2, and CH_4 should be positively related to organic-carbon content because uptake processes are biological. Here, however, we did not model the in-situ uptake rates as a function of organic-carbon content, because the positive relationship between the in-situ uptake rate and the organic-carbon content holds for higher atmospheric concentrations than are observed or cannot be simply applied to the top soil responsible for the oxidation of CO, H_2, and CH_4 (for CH_4, Hütsch et al., 1993; Goldman et al., 1995; Czepiel et al., 1995; for CO, Hendrickson and Kubiseski, 1991; Moxley and Smith, 1998a).

6.2.2 Dependence of in-situ uptake and production rates of CO, H_2, and CH_4 on soil temperature and moisture content

There are large variations in the estimated values for the maximum in-situ uptake rate, u_{max}, of CH_4 in arable fields, forest, and other ecosystems available from previous results

of core/incubation studies performed in the laboratory under atmospheric CH_4 concentrations. Therefore, we divided the experimental values into three scenarios (low, middle, and high) for each soil type (arable-field soil, forest soil, and other; Table 6.1). The u_{max} of CO and H_2 was set to 0.15 s^{-1} (see Chapter 5). The functions of f_{uT} and f_{uW} for CO, H_2, and CH_4 that we used are shown in Fig. 6.1. They are based on previous results for CH_4 (Whalen and Reeburgh, 1996; Priemé and Christensen, 1997) and CO (Heichel, 1973; Liebl and Seiler, 1976; Moxley and Smith, 1998a; Kuhlbusch et al., 1998). Note that temperature is not a major controlling factor on the uptake rates of CO, H_2, and CH_4 in the physiological temperature from 5 to 35°C.

In Fig. 6.1b, f_{uW} is given as a function of the soil wetness index (*SWI*). Since a global data set of soil-moisture content is required to evaluate the values of f_{uW} globally, we used soil-moisture data from the results of the Colorado State University, Atmospheric General Circulation Model (CSU-AGCM) with the Simple Biosphere Model version 2 (SiB2) land-surface process model (Zhang et al., 1999). These data are available from the Global Soil Wetness Project Web site (http://www2.tkl.iis.u-tokyo.ac.jp/DV/gswp/index.html). Figure 6.2 shows the output of the run for 1987. Even though the data are restricted to 1987, we considered that the distribution of soil-moisture content estimated from the AGCM with the land-surface process model (SiB2) is far more reasonable than that estimated using a bucket model, which shows pronounced geographical variation with precipitation and often shows saturation in moist regions, far from reality. The outputs for soil moisture of the GCM model were given by the *SWI*:

$$SWI = \frac{V_l - WP}{FC - WP}. \tag{6.3}$$

Where, V_l is the volumetric water ratio in soil (dimensionless); *WP* and *FC* are wilting point and field capacity (dimensionless), respectively, determined from soil types. Then, V_l is given by

$$V_l = WP + SWI\ (FS\text{-}WP), \tag{6.4}$$

From the *SWI* and soil-texture data, three phase ratios (V_a, V_l, V_s; eq. (5.6)) of soils were calculated. Then, the soil gas diffusivity, D_s, was calculated (eq. 5.9).

The AGCM approach to the evaluation of soil moisture cannot describe the dependence of f_{uW} on soil moisture at low soil-water content where inhibition sets in, as suggested by Ridgwell et al. (1999), because the AGCM does not calculate soil moisture below the wilting point. We assumed that there was no water stress even under dry climatic conditions, because a certain amount of water is also available as soil water at the *WP*. Therefore, we took f_{uW} as a function of *SWI*. The function increases linearly with *SWI* and reaches a saturated value. The threshold value 0.2 (Fig. 6.1b) was tentatively determined from previous studies, assuming that *WP*=0 (Heichel, 1973; Whalen and Reeburgh, 1996; Mosier et al., 1997; Moxley and Smith, 1998a). The bias introduced by the determination of the threshold value should control the uptake strengths at rim regions (e.g., savannah) around deserts and therefore lead to a large control on the global uptake strengths.

Also note that the in-situ uptake rates did not decrease under high *SWI*, although previous studies showed a decrease of in-situ uptake rates when soil moisture was high (Heichel, 1973; Moxley and Smith, 1998a), because we considered that even data of in-situ uptake obtained from laboratory core/incubation experiments are subject to a decrease in molecular diffusion.

Production in soil is considered only for CO because H_2 and CH_4 productions in aerated soils are small. CO production is an abiological process and is proportional to the amount of soil organic carbon. The form of the function P_T was determined from previous results (Conrad and Seiler, 1985b; Zepp et al., 1996) as:

$$P_T = 1.24 \times 10^{25} \exp\left(-\frac{E_a}{R_g (T_0 + T)} \right), \tag{6.5}$$

where R_g is a gas constant (=8.31 J mol^{-1} K^{-1}), T_0 is the absolute temperature for 0°C

(273.15K), and E_a is activation energy (set at 80 kJ mol^{-1}). Under very dry conditions, production is suppressed (Conrad and Seiler, 1985b; Moxley and Smith, 1998b). Therefore, we set f_{PW} as follows:

$$f_{PW}=1, \quad \text{for } (SWI>0.1). \tag{6.6}$$

$$f_{PW}=SWI/0.1, \quad \text{for } (SWI<0.1). \tag{6.7}$$

This equation (6.7) shows that under completely dry conditions (SWI=0) such as in desert soil, production cannot occur even if organic carbon is present because CO production needs water (Conrad and Seiler, 1985b). We assumed the same dependence-function form for f_{PW} as for f_{uW}, in which the threshold value of 0.1 was set based on previous studies (Conrad and Seiler, 1985b; Moxley and Smith, 1998b).

6.2.3 Surface environmental data

Model calculations were carried out monthly. We used surface environmental data listed in Table 6.2 as the input for the above model. Climatic data such as monthly mean temperature was derived from the CRU Global Climate Datasets (http://ipcc-ddc.cru.uea.ac.uk/ddc_provide.html; New et al., 1999). The values for wilting point, WP; field capacity, FS; total pore capacity (the sum of A and W), PC; and cultivation index were set according to the FAO texture class (Zobler, 1986) and the equations of Saxton et al. (1986) and Potter et al. (1996a, b). Organic carbon-content data were obtained from Potter and Klooster (1997), who generated a global map grid for total C content to 1-m soil depth by assigning average measured values (g m^{-3}) from Post et al. (1985) to ecosystem classes in the global data set produced by Leemans (1990). The carbon content is highest in northern high-latitude soils and lower in the tropical region soils and is lowest in desert regions.

Soil temperature changes diurnally and depends upon weather conditions and soil depth. However, we used the monthly mean air temperature as the soil temperature, because it is sufficient for estimating the monthly strength of uptake and production. Furthermore, the in-situ production of CO in soils is affected synchronously by the diurnal temperature

cycle (e.g., Conrad and Seiler, 1985a, Scharffe et al., 1990). Considering this fact and the exponential dependence on temperature (eq. 6.5), the actual soil-temperature values used for the present model should be higher than the monthly mean air-temperature values. We assumed in eq. (8.5) that soil-temperature values were higher than air-temperature values by 5°C in forest soils and by 15°C in non-forest soils (Chapter 4).

6.2.4 Atmospheric concentrations of CO, H_2, and CH_4

Both CO and CH_4 concentrations are higher in the northern hemisphere than in the southern hemisphere because large sources such as wetlands and industrial countries are situated in the northern hemisphere. However, because of the longer lifetime of H_2 and CH_4 in the atmosphere (Chapter 1), the spatial differences in H_2 and CH_4 concentrations are small, so H_2 and CH_4 concentrations were set uniformly at 500 ppbv and 1.8 ppmv, respectively. The H_2 concentration was somewhat smaller than 520 ppbv; the CH_4 concentration is somewhat larger than the 1.7- ppmv background level, to reflect the concentration over land (Dlugokencky et al., 1994).

CO concentration differs greatly in the two hemispheres. Generally, the background level of CO is 75 to 200 ppbv in the northern hemisphere and 40 to 80 ppbv in the southern hemisphere (Novelli et al, 1998). Ground-level concentration is higher than these values because of local sources on the land. However, it should be noted that CO concentration is variable from year to year and highly variable spatially even in the free troposphere (Pochanart et al., 1999). We therefore postulated three atmospheric CO-concentration scenarios as shown in Fig. 6.3. These concentrations are within a reasonable range of recent ground-station data (Novelli et al., 1998). The low scenario is similar to background values and may be lower than actual values because the ground stations are situated so as not to receive direct pollution. The estimation of atmospheric CO concentration leads to large differences in the estimation of CO-uptake strength because CO uptake obeys first-order kinetics with respect to concentration.

6.2.5 Global gross uptake and net uptake

Net CO-uptake strength is apparently affected by the production process in soil. When there is no soil-production term, we refer to gross CO-uptake strength; when a soil-

production term is present, we refer to net CO-uptake strength. Usually, CO soil uptake and production is divided into sink and source inventories, respectively. Although strictly speaking we consider that both the uptake and production processes are interactive and furthermore that production is affected by atmospheric concentration, we calculated global CO-production strength by subtracting net global CO-uptake strength from gross global CO-uptake strength.

6.2.6 Comparison of process-based models to estimate global uptake strengths of CO and H_2

There are only two process-based models to estimate global CO-uptake strength by soil. This study is the first to propose a process-based model to estimate global H_2-uptake strength by soil. Comparison of the process-based models is shown in Table 6.3. Striking feature of the process-based model of the present study is that both biological uptake processes in soil and abiological production processes are incorporated.

6.3 Results and Discussion

6.3.1 Global CO and H_2 uptake

Net and gross global CO-uptake strengths were estimated to be 79.1 and 85.2 Tg yr^{-1} (gross production: 6.1 Tg yr^{-1}), respectively. These values are much smaller than previous estimations but much larger than the results by Potter et al. (1996a).

Measurement data on CO uptake are available from several locales in the world (Table 6.3): Manitoba, Canada (Zepp et al., 1997; Kuhlbusch et al., 1998); Darmstadt, Germany (Sanhueza et al., 1998); Mainz, Germany (Liebl and Seiler, 1976; Conrad and Seiler, 1980b); Tsukuba, Japan (Chapter 4); Andalusia, Spain (Conrad and Seiler, 1985a); Namib, Namibia (Conrad and Seiler, 1985a); Transvaal, South Africa (Conrad and Seiler, 1985a); and Guri, Venezuela (Scharffe et al., 1990). The present estimated gross-deposition velocities are compared with the observed velocities in Fig. 6.4a. The estimated values for deposition velocity were averaged over the period of measurement of the real data. It appeared that there was no relationship between them. Considering that CO is absorbed mostly by top soil within several centimeters of the ground surface, it is essential to correct for soil physical parameters. Top soil should have a higher air-filled porosity and a lower soil-moisture

content, which should be positively dependent on temperature. From these characteristics of top soil, we made the following corrections to adjust the flux values:

for the total pore capacity, PC,

$$PC_{corrected} = PC_{uncorrected} + 0.1; \tag{6.8}$$

for the volumetric solid ratio of soil,

$$S_{corrected} = S_{uncorrected} - 0.1; \tag{6.9}$$

for the wilting point,

$$WP_{corrected} = \frac{S_{corrected}}{S_{uncorrected}} WP_{uncorrected}; \tag{6.10}$$

for the field capacity,

$$FC_{corrected} = \frac{S_{corrected}}{S_{uncorrected}} FC_{uncorrected}; \tag{6.11}$$

for the soil wetness index,

$$SWI_{corrected} = SWI_{uncorrected} - 0.018T. \tag{6.12}$$

$SWI_{corrected}$ was set to zero when the value of $SWI_{corrected}$ was less than zero. These corrections are within a reasonable range compared to values from previous studies (Ball et al., 1997a; Fukumoto, 1999) and reflect the highly porous condition of the top soil. It was assumed that the value of eq. (6.12) reflects the lower moisture of top soil induced by evaporation at higher temperatures.

The revised relationship between the corrected estimates and the observed deposition velocities is shown in Fig. 6.4b. There exists a clear positive correlation between the values except for forest sites. However, it should be noted that the observed data represent values measured from only a narrow surface area during a short period of time, and our calculations were done on a grid scale of 1° latitude ×1° longitude. Thus, the scales are quite different. However, based on the current knowledge of CO uptake by soil, we consider a correction to be necessary.

For the corrected estimation of global CO uptake, the deposition velocities in forest regions were independently set apart from agricultural and grassland regions, using the relationship between deposition velocities and yearly averaged temperature. It has been shown by recent study (Sanhueza et al., 1998) and the results in Chapter 4 that diffusion controls on CO deposition at forest sites are weaker than in arable fields. In forests, the layer of leaf litter acts to resist the diffusion of gas between the atmosphere and the soil. The leaf-litter layer is expected to be thicker in low-temperature forest regions, because the destruction rate of the organic matter in the leaf litter should be small. Thus, although the data are quite limited, the positive relationship shown in Fig. 6.5 may be reasonable.

After the flux corrections, gross and net global CO-uptake strengths and global H_2-uptake strength were estimated to be 117.6 and 103.8 Tg yr^{-1} (CO production: 13.7 Tg yr^{-1}) from middle scenarios of atmospheric CO concentrations (Fig. 6.3), respectively, and global H_2-uptake strength was 69.7 Tg yr^{-1}. The net global CO-uptake strength was estimated to range between 88 and 150 Tg yr^{-1}. The estimated gross CO-uptake strength is about 5% of the total global CO-sink strength and is on the lower edge of the 115 Tg yr^{-1} estimated by Sanhueza et al. (1998) but significantly larger than the 16 to 50 Tg yr^{-1} estimated by Potter et al. (1996a), who employed a similar diffusion model that assumed the concentration gradients in soil to be in reality low. The low value of Potter et al. (1996a) could be attributed both to the assumption of their low-pitched CO gradient soil and to the high moisture content in wet climate regions estimated by bucket model. Our global CO-production value of 13.7 Tg yr^{-1} is of the same order as the values of 17 (2 to 34) Tg yr^{-1} by Seiler and Conrad (1987) and 9.4 (6.9 to 11.9) Tg yr^{-1} by Potter et al. (1996a). The H_2-uptake strength is about 75% of the total global H_2-sink strength.

Global estimation of CO- and H_2- uptake strengths by soil from previous studies is summarized in Table 6.4 (see Appendix C on the detailed estimation of global H_2-uptake strength by soil obtained from the balance of deuteirum content). The large CO-uptake strength estimated by Conrad and Seiler (1985a) which has been authorized, is partly because their estimation of deposition velocity was larger than those of Sanhueza et al. (1998) and this study, and partly because they estimated the contribution from northern hemispheric winter, and largely because they set high concentration of CO in the boundary layer. The H_2-uptake strength of the present study is in the middle of those of Seiler and Conrad (1987) and Ehhalt (1999). The reduction of H_2-uptake strength from Seiler and Conrad (1987) to the present study is partly because their estimation in deposition velocity is lower in the present study and because they incorporated northern-high latitudes uptake in northern-hemispheric winter.

Large errors in the estimation of global CO-uptake strength are due to the uncertainty in the CO concentration at the land surface. Conrad and Seiler (1985a) estimated a large value, assuming a high concentration of CO at the land surface. Taking into account the seasonal variation, since CO concentration is low in summer, could decrease the estimated values of global CO-uptake strength. The sink strength of CO should be low in the northern hemisphere. The assumption that the concentration at the land surface is much higher than the background concentration could positively increase the predicted value for global CO-uptake strength. Because most of the active areas of CO uptake correspond to anthropogenically active areas such as the developed countries in the northern hemisphere with a high level of industrial activity or to vegetation areas with CO emissions from burning and photooxidation of organic matters , CO concentration in the boundary layer in active areas is high. However, it is very difficult to totally grasp concentrations at the land surface because of the complexity of the problem.

The estimated distributions of global CO- and H_2- uptake strengths after the corrections are incorporated are shown in Figs. 6.6 and 6.7. It can be expressed in or seen from the maps that: desert regions do not contribute to the exchange of CO and H_2; in the Eurasian and North American continents in the winter, the uptake strengths of CO and H_2 fade away over large areas because the temperature in those areas is less than 0°C; at low latitudes, on the

other hand, grasslands or agricultural fields show a larger uptake strength than do forest regions because of the resistance by the leaf-litter layer above soil; and there exist high uptake-strength regions in agricultural fields in the United States and in Russia and the Ukraine.

Figure 6.8 shows the latitudinal distribution of CO-uptake and production, and H_2-uptake strengths. Seasonal variations in CO- and H_2-uptake strengths (Fig. 6.9) are mostly accounted for by the variation in the northern hemisphere; CO- and H_2-uptake in the southern hemisphere have no clear seasonal variations. The global uptake strengths show maximum in summer and minimum in winter of the northern hemisphere. In the summer (January) in the southern hemisphere, net CO uptake decreased due to the high CO-production strength at high temperatures. CO production is also important in the southern hemisphere because of the low atmospheric CO concentration. CO production is conspicuous in summer (July) in the northern hemisphere as well as in tropical latitudes because of high organic-carbon content and a high equilibrium CO concentration in these regions induced by small in-situ uptake velocities reflecting resistance by the layer of leaf litter.

6.3.2 Influence of global CO- and H_2- uptake by soil on global CO and H_2 concentrations

The relationship between the seasonal variation in CO-uptake strength by soil (Fig. 6.9) and the seasonal variation in CO concentrations (Figs. 1.3 and 1.4) is unclear because the CO uptake strength is small within several percentage of global CO sink and because both sink strengths of soil uptake and the reaction with OH are similar in seasonal variation.

On the other hand, H_2 concentration (Figs 1.3 and 1.5) can be considered to be much influenced by H_2-uptake by soil because of the following 3 points:

1 H_2 concentrations in the northern hemisphere are lower than those in the southern hemisphere.

2 H_2 concentrations in the northern hemisphere decrease in summer when the H_2-uptake is large in the northern hemisphere. Here, please note that small seasonal variation in southern hemisphere shows that the increase in OH radical in southern hemispheric summer does not lead to large destruction of H_2; rather, the increase in OH radical could lead to the formation of H_2 due to the reaction with CH_4 (eqs. 1.4-1.8a).

3 Continental H_2 concentrations (Mongol, Utah) are lower than marine concentrations.

6.3.3 Global CH_4 uptake

Globally, the total CH_4 uptake strength was 19.8 Tg (Tg=10^{12}g) yr^{-1} for the middle scenario (Table 6.1). The estimated values among the three scenarios range from 9.9 to 39.6 Tg yr^{-1}, which is comparable to or smaller than previous estimates (Seiler and Conrad, 1987; Born et al., 1990; Dörr et al., 1993; Potter et al., 1996b; Ridgwell et al., 1999). It should be noted that the determination of u_{max} directly affected the global uptake strength of CH_4. The estimation of 38 Tg yr^{-1} by Ridgwell et al. (1999) is attributed to an oxidation rate (here, the in-situ uptake value) of 8.7×10^{-4} (R^2=0.55), based on data obtained in Europe and Alaska (Whalen et al., 1992; Dörr et al., 1993; Striegl, 1993; Koschorreck and Conrad, 1993). This rate corresponds to u_{max} in this study, although the formulation of the model is different. The value of u_{max} in Ridgwell et al. (1999) is higher than the values shown in Table 6.1, which are based on limited data from core/incubation experiments in the laboratory. To obtain a much more accurate estimation of the global uptake strength of CH_4, it would be necessary to validate u_{max} based on much more soil-moisture data as well as other data from various places in the world. Further intensive measurements including soil physical characteristics such as soil moisture are needed.

In the summer in the northern hemisphere, CH_4 uptake reaches maximum strength because the land in that hemisphere is free from snow cover then (Figs. 6.10 and 6.11). Geographically (Fig. 6.10), the following points were simulated in the model: soils in extreme desert regions do not contribute to the exchange of CH_4; in the Eurasian and North American continents during the northern-hemisphere winter, the temperature over large areas is under 0°C, and the uptake of CH_4 approaches 0; agricultural regions in Eurasia and North America show small CH_4 uptakes reflecting low uptake ability; considerable regions of South America and Southern China show small uptakes due to the fine soil-texture class. The distribution found by this study was different from that found by Ridgwell et al. (1999) in wet regions and savannah regions, mainly because of the difference in the input of soil-moisture data (Fig. 6.2).

Figure 6.11 shows the latitudinal distribution of CH_4-uptake strengths. Note that in low latitudes of the southern hemisphere, CH_4 uptake showed small seasonal variation. Globally, seasonal variation in CH_4 uptake strengths is mostly due to variation in the northern

hemisphere.

6.3.4 Comparison of global CO-, H_2-, and CH_4- uptake and their changes under global changes

Comparing global distributions of CO, H_2, and CH_4 uptake strengths, we can see that: although the atmospheric concentrations of CO and H_2 are far smaller than that of CH_4, but its uptake flux is larger because of large in-situ uptake rates; the uptake regions of CH_4 extend farther into desert regions than those of CO and H_2, reflecting the fact that CH_4 uptake is less affected by low soil moisture because CH_4 uptake occurs in a deeper soil layer than does CO and H_2 uptake. These results are consistent with those of Striegl et al. (1992), which indicate that soil layers deeper than 2 m show CH_4 uptake ability and with Zepp et al. (1996), which indicate that no uptake flux is shown in arid-soil.

The effects of temperature on global CO-, H_2-, and CH_4- uptake strengths are shown in Fig. 6.12a. All the CO-, H_2-, and CH_4-uptake strengths increased with temperature, mostly because of the enlargement of the uptake regions as the temperature rose and snow cover shrank. Secondly, uptake strengths increased because of the enhancement of soil diffusivity with the rise in temperature. Thirdly, biological uptake ability was also enhanced by the rise in temperature (Fig. 6.1a). The gross CO-uptake strength is more sensitive to changes in temperature than is the CH_4-uptake strength, because the temperature dependence of CO in-situ uptake rates is larger than is the case for CH_4. However, variation in the net global CO uptake was less than was the case for CH_4 because temperature positively affects the CO-production rates in soil. Global CO production (gross uptake - net uptake) increased exponentially with temperature (Fig. 6.12b).

The changes in global CO, H_2, and CH_4 uptake with *SWI* are shown in Fig. 6.13. CO-, H_2-, and CH_4- uptake strengths were positively dependent on *SWI*, which is contrary to the results of Potter et al. (1996a, b), who show a negative dependence of global uptake strength on precipitation. This difference is because of the reduction in size of the area of extreme desert having no uptake of CO, H_2, and CH_4 and the lesser effect of drought on top soil. The mechanisms involved in CO being absorbed only by surface soil and CO uptake being sensitive to drought can be deduced from Fig. 6.12. Note that global CO production (gross uptake - net uptake) decreased as *SWI* increased, reflecting the increase in in-situ

uptake by soil and the decrease in the CO equilibrium concentration.

Under conditions of global warming, it is expected that temperature will increase and that the variation in soil moisture (*SWI*) may be large and the absolute value of *SWI* may be somewhat smaller because of high precipitation and evapotranspiration. Thus, the changes in CO, H_2, and CH_4-uptake strengths resulting from global warming cannot be simply predicted. We must wait for much more progress in GCM. Actually, global uptake strength should change its magnitude year by year with the variation in soil moisture and temperature. Furthermore, human management of the land is an important factor, for instance, in agricultural regions and when land use changes: the tropical forest is a large sink for CO, H_2, and CH_4 due to the high level of bacterial activity. Destruction of the tropical forest lessens the capability of the soil to act as a sink for CO, H_2, and CH_4.

6.5 Summary

This Chapter proposed a process-based model that explicitly incorporates biological uptake processes as well as the physical diffusion process to investigate the characteristics and distribution of the global uptake strengths of CO, H_2, and CH_4 (Yonemura and Yokozawa, 1999). The mechanisms revealed in previous Chapters 4 and 5 are incorporated into the model.

The model consists of a biological part, given as functions of soil temperature and moisture, and a soil physical part, calculating soil diffusivity between the atmosphere and the soil. Calculations were carried out a grid scale of 1.0° latitude by 1.0° longitude. Climatic data and the soil wetness index (*SWI*) from an Atmospheric General Circulation Model with a land-surface process model were used and plausible atmospheric concentrations were assumed. The global uptake strengths of CO, H_2, and CH_4 were estimated to be 110 (88 to 150) , 70, and 20 (14 to 28) Tg yr^{-1}, respectively. The figure for H_2 corresponds to about 75% of the global sink for the gas; the figures for CO and CH_4 correspond to about 5% of the global sink for these gases. The global uptake strengths are at maximum in July and minimum in February. This seasonal pattern is related to the variation in uptake rates in land ecosystems in the northern hemisphere. If the temperature increases by 5°C and the *SWI* increases by 0.05 uniformly around the world, global uptake strengths of CO, H_2, and CH_4 increase by

several percentage points due to the increase in diffusivity and microbial activity, and due to the enlargement of the active uptake area in dry regions.

The difference in H_2 concentrations between the northern and southern hemispheres should be attributable to the uptake by soil because of the large H_2-uptake strength by soil and its seasonality in the northern hemisphere. H_2 uptake by soil is very important to explain H_2 concentrations in the atmosphere.

Table 6.1 CH_4 u_{max} scenarios. The u_{max} was determined from previous core/incubation laboratory studies (Crill, 1991; Adamsen and King, 1993; Whalen and Reeburgh, 1996; Priemé and Christensen, 1997; Priemé et al., 1997).

scenarios	CH_4 u_{max} $10^{-6}s^{-1}$ Arable	Forest soil	Other soils
low-scenario	5	25	100
middle-scenario	20	100	400
high-scenario	80	400	1600

Table 6.2 Data sets used.

Data	Resolution (°)	Reference
Climate data	0.5x0.5	from IPCC
Soil texture	1.0x1.0	Zobler (1986)
Soil organic carbon	1.0x1.0	Potter and Klooster (1997)
Soil Wetness Index	1.0x1.0	CSU-AGCM
Vegetation Cultivation index	1.0x1.0	Mathews (1983)

Table 6.3 Comparison of process model to estimate global uptake strengths of CO and H_2

Items	This study	Potter et al. (1996a, b)
Target gases	CO, H_2, (CH_4) (H_2 was obtained from COv_d)	CO, (CH_4)
Soil moisture	SIB2	Bucket model
Incorporation of biological processes	○ (Temperature and moisture dependence are given by stress factors)	×
CO production in soil	Process-modelled	Not process-modelled
Concentration profile in soil	Exponential	Linear (set constant)
Arid soils	Water stress factors on biological uptake on biological process	Calculated from CO_2 flux
Forest	Correlation with yearly-temperature (based on the presence of dead leaf layer)	Normal model

Table 6.4 Comparison of estimation of CO and H_2 uptake strength by soil

References	Tg yr^{-1}	Features
CO		
Conrad and Seiler (1985a)	170-560	$v_d \times C_{atm} \times$ Land area
Potter et al. (1996a)	7-40	Process model with no biological process
Sanhueza et al. (1998)	85-200	$v_d \times C_{atm} \times$ Land area
This study	90-150	Process model with biological process
H_2		
Seiler and Conrad (1987)	70-110	$v_d \times C_{atm} \times$ Land area
Ehhalt (1999)	10-70	Estimation from H-D ratio
This study	60-80	Process model with relationship to CO

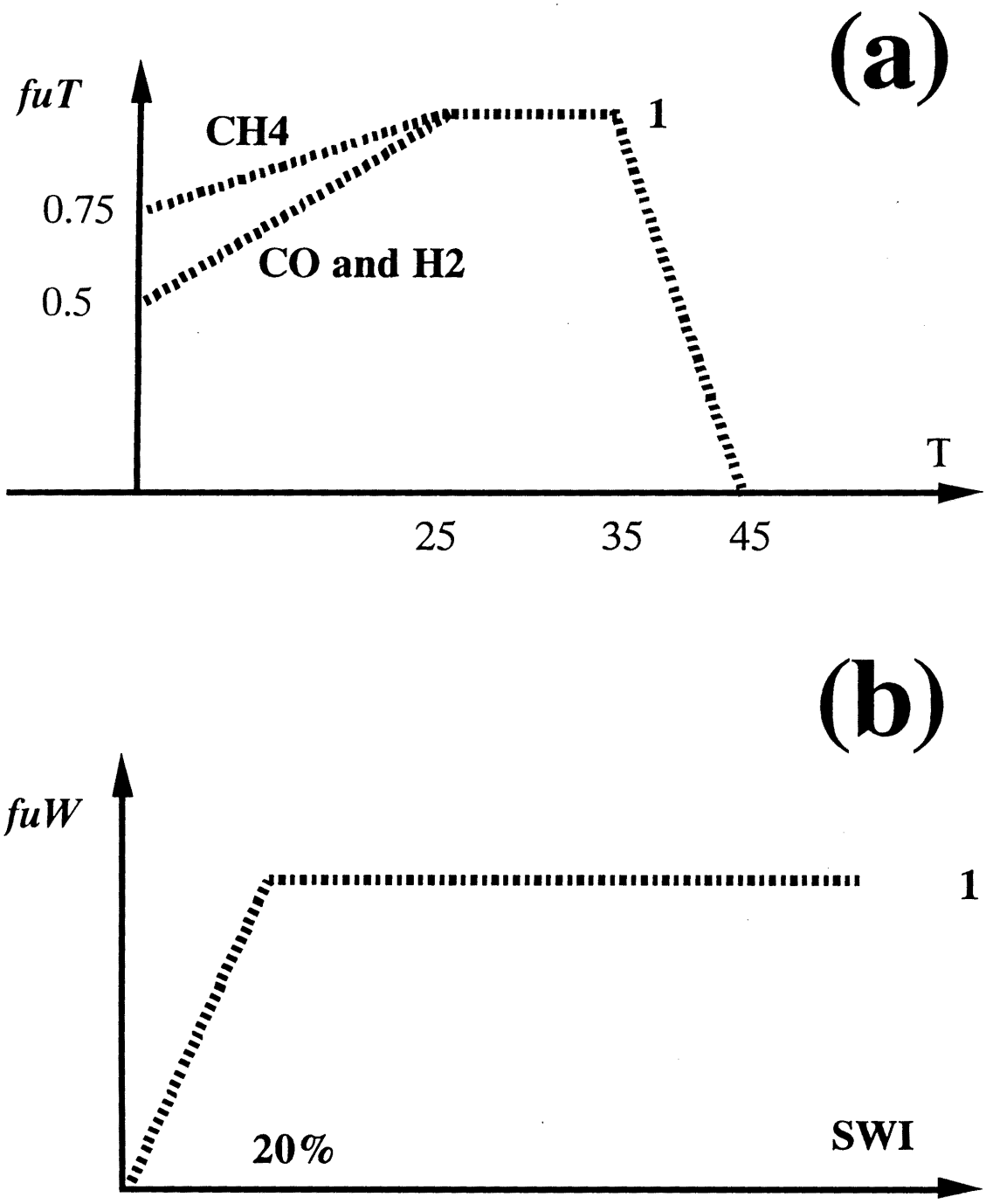

Figure 6.1 Dependence of f_{uT} and f_{uW} on (a) soil temperature and (b) soil moisture, respectively.

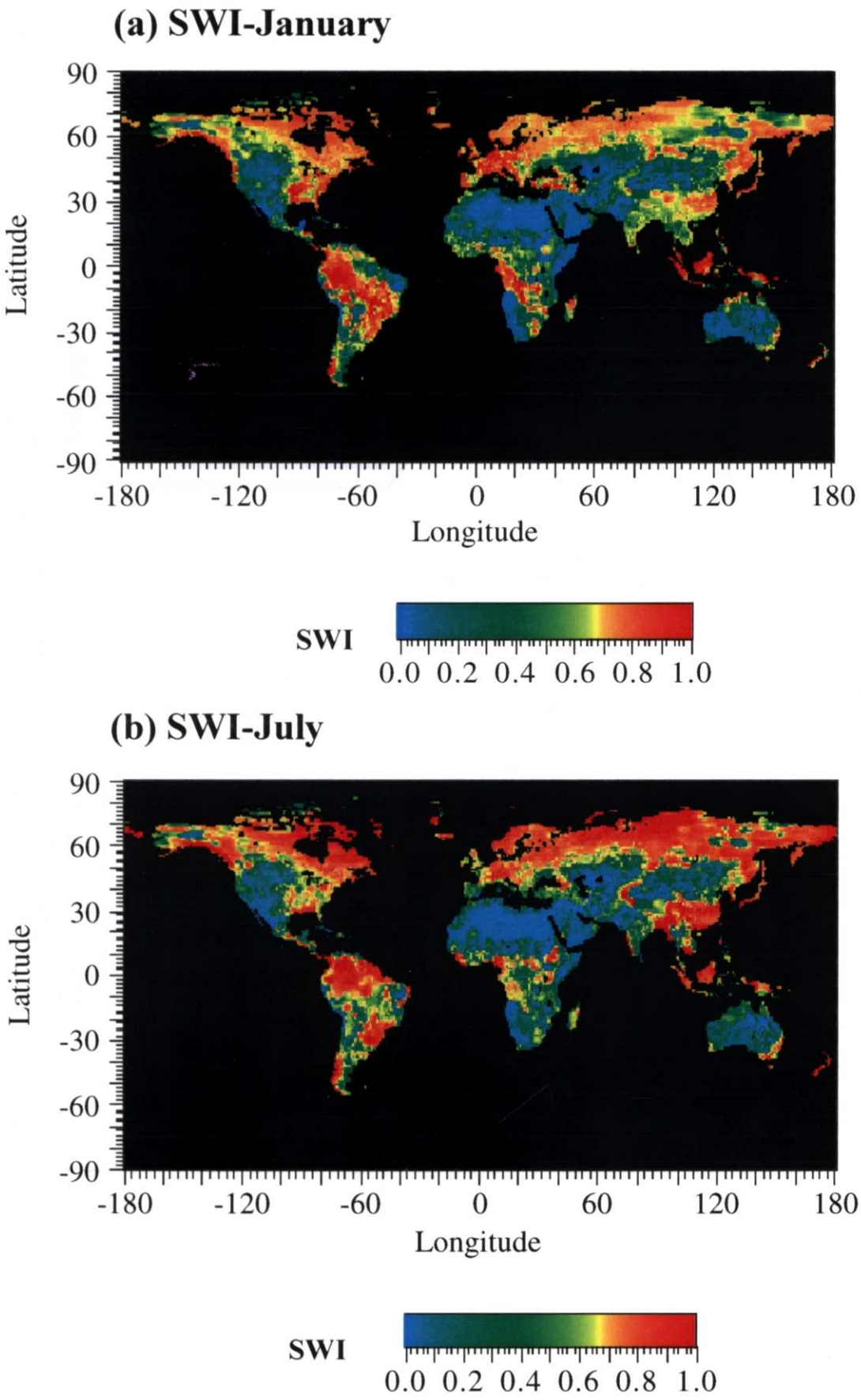

Figure 6.2 SWI (soil wetness index) distribution map in (a) January and (b) July from outputs of the Colorado State University Atmospheric General Circulation Model with the Simple Biosphere Model version 2 land-surface process model.

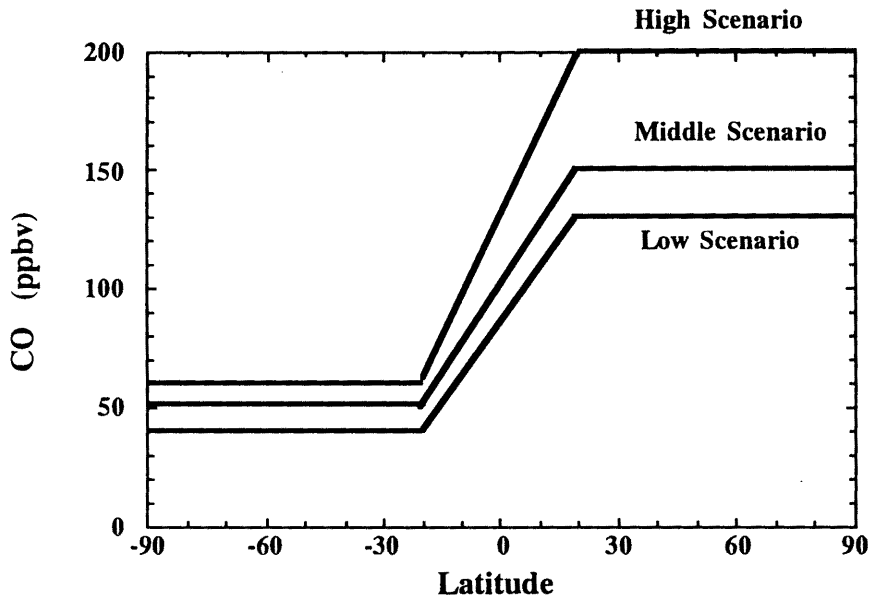

Figure 6.3 Scenarios of atmospheric CO concentrations.

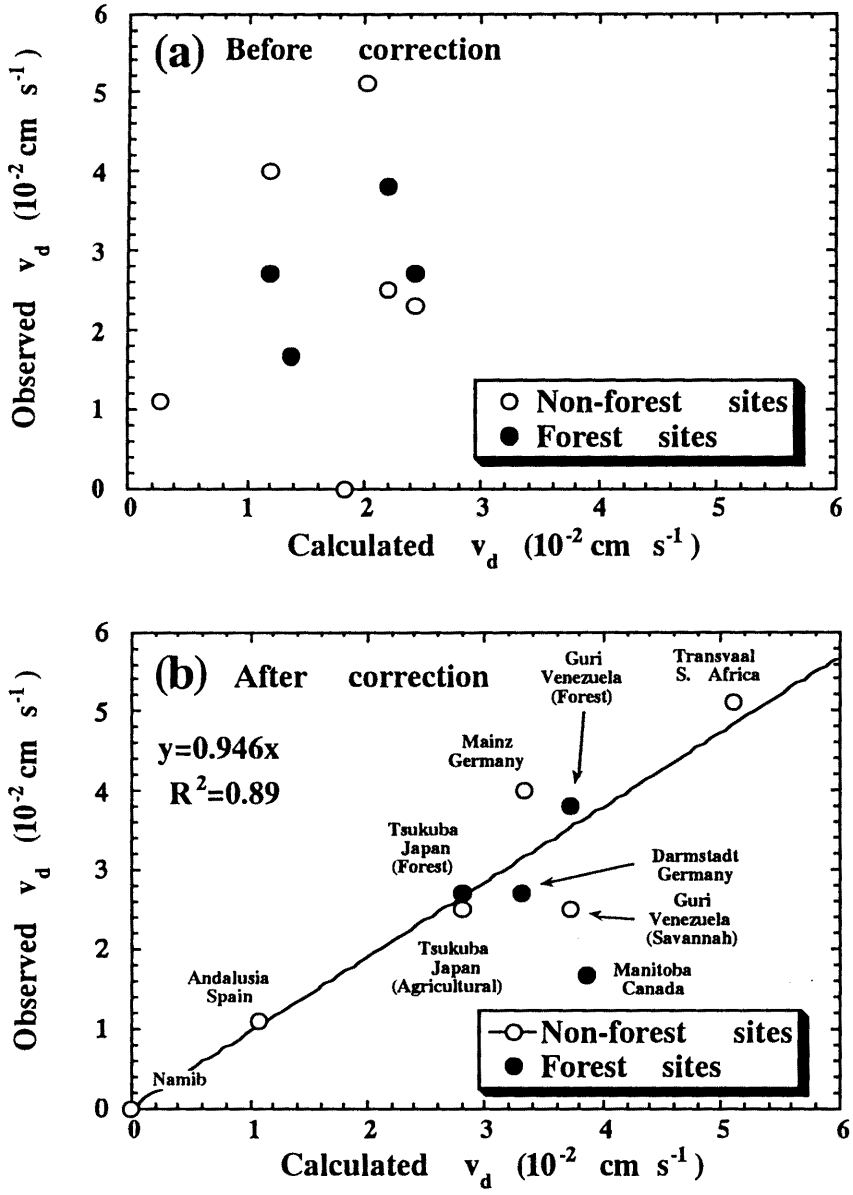

Figure 6.4 Relationship between calculated deposition velocities and observed deposition velocities of selected sites (a) before correction and (b) after correction (eqs. 6.8-6.12).

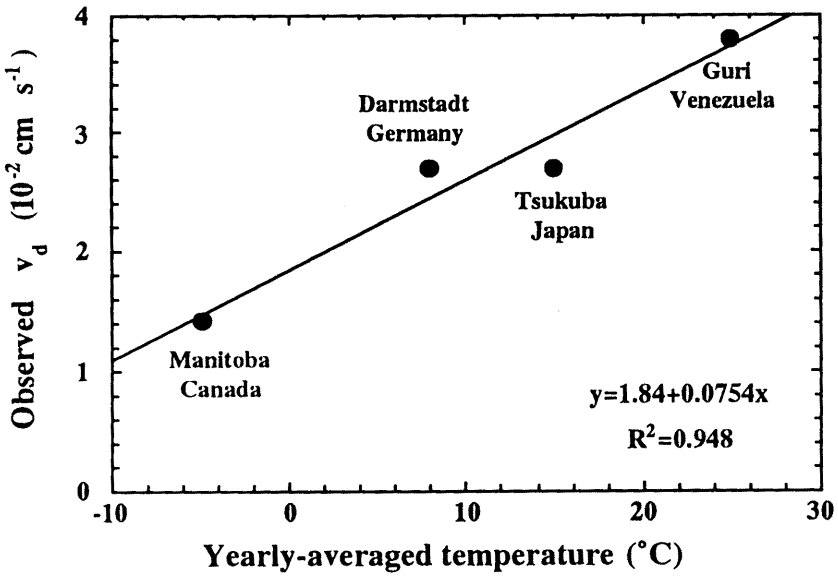

Figure 6.5 Relationship between yearly averaged temperature and observed deposition velocities at forest sites.

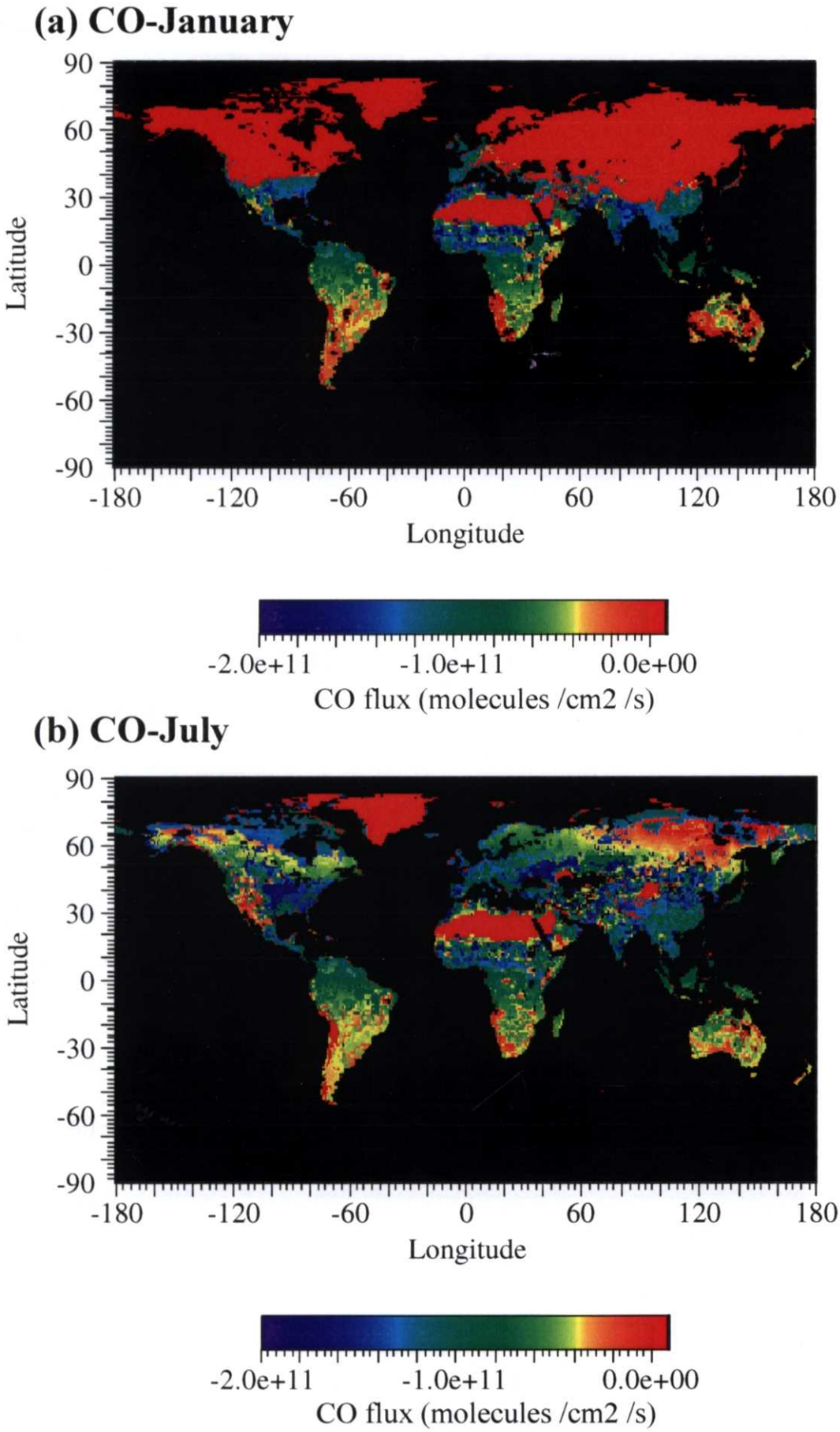

Figure 6.6 Global CO-uptake flux maps in (a) January and (b) July.

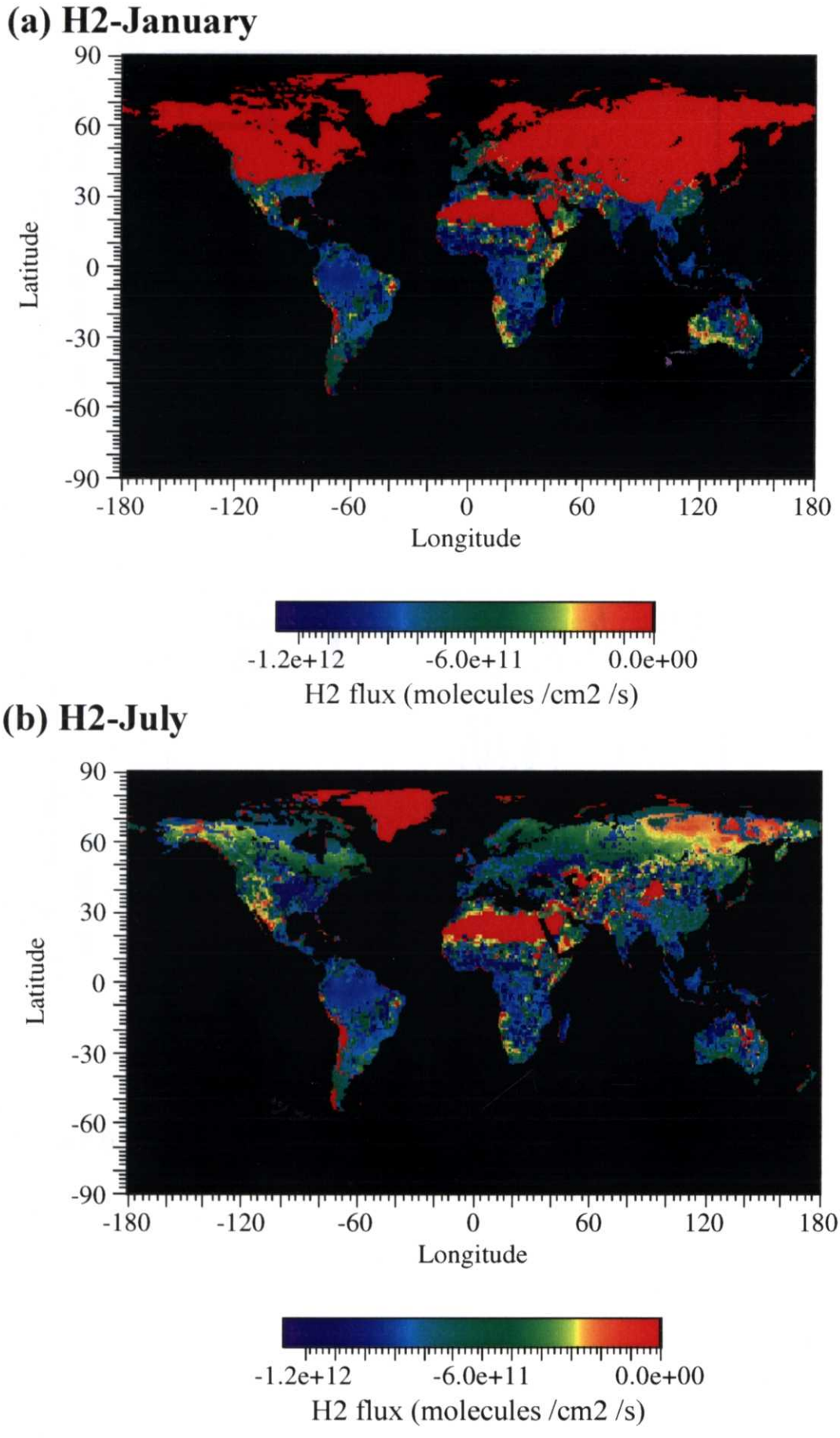

Figure 6.7 Global H_2-uptake flux maps in (a) January and (b) July.

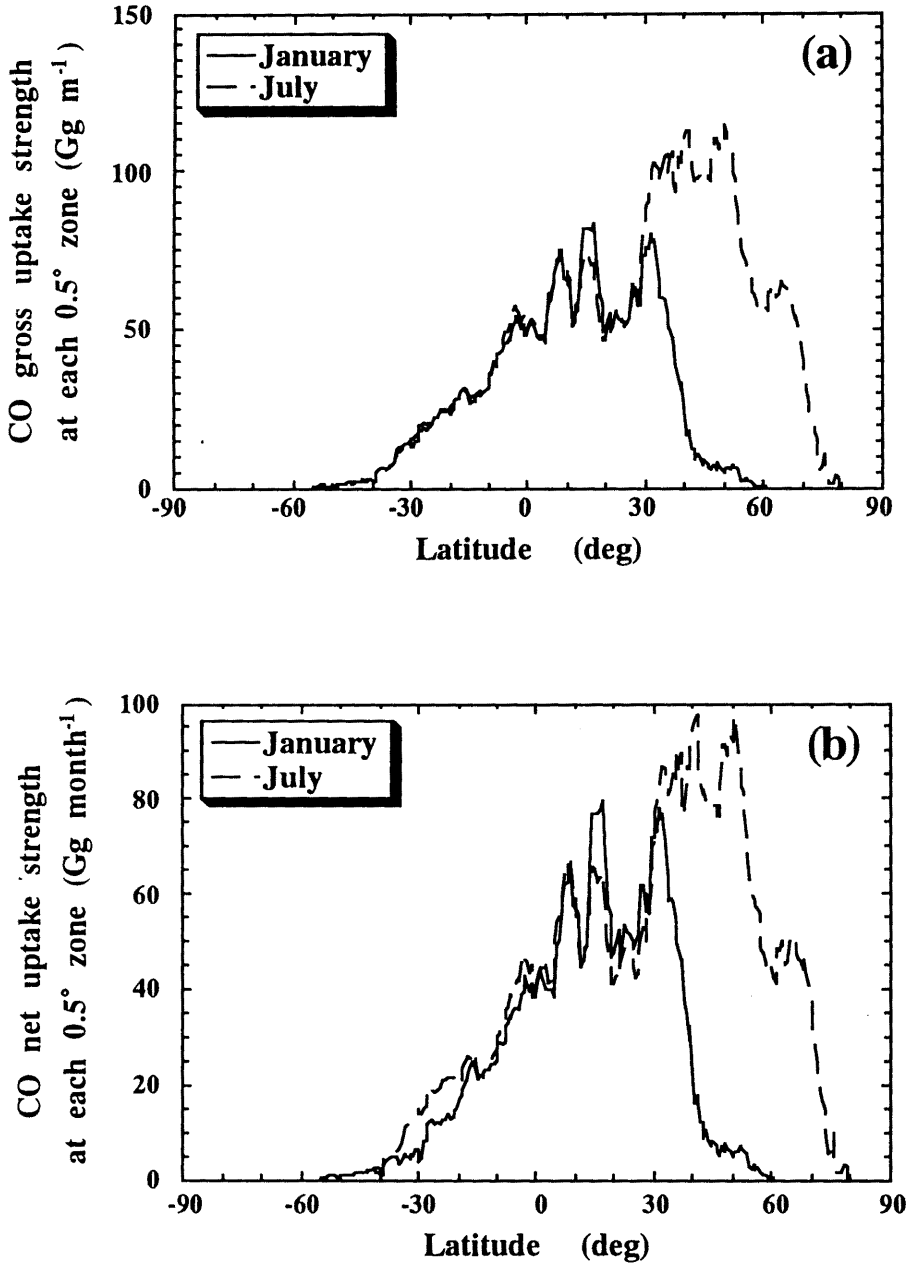

Figure 6.8 continues to next page.

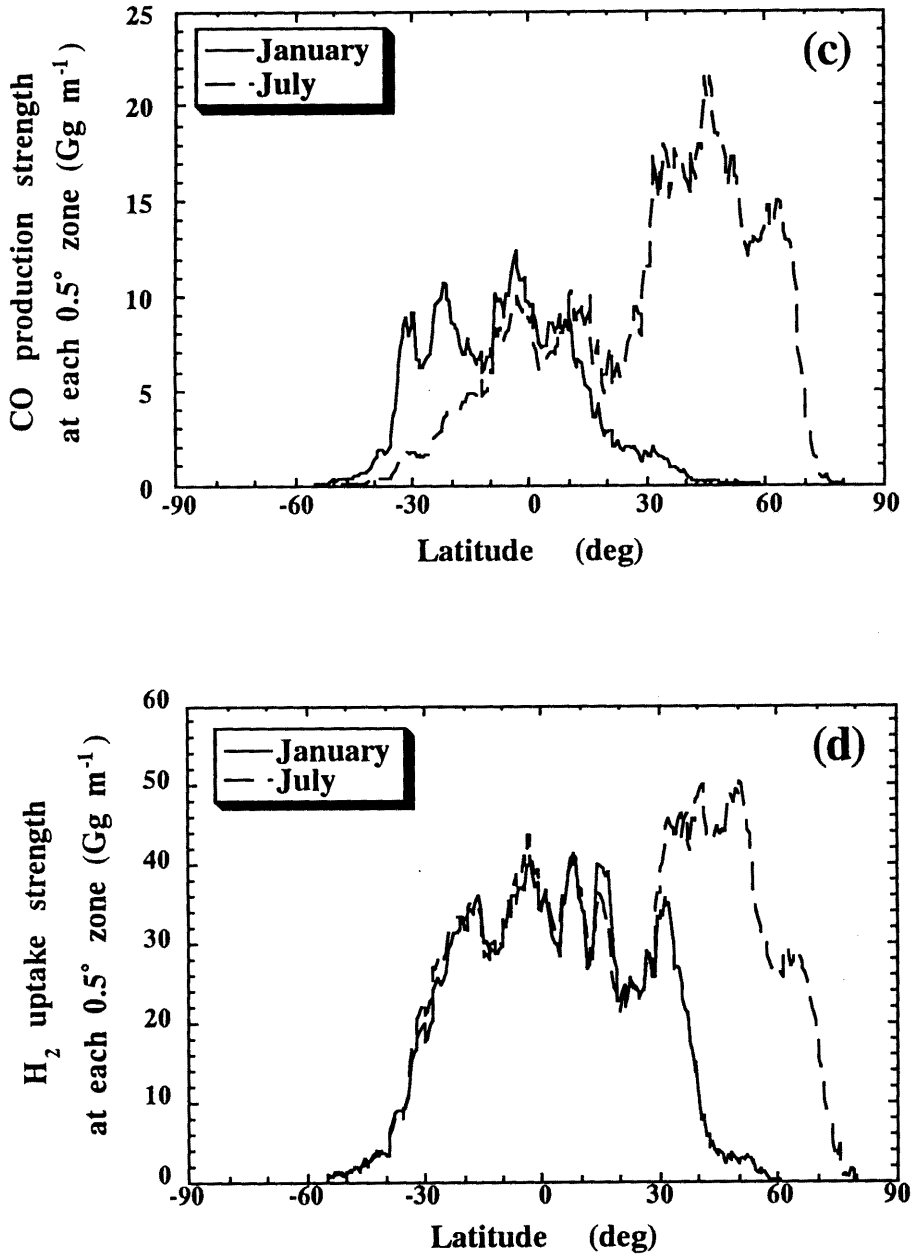

Figure 6.8 Latitudinal distribution of (a) gross CO uptake, (b) net CO uptake, (c) CO production, and (d) H_2 uptake by soils in January and July.

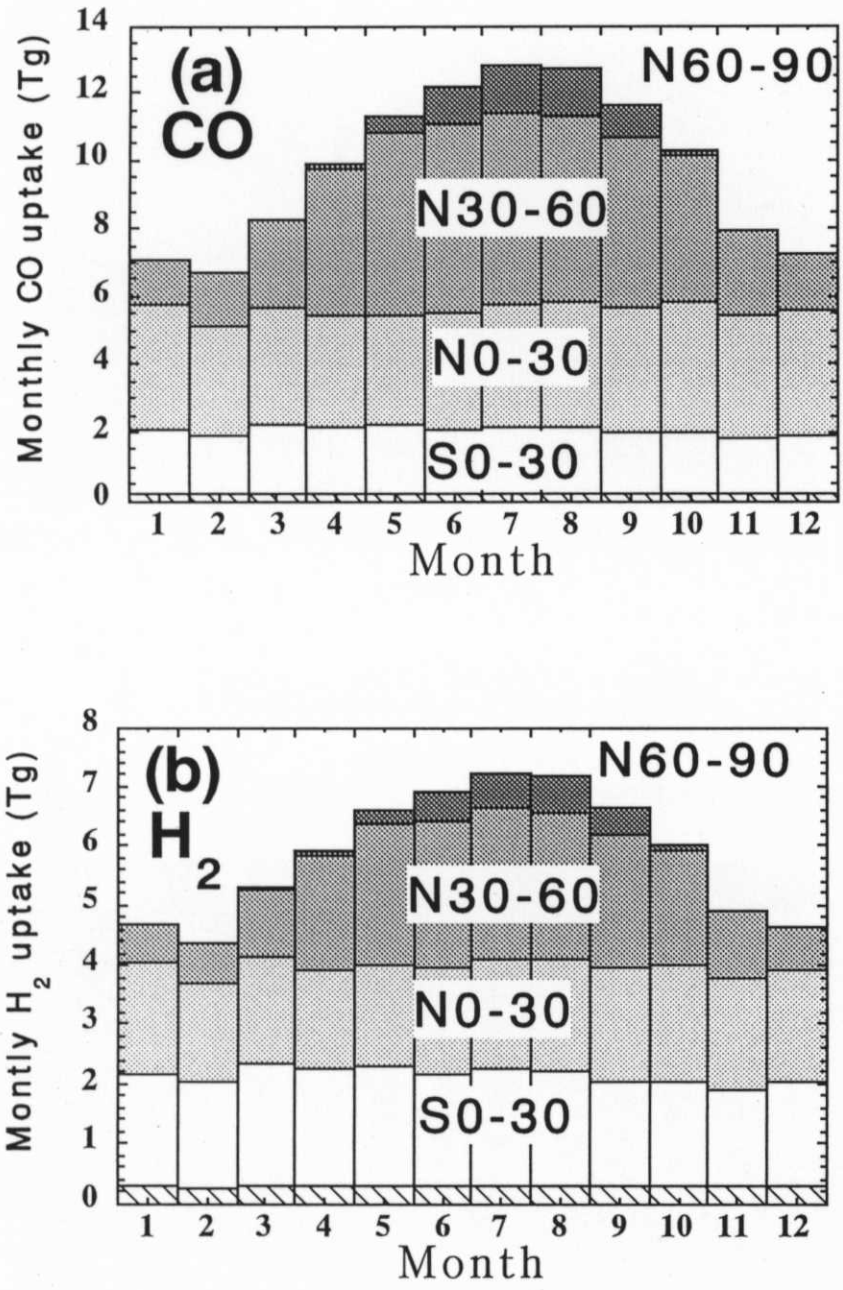

Figure 6.9 Seasonal variation in (a) CO gross uptake and (b) H_2 uptake strengths by soil

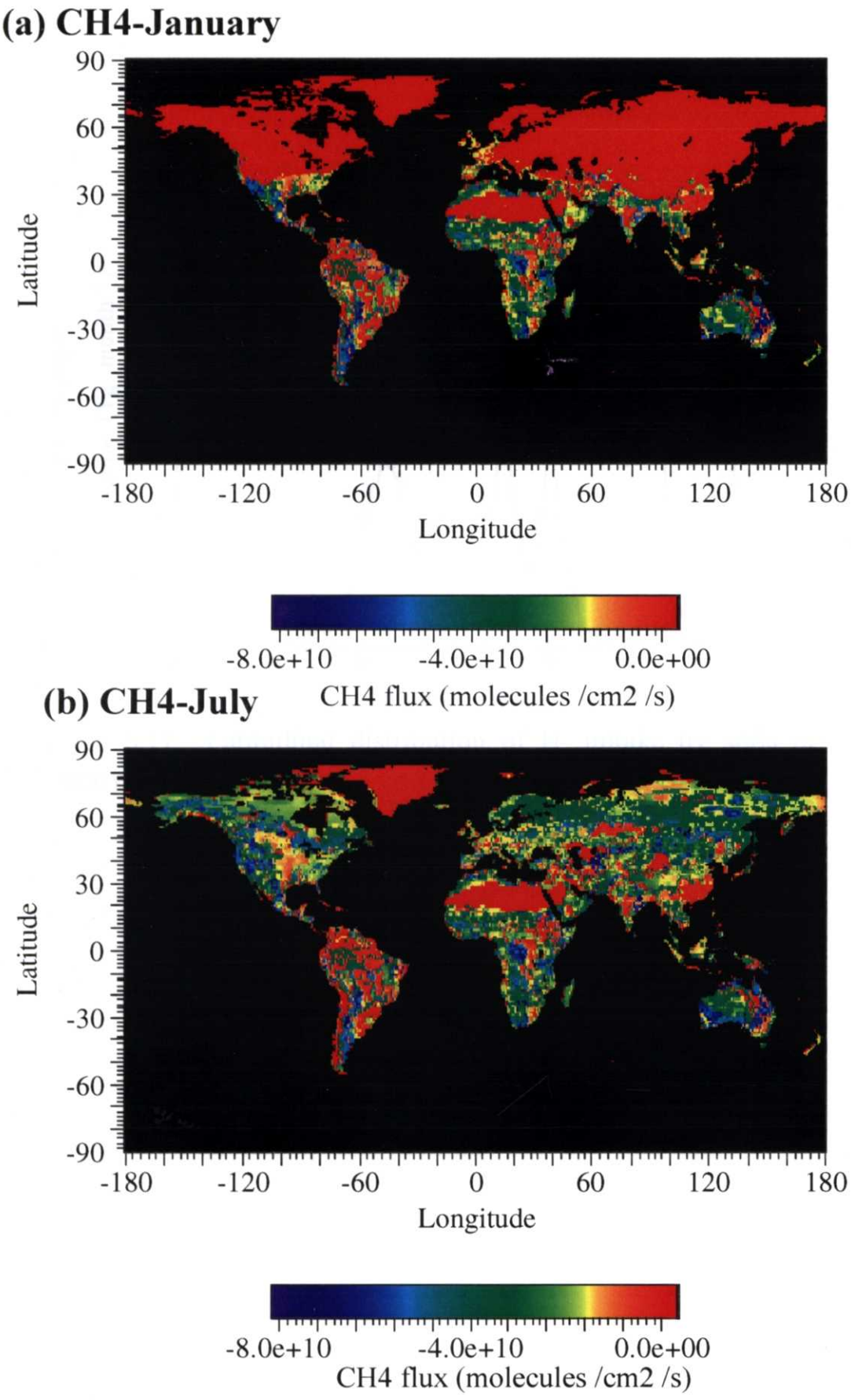

Figure 6.10 Global CH_4-uptake flux map in (a) January and (b) July.8.0×10^{10} molecules cm^{-2} s^{-1} corresponds to about 1.84 mg CH_4 m^{-2} d^{-1}.

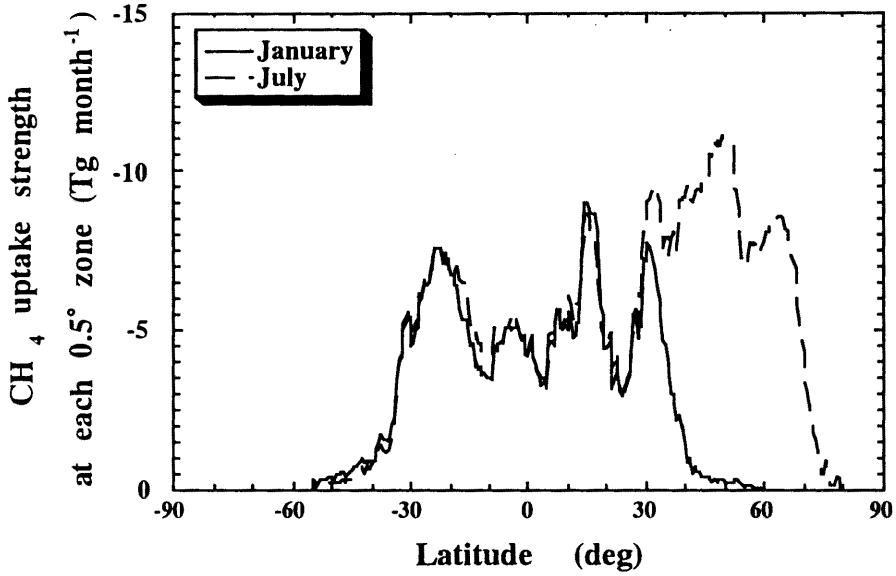

Figure 6.11 Latitudinal distribution of H_2 uptake by soils in January and July.

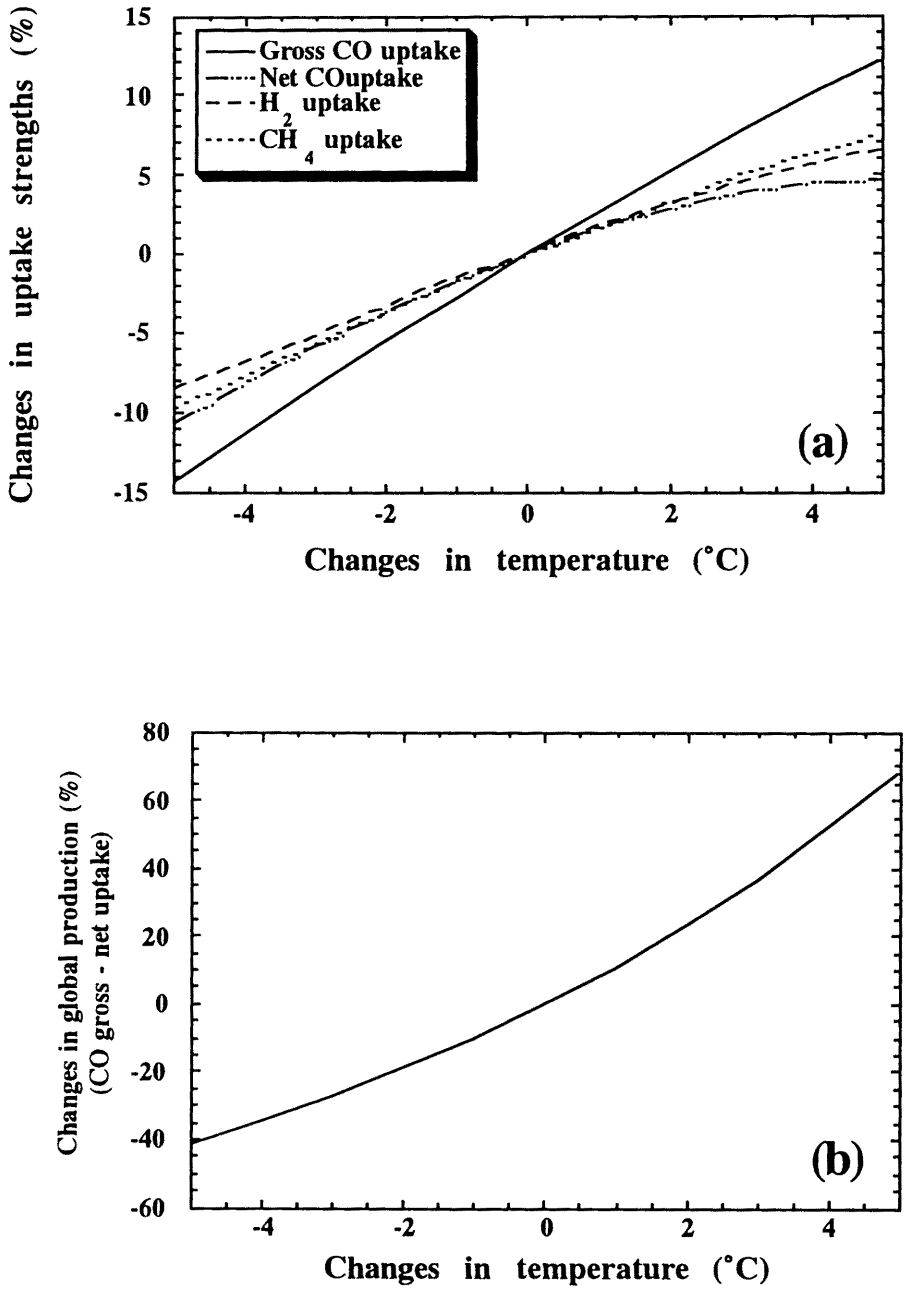

Figure 6.12 Variations in global (a) CH_4 and CO gross and net uptake and (b) CO production with changes with temperature.

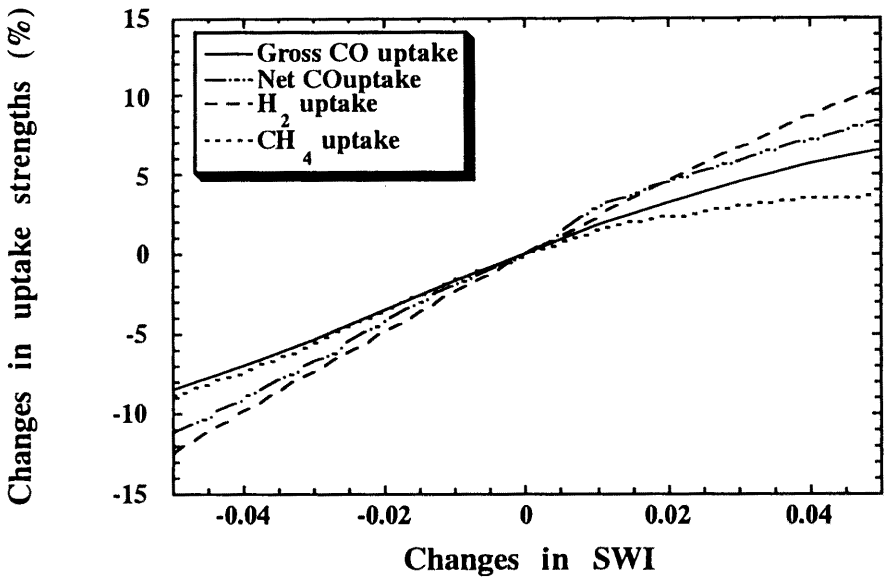

Figure 6.13 Variations in global CH_4 and CO gross and net uptake and CO production with changes in SWI.

Chapter 7

CO emission process from vegetation: CO photoproduction from rice and maize leaves

7.1 Introduction

This Chapter have focused on the photoproduction of CO by rice and maize as representatives of the *Gramineae* that includes major crops and occupies plant species grown in grass lands (Yonemura et al., 1999a). Rice and maize were selected because both crops belong to the *Gramineae*, and because rice is a C_3 grass and maize is a C_4 grass and they might therefore show large mechanistic differences in CO photoproduction. Lüttge and Fischer (1980) reported a difference in CO photoproduction between C_3 and C_4 plants and attributed it to the metabolism of photorespiration.

7.2 Material and methods

Rice (*Oryza sativa L.*, cv. "Nipponbare") seedlings were transported to 1/5000a Wagner pots™ in the middle of May and were grown the pots in the field. Leaf samples were taken the day before ear emergence at the beginning of August. Dead leaves used had no green or yellow parts and were taken from live plants just before measurement.

Maize (*Zea mays L.*, cv. "Petercorn") was sown in the field in May. Whole plants were carefully lifted with soil not to give damage to the plant body just before ear or tassel emergence and brought to the laboratory within 5 days of lifting.

The experimental setup is shown in Fig. 7.1 and Photo 7.1. Synthetic air mixed with CO_2, N_2, O_2, or indoor air was introduced into a platinum-catalytic CO combustion purifier where any CO was reduced to a concentration of < 1 ppbv. The air was introduced into a Pyrex® glass chamber of internal volume of approximately 750 cm^3. The removable top plate was made of quartz. The gaskets between glass and leaves were made of Viton®. To avoid extraneous CO photoproduction from the gaskets, the top part of the chamber above the

gaskets was covered with aluminum foil.

Live leaves were placed in the middle of the chamber, intact on the plant body. The leaves were carefully placed to avoid damage and arranged so as not to overlap. On average, a dozen rice leaves or several maize leaves were used.

Dead rice leaves were removed just before measurement. Dead rice leaves were placed on the bottom of the chamber, stretched out to absorb all the incident light in the chamber.

The flow rate of the introduced air was set to either 500 or 1000 $cm^3\ min^{-1}$ with a mass flow controller. A water trap loop was connected to the chamber to protect the chamber from water vapor. The trap loop flow rate was set to 500–2500 $cm^3\ min^{-1}$.

Metal halide positive glow lamps (D400; Toshiba Lighting and Technology Corporation, Tokyo, Japan) were used as a light source because their visible spectrum is similar to that of sunlight. A water filter was placed between the lights and the chamber to protect the leaves from the heat. The light intensity was controlled by piling up cheesecloths under the water filter and measured by a pyranometer (Eiko Instruments Co., Ltd., Tokyo, Japan). The light distribution in the chamber was measured by small sensors (G1118; Hamamatsu Photonics, Hamamatsu, Japan), sensitive to photosynthetically active radiation. From these measurements, the strength of the incident light on the leaves was calculated. The temperature of the chamber air was measured by thermocouple (Copper-Constantan) thermometers. Light strength and temperatures were recorded automatically by a hybrid recorder on a PC.

Sample gases that entered and exited the chamber were introduced into the gas analyzer through Teflon® tubes (< 1 m long). The CO emission from the chamber (F_c, molecules s^{-1}) was calculated from the difference in concentration entering (C_{in}, ppbv) and exiting (C_{out}, ppbv) the chamber with eq. (7.1):

$$F = \rho f(C_{out} - C_{in}) \tag{7.1}$$

where ρ is the volumetric number density (molecules cm^{-3}) and f is the gas flow rate ($cm^3\ s^{-1}$). F_c was converted to flux (F_l, molecules $cm^{-2}\ s^{-1}$) per leaf area (L_A, cm^2) perpendicular to the light direction with eq. (7.2):

$$F = \frac{F_{\cdot}}{L_{\cdot}} \qquad (7.2)$$

7.3 Results and discussion

The average CO photoproduction was 2.6 ± 0.3 × 10^{10} molecules cm^{-2} s^{-1} from live rice leaves and 2.2 ± 0.1 × 10^{10} molecules cm^{-2} s^{-1} from live maize leaves (n = 5) at a radiation intensity of 49 mW cm^{-2} (errors are standard deviation). The difference is not striking. These values are reasonably similar to those from other plants (Seiler et al., 1978; Tarr et al., 1995). CO photoproduction from dead rice leaves was 25.7 ± 1.5 × 10^{10} molecules cm^{-2} s^{-1} (n = 2), 9 times the rate from live leaves. The emission of CO from dead leaves supports the hypothesis that CO is emitted as a product of photodegradation of plant cellular material. Live leaves may use protective mechanisms to prevent photooxidative damage (Batschauer, 1993; Nouchi and Kobayashi, 1995).

For both live and dead leaves, CO emission increased almost linearly with increasing light intensity (Fig. 7.2). This linearity is consistent with the results for the leaves of 3 trees and a bean (Seiler et al., 1978) and of cell suspension samples of phototrophic bacteria (Bauer et al., 1980). Dead leaves needed much more time (> 1 h) for the emission value to equilibrate than live leaves. This could be due to heating of the leaf after absorption of visible and UV radiation. Dead leaves emitted CO even without irradiation. This abiological CO production is discussed by Conrad and Seiler (1985b).

CO_2 concentration was controlled (Fig. 7.3) at values ranging from the CO_2 compensation point, which is about 60 parts per million by volume (ppmv) for rice and 10 ppmv for maize, to > 1400 ppmv. No clear dependence on CO_2 concentration was found for CO photoproduction. This result supports the results of Seiler et al. (1978) and Tarr et al. (1995) but not those of Lütte and Fischer (1980), who related CO photoproduction to carbon metabolism by photorespiration, which is different in C_3 and C_4 plants. It can be concluded that photorespiration

had no direct relationship to CO photoproduction in rice and maize.

In contrast to CO_2 concentration, O_2 concentration had a positive influence on CO photoproduction by live leaves (Fig. 7.4). Figure 7.4 shows that most CO photoproduction is from reactions connected with O_2. CO photoproduction from live leaves showed a fast response (several minutes) to changes in ambient O_2 concentration (Fig. 7.5a). However, dead leaves needed much more time (several hours) to respond to changes in O_2 concentration (Fig. 7.5b). This suggests that O_2 must penetrate to isolated sites or that precursors must be formed before CO is produced.

Tarr et al. (1995) reported that CO was emitted from leaves through their stomata, based on experiments comparing CO emissions from the top and bottom of leaves. The conductance of stomata might have some influence on CO efflux.

In gas diffusion from a leaf, cell walls, intercellular spaces, and stomata are in a row; stomata and are parallel. Gas conductances from intercellular spaces and cell walls are far larger (about 10 times) than stomatal conductance (Jones, 1992); stomatal conductance is at least several times larger than cuticular conductance. These facts show that stomatal conductance is a major controlling factor for gas diffusion from leaves.

Generally, humidity and CO_2 concentration have a large influence on stomatal conductance in rice and maize leaves (Morison and Gifford, 1983). By changing the loop speed of the water trap (Fig. 7.1), the present study controlled the humidity in the chamber. According to Morison and Gifford (1983) and Fig. 7.6, the treatments of humidity lead to a several times control of stomatal conductance for rice leaves. As shown in Fig. 7.6, there was no relation between the difference in leaf-air vapor pressure and CO efflux. At concentrations of CO_2 below ambient, stomata of rice and maize leaves tend to open under irradiation (Morison and Gifford, 1983). However, no clear influence of CO_2 concentration on CO photoproduction was found (Fig. 7.3). The lack of dependence of CO photoproduction on humidity and CO_2 concentration leads to the conclusion that stomatal conductance does not directly control CO efflux from leaves. CO photoproduction by rice and maize leaves is directly proportional to light intensity with no apparent influence of stomatal conductance. This is consistent with results for other plant materials (Troxler and Dokos, 1973; Bauer et al., 1980; Tarr et al., 1995). This does not deny, however, that the transport of gaseous oxygen has importance for dead leaves, because a long response time was needed for dead

leaves when the oxygen concentration was changed (Fig. 7.5).

7.4 Summary

In this Chapter, in order to understand CO emission from vegetation (plants), CO photoproduction from intact leaves of rice (*Oryza sativa L.*) and maize (*Zea mays L.*) under radiation was investigated by laboratory experiments. CO photoproduction rate showed positive correlation with light intensity and oxygen concentration. The average CO photoproduction rate from rice leaves was $2.6 \pm 0.3 \times 10^{10}$ molecules $cm^2 s^{-1}$ from rice leaves and that from maize leaves was $2.2 \pm 0.1 \times 10^{10}$ molecules $cm^{-2} s^{-1}$ at a radiation intensity of 49 mW cm^{-2}. The CO photoproduction rate from senescent rice leaves was 9 times greater ($25.7 \pm 1.5 \times 10^{10}$ molecules $cm^2 s^{-1}$) at the same radiation intensity than from live leaves, and responded slowly to changes in oxygen concentration and light intensity. This reassured the previous result (Tarr et al., 1995) that the CO photoproduction from senescent leaves which is much larger (~ 10 times) than that from live leaves.

The results that CO photoproduction showed no correlation with CO_2 concentration or humidity, indicate that CO photoproduction in leaves is not directly controlled by carbon metabolism or stomatal conductance. The lack of dependence on stomatal conductance leads to the conclusion that the diffusion of CO from inside the leaves to the atmosphere is not a controlling factor for CO photoproduction from rice and maize leaves.

CO emission is linearly dependent on radiation and is not controlled by physiological parameters as stomatal conductance. This means that global uptake strengths of CO emission from plants can be easily estimated apart from biological processes. Previous studies (Seiler and Conrad, 1987; Khalil and Rasmussen, 1990a) estimated that direct CO emission from living plants have been estimated to range from 50 to 200 Tg yr^{-1}. This estimation should be enhanced by incorporating CO emission from dead plant matters. To estimate CO emission from dead plant matters need exposure of dead plant matter under solar irradiation. Tarr et al. (1995) estimated global CO emission from dead plant matters to be 60-90 Tg yr^{-1}.

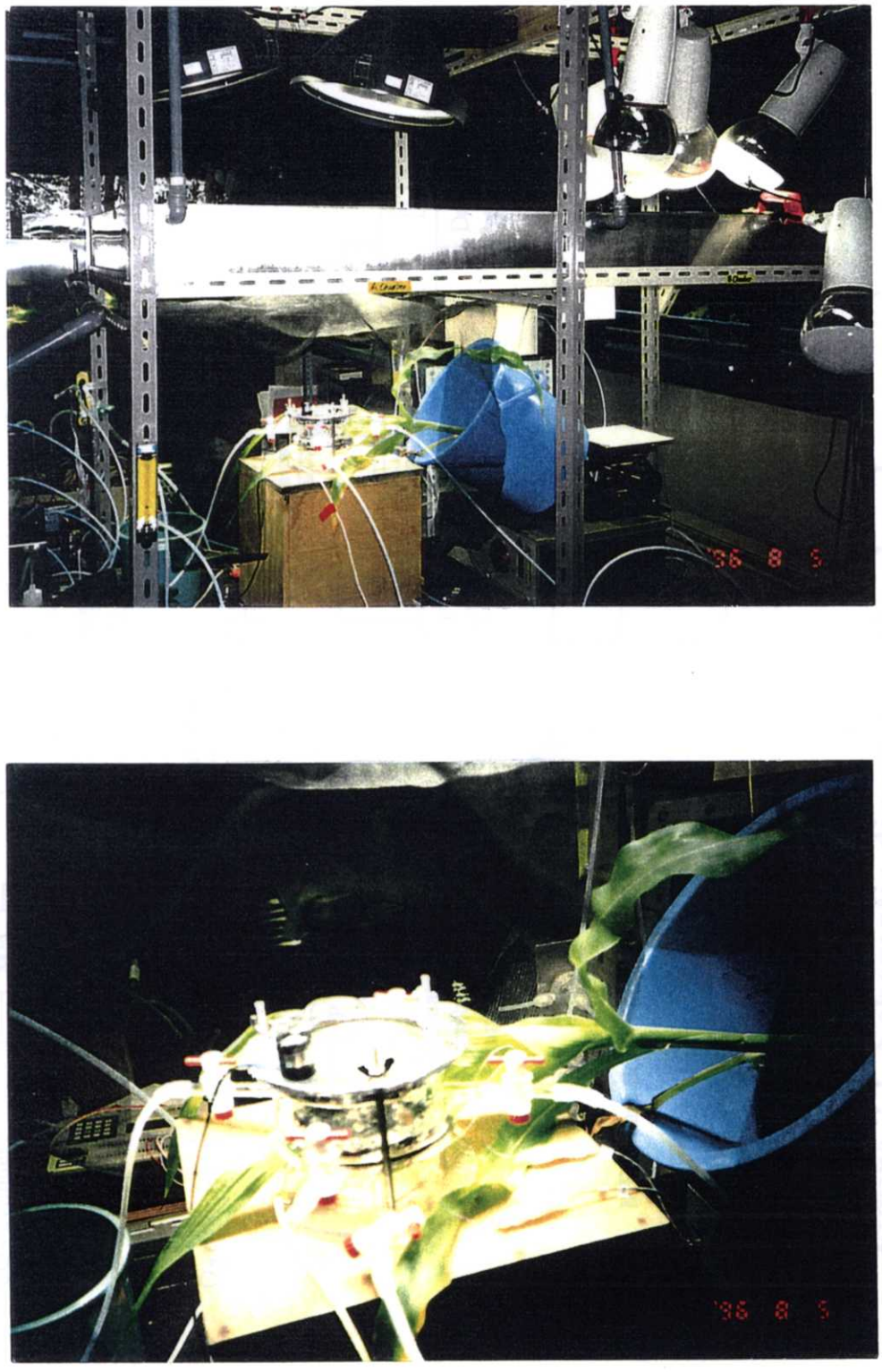

Photo 7.1 Chamber experiments for plants in laboratory.

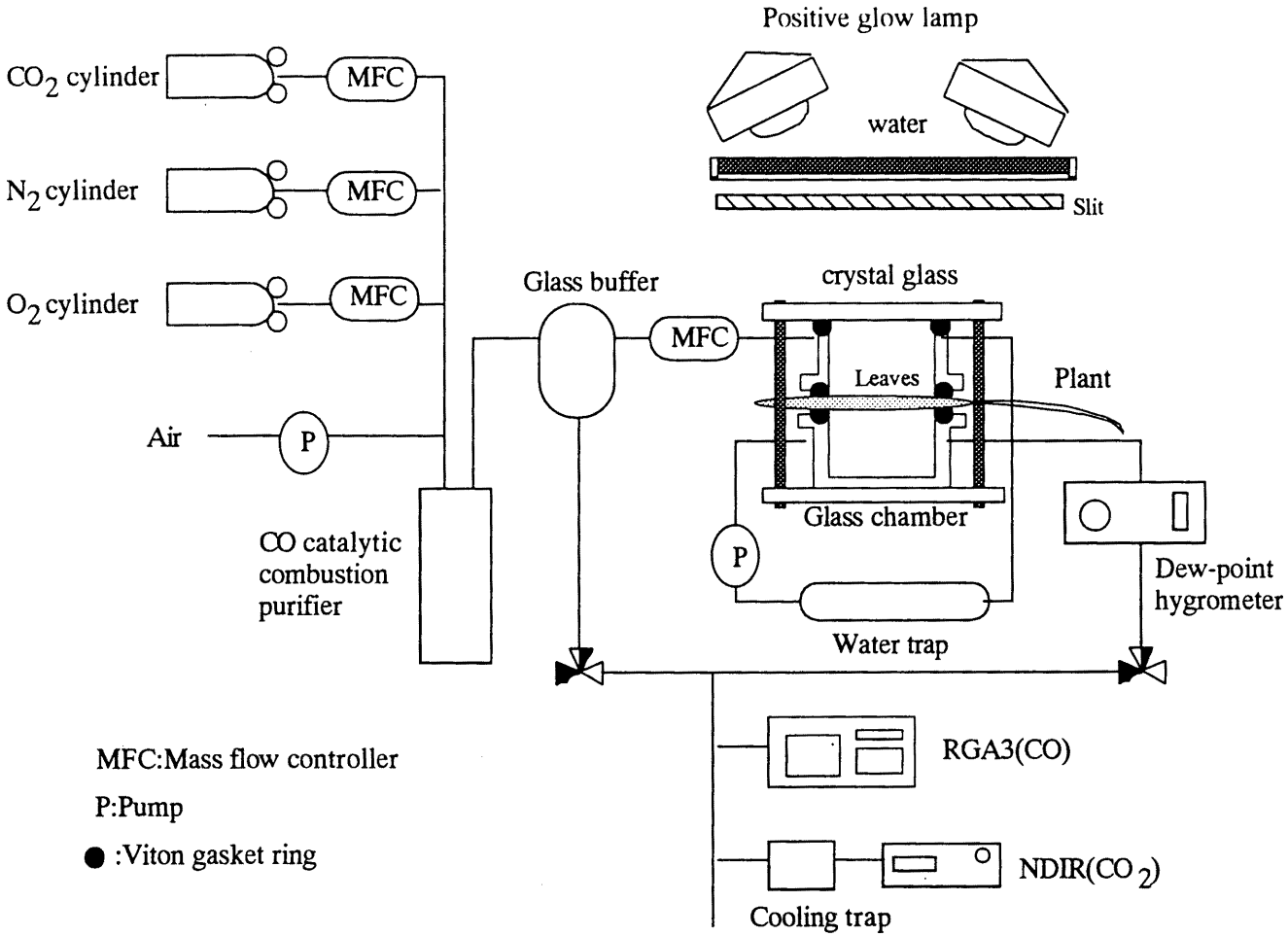

Figure 7.1 Schematic diagram of the chamber experiment system.

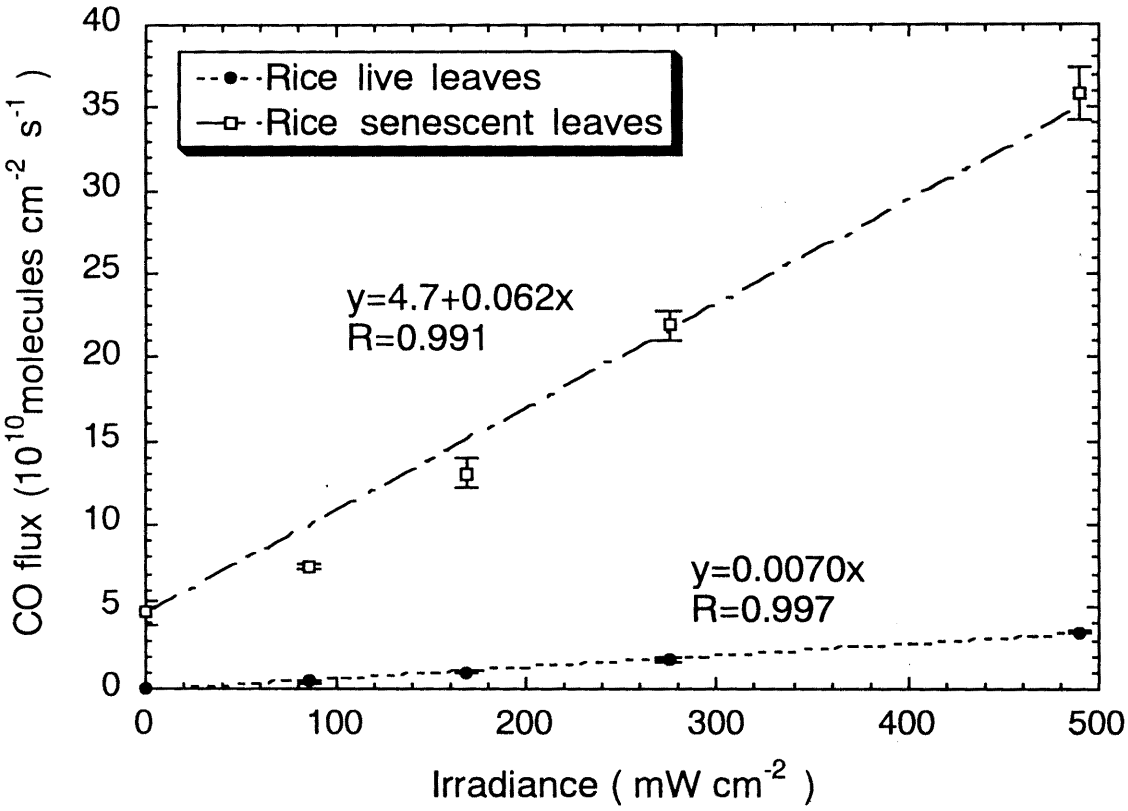

Figure 7.2 Dependence of CO emission on light intensity in live and dead rice leaves. CO flux is expressed as molecules per leaf area perpendicular to light direction per second; light intensity is expressed as irradiance. Error bars are standard deviations of measurements.

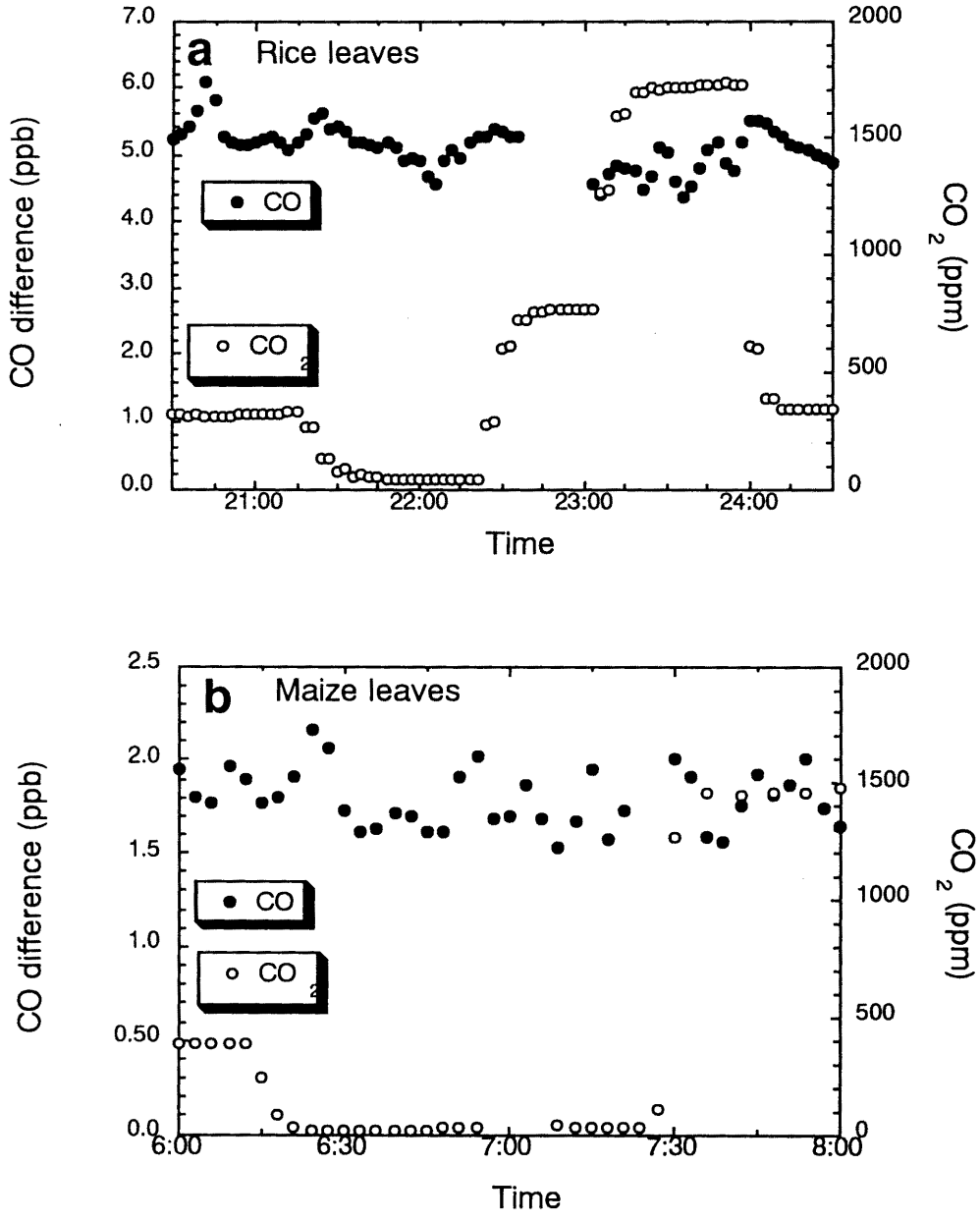

Figure 7.3 Response of CO concentration difference to changes in CO_2 concentration for (a) rice leaves and (b) maize leaves. The air temperature in the chamber was 29°-33°C.

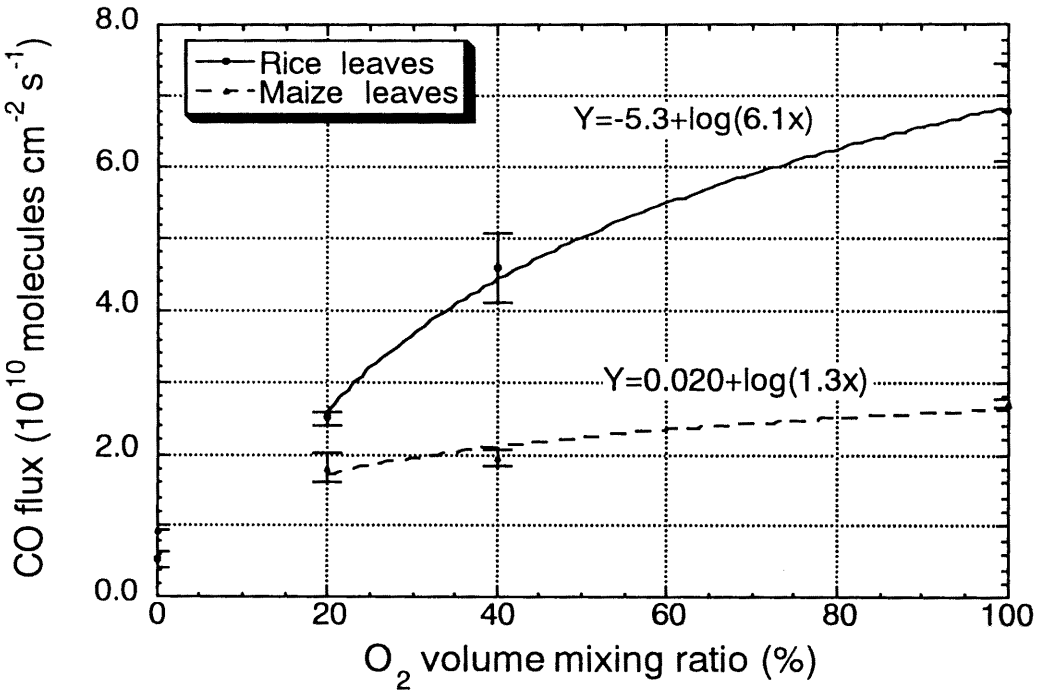

Figure 7.4 Dependence of CO photoproduction on oxygen concentration by live rice and maize leaves. The light intensity was 38.8 mW cm^{-2}. Error bars are standard deviations of measurements.

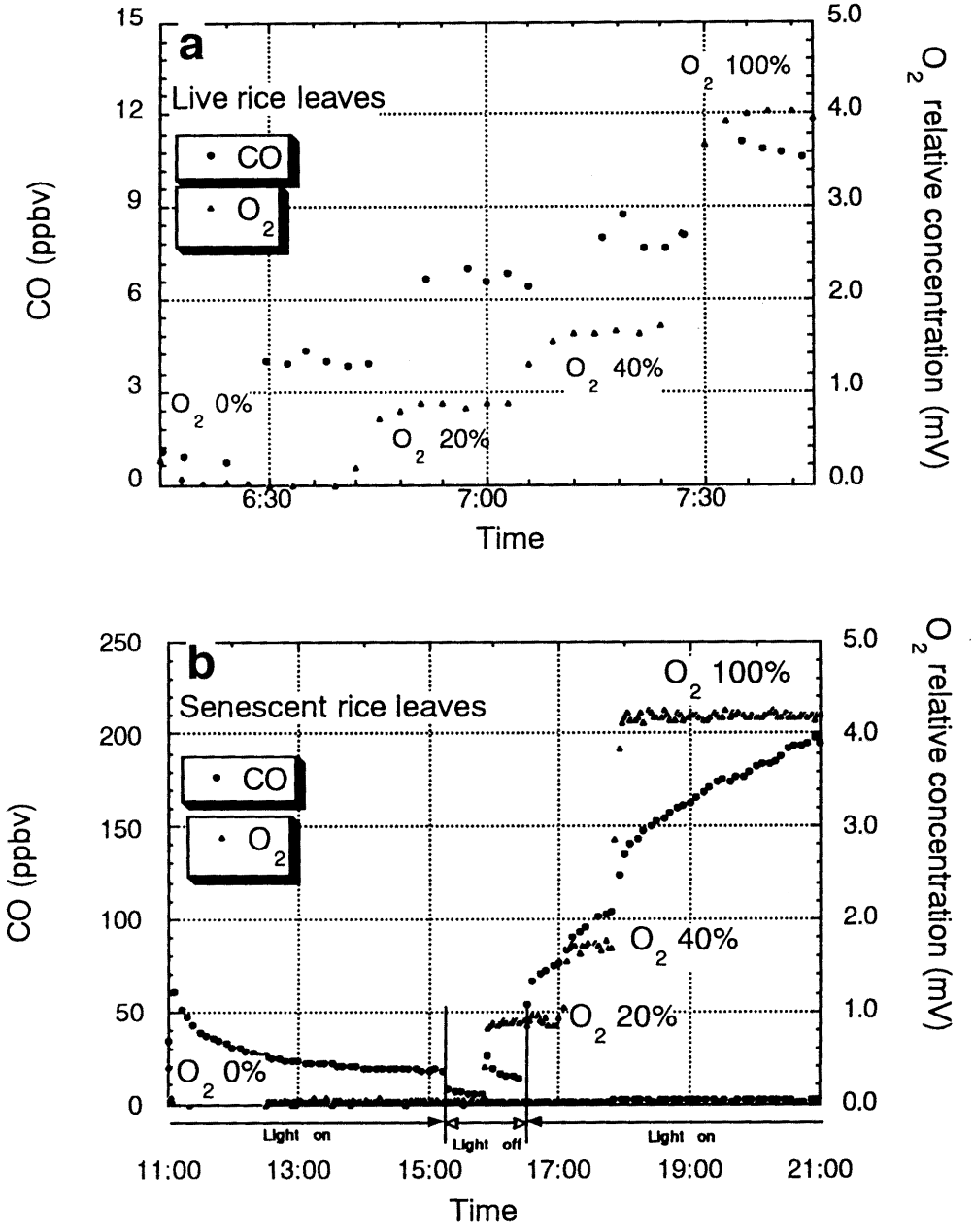

Figure 7.5 Response of CO photoproduction to changes in O_2 concentration for (a) live rice leaves at a light intensity of 42.5 mW cm^{-2} and leaf area of 59.5 cm^2 (0.26 g); and (b) dead rice leaves at a light intensity of 51 mW cm^{-2} and leaf area of 70.8 cm^2 (3.3 g). In (a) the light was always on; in (b) the light was on or off as shown under the X-axis. The flow rate was 1000 cm^3 min^{-1}. The CO concentration is that exiting the chamber and is interpreted to be approximately proportional to CO efflux.

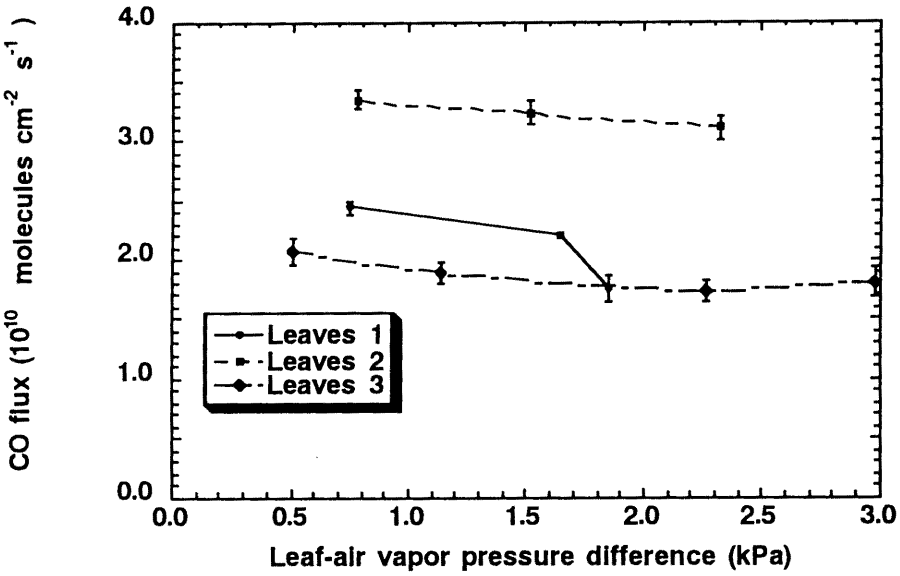

Figure 7.6 The relationship between relative humidity and CO photoproduction rate for 3 live rice leaves. The light intensity was 49 mW cm^{-2}. Error bars are standard deviations of measurements. The difference in leaf-air vapor pressure was calculated from the dew point and the chamber air temperature on the assumption that the leaf temperature was 2°C higher than the chamber air temperature.

Chapter 8

Production of CO and other gases during combustion processes : Mechanism of carbon monoxide, carbon dioxide and light hydrocarbon emissions from the combustion of plant material

8.1 Introduction

Large amount of CO are emitted from combustion processes such as technological sources and biomass burning to the atmosphere (Table 1.1). In this Chapter, the emissions of CO as well as CO_2 and light hydrocarbons from dead plant material, were investigated by combustion experiments using a furnace and a closed-chamber (Sudo et al., 2000; Yonemura et al., 2000e). Experiments were done in view of oxidation process from organic matter, hydrocarbons to CO_2 via CO. First, the gas emissions were analyzed and correlated. Second, time-series of concentrations of these gases were investigated and compared with previous results. The total emission ratios, estimated by the closed-chamber experiments, were then estimated from the time-series of gas concentrations.

Until now, several studies on gas emission from biomass burning have been conducted using airborne sampling (e.g., Laursen et al., 1992; Blake et al., 1996). However, mechanical studies in the field or in the laboratory incorporating combustion processes are relatively limited (Lobert et al., 1991). The composition of air in the atmosphere is gradually transformed by chemical reactions of gases after they are emitted from ground sources into the atmosphere. Hence, direct investigations of the composition of air immediately after combustion are essential for understanding the impact of biomass burning on atmospheric chemistry.

8.2 Materials and methods

Fuel sample materials used for the combustion experiments were dead weeds mainly *Imperata* grass which belongs to *Gramineae*. The sample also contained other weeds most of which also belonged to *Gramineae*, roots with small amounts of soil and some deciduous leaves. The samples were taken from the agricultural fields of the National Institute of Agro-Environmental Sciences during weeding in spring 1998, and were stored in a chamber until winter 1999, when this experiments were carried out. The carbon-nitrogen contents of the fuel samples are given in Table 8.1.

8.2.1 Closed-chamber experiments

The closed-chamber technique was applied to estimate the emission ratio of gases (Fig. 8.1, Photo 8.1). Combustion tests were carried out in a cube-shaped chamber of stainless steel and glass, with inner volume of 4.56 m^3. The combustion process could be observed through the glass wall. The chamber was closed during the experiments.

In the chamber, a commercial combustion furnace of stainless steel, 45 cm high and 35 cm in diameter, in the top of which was a 45-cm stack, was installed. During combustion, air was drawn in by convection via intakes at the bottom of the furnace. Before combustion, fuel samples were placed on a 2-mm mesh stainless steel sieve (20 cm in diameter, 6 cm high) placed on the floor of the furnace. Samples were uniformly spread to avoid any density effect of fuel on the combustion. Temperatures were measured by chromel-alumel thermocouple thermometers coated with a ceramic sheath at four sites: in the stack, in the upper part of the furnace, and at two points in the fuel material. The temperature signals were automatically transmitted every second to a data logger (21XL; Campbell Co. Ltd., California) and were transferred to a microcomputer.

The air inlet for THC (total hydrocarbon) monitoring was attached to the inner stack where the combustion plume entered the chamber from the furnace. After combustion, the chamber air was pumped from the mid-level of the chamber into 0.5- or 1.0-l Tedler® bags outside the chamber. The flow rate of the pumps was about 6 l min^{-1}. CO_2, CO, and CH_4 were measured within a day after the samples were packed in the Tedler® bags. Non-methane hydrocarbons (NMHCs) were measured within several days of the combustion experiments.

The O_2 concentration in the closed-chamber experiments decreased during combustion. Consumed O_2 estimated from total carbon emitted to the air was <1.3%; thus, the chamber effect due to decrease in O_2 content was considered to be negligible.

8.2.2 Time-series experiments

Time-series of gas concentrations at the stack of the furnace were made. The furnace was placed in an open area where wind was blowing at 1 to 2 m s^{-1}, which represented a more natural condition than the closed-chamber experiments. THC and temperatures were monitored by the same method as in the closed-chamber experiment. Gas samples were pumped from the stack to the Tedler® bags. Gas sampling was conducted at 15-s intervals at ignition and then 15, 30, 45, 60, 75, 90 and 105 s after; then at 120, 150, 180, 240 and 300 s.

In the time-series, the response time of each measured component is needed to compare variation patterns. The THC response time was adjusted in accordance with the time-series of temperatures. The delay in THC response was from 20 to 50 s as a result of the buffering effect of the humidifier and filter attached to the gas sampling line. Furthermore, the THC response was smoothed on a time scale of several seconds due to the buffering effect. Sampling by the Tedler® bags was conducted within 5 s. The delay in gas sampling was considered insignificant because the sampling line from the furnace to the bags was only 2 m long.

8.2.3 Method for expressing gas emissions

There are several indices used to express trace gas emissions during biomass burning. A key point is which gases to use as the base (denominator) in the calculation. Previous authors have used CO_2 and CO (e.g., Lobert et al, 1991), CH_4 (Hao et al., 1996) or C_2H_6 (Blake et al., 1994) as the base for their purposes and situations.

The emission factor (EF) is defined as the mass of a gas species emitted to the air per unit mass of fuel burnt. EF requires knowledge of the fuel, which is difficult to assess in field studies. Therefore, EF is mostly used in laboratory studies. Similarly, combustion efficiency (CE), defined as the ratio of carbon as CO_2 to total carbon emitted to the atmosphere, is difficult to use in field studies.

This study described data mainly by taking both CO and CO_2 as bases for comparison

with other studies, and only included EF values in Table 8.2. The emission ratio of a gas (X: formulated by chemical equation) concentration to a gas (Y) concentration is expressed by:

$$ER_Y(X) = \Delta[X]/\Delta[Y] = ([X]-[X]_0)/([Y]-[Y]_0). \quad (8.1)$$

For Y = CO_2 and CO,

$$ER_{CO2}(X) = \Delta[X]/\Delta[CO_2] = ([X]-[X]_0)/([CO_2]-[CO_2]_0), \quad (8.2)$$

$$ER_{CO}(X) = \Delta[X]/\Delta[CO] = ([X]-[X]_0)/([CO]-[CO]_0). \quad (8.3)$$

The background concentration level, $[X]_0$, was taken into account only for $[CO_2]_0$ (= 380 ppmv) and $[CH_4]_0$ (= 1.7 ppmv) and was set at zero for other gases because the concentrations of other gases in the combustion experiments were much higher than the background levels. The ratio $[CO]/\Delta[CO_2]$, which has been used for describing the quality of combustion, was expressed as $ER_{CO2}(CO)$.

8.3. Results

8.3.1. Estimation of gas emission in closed-chamber experiments

Table 8.2.1 shows the carbon partitioning to each gas in the closed-chamber experiments calculated by carbon balance. Judging from the values of $ER_{CO2}(CO)$, which is a suitable parameter to describe combustion stages of hydrocarbons (Lobert et al., 1991), tests Nos. 1 and 2 showed efficient combustion; Nos. 4 and 5 showed inefficient combustion; test No. 3 was between the two. In Nos. 4 and 5, a considerable quantity of particles was emitted and the chamber was filled with white smoke from 30 s until more than 1200 s after ignition.

The residual, estimated by subtraction from carbon emitted (Table 8.1) of the carbon in the chamber air calculated from the sum of CO_2, CO and CH_4, could be regarded as the carbon partitioned to particles, namely black carbon. However, in this study, a low value of the residual was only observed in test No.2. Nos. 4 and 5 were similar to the combustion of wood (Kuhlbusch and Crutzen, 1996).

Carbon partitioning to hydrocarbons showed high values in the inefficient combustion cases, Nos. 4 and 5. For NMHCs, carbon partitioning to C_2H_4 was the highest, in agreement with the results of Bonsang et al. (1995).

$ER_{CO2}(X)$ and $ER_{CO}(X)$ values from the closed-chamber experiments are shown in Tables 8.2.2 and 8.2.3. The C_2H_2 showed close correlation with $[CO_2]$. The C_4 gas species have a tendency to relatively higher correlation with $[CO_2]$ than do C_3 and C_5 species. CH_4 and C_4 species had close correlation with CO. The emissions of gases with higher carbon numbers were less than those with smaller carbon numbers.

Correlation between $ER_{CO2}(CO)$ and $ER_{CO2}(HCs)$ (Table 8.3) was closer than the correlation of gas concentrations and [CO] probably because $ER_{CO2}(X)$ reflected the combustion process better than did gas concentration. The correlations for all the hydrocarbons exhibited $R^2 > 0.80$ except that for C_2H_2. CH_4 showed the highest correlation ($R^2 = 0.996$). The correlation coefficients of the unsaturated C_2 and C_3 species were lower than those of saturated species. Normal-chain alkanes exhibited high correlation ($R^2 > 0.96$). For the C_4 and C_5 species, the correlations of iso-chain species were lower than those of normal-chain species. The slope values decreased as the carbon number increased. Iso-chain gas species had lower slopes than normal-chain species.

8.3.2. Time-series of gas concentrations in combustion plume

Here, time-series of gas concentrations for efficient and inefficient combustion are shown.

8.3.2.1 Case 1: efficient combustion (Fig. 8.2)

The temperature at the top of the furnace exceeded 600°C. The amount of carbon emitted to the air was 52.8 g. There was little emission of smoke particles.

Temperatures were maximum at 45 to 60 s. The $[CO_2]$ and [CO] showed maxima at 30 s. The variations in $[CO_2]$ and [CO] showed similar patterns until 90 s when $ER_{CO2}(CO)$ became relatively constant (0.03 to 0.05). The absolute concentrations decreased rapidly with increasing carbon number (see y-axis of Fig. 8.2).

The THC had 3 peaks corresponding to different gases. The first peak at 30 s, the weakest, was synchronized with the peaks of $[CO_2]$, [CO], $[C_2H_4]$, $[C_2H_6]$, and $[i\text{-}C_4H_{10}]$. The

second peak at about 60 s was synchronized with the peak of $[C_3H_6]$, and the third peak at about 165 s was synchronized with the maximum of $ER_{CO2}(CO)$ and peaks in the concentrations of CH_4, C_4 and C_5 species.

The first peak of $[CH_4]$ at 30 s was stronger than that in the THC. Peaks of $[C_2H_2]$ and $[C_2H_4]$ at 30 s were stronger than those of other hydrocarbons. The $[C_2H_6]$ peaks corresponded weakly to the first and strongly to the third peak of THC. The C_3 gas species had 3 peaks corresponding to those of THC. The second peak was strong in $[C_3H_6]$ rather than in $[C_3H_8]$. For the C_4 gas species, two peaks of concentrations were observed, corresponding to the first and third peaks of THC. Only one C_5 gas species peak was observed, corresponding to the third peak of THC. In C_4 and C_5 gas species, the peaks of iso-chain species tended to be earlier than those of normal-chain species, and the absolute concentrations of iso-chain species were approximately one third those of normal-chain species. It should be noted also that at 15 s, just before the peaks of $[CO_2]$ and [CO], small peaks of $[C_3H_8]$, $[C_3H_6]$, and $[i\text{-}C_4H_{10}]$ appeared.

8.3.2.2 Case 2: inefficient combustion (Fig. 8.3)

The temperature at the top of the furnace did not exceed 300°C. The proportion of moisture in the fuel in case 2 was 5.5%, a little higher than in case 1 (4.7%). The carbon remaining in burnt ash was 18%, higher than in case 1 (12%). The amount of emitted carbon in case 1 was 38.2 g, which was 75% of that in case 2. The strength of the fire was visibly weak throughout combustion.

The pattern of smoke emission in case 2 was as follows: until 30 s, smoke was not observed; from 30 to 45 s, there was a little smoke; from 45 to 60 s, smoke gradually became intense; from 60 to 90 s, massive smoke was observed; from 90 to 120 s, the massive smoke gradually subsided; after 2 min, the smoke continued to subside until 300 s. From this smoke emission profile, a considerable amount of carbon should have been emitted as smoke particles similar to Nos. 4 and 5 in the closed-chamber experiments.

The THC emission showed a large peak around 160 s. There were several minor peaks or rises, and one small maximum was synchronized with the peaks of $[CO_2]$ and [CO]. The rise in THC at about 45 s corresponded to peaks of $[C_2H_6]$, $[C_3H_8]$, and peak concentrations of C_4 and C_5 gas species. None of the light hydrocarbons seemed to correspond to the peaks

or rises in THC after 120 s.

Concentrations of gas species decreased with carbon number (see y-axis of Fig. 8.3). The C_2H_6 and C_2H_4 showed similar concentrations after 60 s, while C_3H_8 and C_3H_6 showed similar concentrations throughout combustion. In C_4 and C_5 species, concentrations of normal-chain alkanes were approximately 3 times higher than those of iso-chain alkanes, as in case 1. The patterns of variation of normal and iso-chain alkanes were quite similar.

At 30 s, $[CO_2]$, [CO] and the temperature in the stack showed maxima. The $[CO_2]$ at 30 s was 3.3%, which was far lower than in case 1 (13.3%), even taking into account the amount of fuel.

Until 30 s, $ER_{CO2}(CO)$ was a little lower than 0.15. After 30 s, temperatures gradually decreased, and $ER_{CO2}(CO)$ remained higher than 0.20 until 120 s. In case 2, the concentrations of resulting hydrocarbons were far higher than those in case 1 and had two concentration peaks, at 30 to 45 s and at 75 s, respectively. The first peaks of C_2 and C_3 alkanes were at 45 s and those of unsaturated C_2 and C_3 species were at 30 s. At 75 s, a sudden decrease in CH_4 concentration was observed, corresponding to the peaks of C_2 to C_5 gas species. At 30 s, the order of the C_2 species concentrations was $[C_2H_4] > [C_2H_6] > [C_2H_2]$. The $[C_2H_6]$ at 30 s was higher in case 2 than in case 1 whereas the opposite was true for $[C_2H_2]$. In case 2, C_3H_8 and C_3H_6 showed absolute concentrations similar to those in case 1. Other gas species, C_2H_6, C_3, C_4, and C_5, showed higher concentrations, corresponding to the second peak of THC.

The rate of decrease in concentration (concentration ratio of 75 s to 90 s) of normal-chain alkanes became gradually smaller with increasing carbon number. This shows that the concentration peaks were gradually delayed with increasing carbon number, although sampling in 15-s intervals of this study could not detect the time difference of these peaks.

The decreasing rates of hydrocarbon concentration with increasing carbon number were higher in case 1 than in case 2. In terms of absolute concentrations, $[CO_2]$, $[CH_4]$, $[C_2H_2]$, and $[C_2H_4]$ in the first peak were higher in case 1 than in case 2. Gas concentrations, except those of $[CO_2]$ and $[C_2H_2]$, were higher in case 2 than in case 1. The $[CH_4]$ in case 2 was twice that in case 1 (300 and 150 ppmv, respectively); $[C_2H_6]$ was about 3 times higher in case 2 than in case 1 (50 and 15 ppmv, respectively); the concentrations of C_3 gas species were about 6 times higher in case 2 than in case 1; those of C_4 gas species were 10 times higher in case 2 than in case 1; and those of C_5 gas species were about 15 times higher in case

2 than in case 1. The ratio of concentrations in cases 1 and 2 became higher with increasing carbon number.

8.3.3. Relationship between temperature, $ER_{CO2}(X)$ and THC, and time-series of $ER_{CO2}(X)$

$ER_{CO2}(CO)$ showed maxima between 80 and 300°C, which corresponded to those of THC (Fig. 8.4). In case 1 (b), THC had 2 maxima, which corresponded to emission during the flaming and smoldering phase, respectively. In case 2 (b), the THC peak corresponding to emission in the flaming phase was not observed, probably due to the weak flaming.

The time-series of gas concentrations were converted to $ER_{CO2}(X)$ (Figs. 8.5, 8.6) because CO_2 is a final product in the combustion process; it is the major carbon species emitted, and is considered to be a suitable species for the normalization of data. In case 1 as is shown in Fig. 8.5, the peak in CH_4, which appeared in Fig. 8.2d, disappeared and the pattern of $ER_{CO2}(CH_4)$ corresponded closely with that of $ER_{CO2}(CO)$; hydrocarbons except C_2H_2 showed similar patterns with $ER_{CO2}(CO)$ until 180 s. The $ER_{CO2}(C_2H_4)$ and $ER_{CO2}(C_2H_2)$ showed sharp peaks at 30 s, unlike the variation in $ER_{CO2}(CO)$. The $ER_{CO2}(X)$ of C_4 and C_5 species showed peaks even at 240 s. The $ER_{CO2}(X)$ of C_3 and C_4 species showed small peaks at 15 s (Fig. 8.5c, d) as in Fig. 8.2, although $ER_{CO2}(CO)$ was lower at 15 s.

However, in case 2 as shown in Fig. 8.6, the patterns of variation of gases could not be explained simply by variation in $ER_{CO2}(CO)$. The patterns in $ER_{CO2}(HCs)$ and $ER_{CO2}(CO)$ became similar only after 150 s. When $ER_{CO2}(CO)$ was higher than 0.20 during 45 to 120 s, the variations in ER_{CO2} (light HCs) and $ER_{CO2}(CO)$ were opposite. The $ER_{CO2}(X)$ of lighter hydrocarbons showed lower values when $ER_{CO2}(CO) > 0.20$. The $ER_{CO2}(X$ = light HCs) increased before and after $ER_{CO2}(CO)$ was higher than 0.20.

8.4 Discussion

8.4.1 $ER_{CO}(X)$ values from the closed-chamber experiments and comparisons with previous studies

The results of closed-chamber experiments in this study showed broad ranges of emission ratios to CO (Table 8.5). The range of $ER_{CO2}(CO)$ values, 0.044 to 0.137, indicates that a wide range of control on combustion conditions was achieved in closed-chamber

experiments in this study. The magnitude of the range of gas emissions is comparable with those of Bonsang et al. (1991) and Lobert et al. (1991). Although the absolute values of $ER_{CO}(X)$ were higher in this study except for C_2H_2, the magnitude of the range (expressed as max/min) increased with increasing carbon number.

We compared the $ER_{CO}(X)$ of the present chamber experiment with previous reports (Table 8.6). Although the emission of C_2H_2 was strongly correlated with CO_2 emission, the C_2H_2 ratio in data of this study was the lowest. This indicates that combustion in the present closed-chamber experiments, especially Nos. 4 and 5, was very inefficient. The $ER_{CO}(CH_4)$ of the present data are in a similar range to other studies. The $ER_{CO}(X = NMHCs)$ values of the present data exceed all the mean values of other studies. This trend became more marked with increasing carbon number, perhaps because fresh air, including O_2, could not be supplied adequately to the fuel from the outside due to weak convection in the furnace in the closed-chamber. This may be also because the phase of gas emission was no longer the same as that of CO under very high $ER_{CO2}(CO)$ values (>0.1), as shown for CH_4 in Fig. 8.3c, d and Fig. 8.7a.

The ratios of i-C_4H_{10} to n-C_4H_{10} and i-C_5H_{12} to n-C_5H_{12} in the present data are similar to those of other studies except the value of 0.46 for high CE in Bonsang et al. (1995). This may be due to uniformity in the synthetic and decomposition processes of C_4 and C_5 alkanes regardless of the large variety of combustion processes and fuels.

The ratios of hydrocarbons to CO (= $ER_{CO2}(X)/ER_{CO2}(CO)$ were positively related to $ER_{CO2}(CO)$ (Table 8.6). Hence, $ER_{CO2}(X)$ against $ER_{CO2}(CO)$ (Fig. 8.7) was plotted. Data from Nos.1 and 2, and Nos.4 and 5, was averaged due to the similarity of the $ER_{CO2}(CO)$ axis. For CH_4, the data except Bs (low) were better correlated using a second polynomial rather than a linear function.

When $ER_{CO2}(CO) < 0.1$, the data were positively correlated with $ER_{CO2}(CO)$. When $ER_{CO2}(CO) > 0.1$, the data for Nos. 4 and 5 showed high values of $ER_{CO2}(CH_4)$, whereas Bonsang et al. (1995) showed low values. One explanation is that the emission rates of hydrocarbons in African fires were lower than those in Brazil (Blake et al., 1996). Another explanation is that in the airborne experiments, samples were not collected in the absence of visible flames and may neglect smoldering samples as depicted by Bonsang et al. (1995).

8.4.2 Time-series of gas concentrations in the combustion plume and $ER_{CO2}(X)$

The slight difference in fuel moisture led to a difference in combustion conditions between cases 1 and 2. Fuel with several percent moisture added before combustion was difficult to ignite due to the low permeability of O_2 in the tissue of the fuel sample or cooling by evaporation. This shows that combustion conditions are sensitive to slight differences in the moisture content of fuel.

Crutzen and Andreae (1990) classified combustion into two phases, flaming and smoldering. They defined the transition time between phases as the time to maximize d[CO]/dt; the transition time was the period between $[CO_2]$ and [CO] peaks. However, this definition is not applicable in all types of combustion, as shown by Gerstle and Kemnitz (1967) who described a case in which the peak of [CO] preceded that of $[CO_2]$. In fact, this definition cannot be easily applied to this study because continuous measurements of CO concentrations were not made. Combustion conditions were not easily described as flaming and smoldering phases from the results of the present time-series experiments. The present study tried to determine the combustion phases first by various combinations of combustion conditions and summarized the conditions during the those phases afterwards.

Gas concentrations in a combustion plume are determined from the net balance of synthetic and decomposition reactions. In the present experiments, the higher rates of decrease in hydrocarbon concentration with increasing carbon number in case 1 than in case 2, are explained by the slower rate of decomposition of hydrocarbons in the lower temperature in case 2. Because the combustion process overall is regarded as the oxidation process of organic compounds, it is not unreasonable that the $ER_{CO2}(CO)$, which is the ratio of CO (which precedes CO_2) to CO_2 (final product of combustion), should reflect some properties of combustion. It is also to be expected that lighter hydrocarbons would have chemical reactions directly or almost-directly related to CO or CO_2, the correlation between the light hydrocarbons and $ER_{CO2}(CO)$ being strong; the opposite is the case for heavy hydrocarbons. Therefore, $ER_{CO2}(CO)$ is considered to be a significant parameter that reflects the combustion process, at least for light hydrocarbons.

Case 1 (Figs. 8.2 and 8.5), which exhibits efficient combustion, is similar to Fig. 8.1 of Crutzen and Andreae (1990), taking into account the time scale. However, there are some

differences. The peak of [CO] in Crutzen and Andreae (1990) was distinctly delayed in comparison with that of [CO_2]. Case 1 showed simultaneous peaks of [CO_2] and [CO], although the time interval was only 15 s and the peaks probably could not be distinguished. The present study estimated the transition from flaming to smoldering phase to be at 105 s when the $ER_{CO2}(CO)$ began to increase. Crutzen and Andreae (1990) showed that the peaks of hydrocarbon concentrations were synchronized with the peak of [CO]. Case 1 showed that the emission of hydrocarbons largely corresponded to the patterns of $ER_{CO2}(CO)$. However, this could not be simply applied to all the gas species. Unsaturated C_2 species such as C_2H_2 and C_2H_4 showed both higher concentrations and ratios to $\Delta[CO_2]$ at 30 s when [CO_2] and [CO] reached maxima, although [C_3H_6] did not show such a peak.

Under flaming conditions, the C_3H_6 produced from higher organic compounds could be decomposed further into C_1 and C_2 gases. This was expected because the rise in [C_3H_6] took place earlier than that of [C_3H_8]. There is a considerable concentration of O, H, and OH radicals in the fire plume, similar to that of OH and HO_2 in the atmosphere (Baulch et al., 1992). With increasing carbon number, the reactivity of hydrocarbons to these radicals increases. Therefore, C_3H_6 could be decomposed in the flaming phase, but survive in the following phase. The present study defined this phase as the transition phase between the flaming and smoldering phases.

C_2H_4 was emitted in both flaming and smoldering phases. These phase features of C_2 and C_3 species correspond well to their proportions in the combustion phases of Lobert et al. (1991). However, their estimated 44% C_2H_2 production in the smoldering phase was different from that in case 1, in which C_2H_2 emission occurred mostly in the flaming phase.

The peaks in $ER_{CO2}(X)$ of C_3 and C_4 species at 15 s (Fig. 8.5) could be attributed to the pyrolytic decomposition of plant matter immediately preceding the flame (Andreae et al., 1996). The present study define this combustion stage as the pre-flaming phase, in which C_3 and C_4 gas species are produced abundantly and not greatly decomposed under the lower temperature.

In Fig. 8.5, it can be seen that the [CO]/$\Delta[CO_2]$ ratios remained high even after 180 or 240 s, although the emission ratio of hydrocarbons to CO_2 decreased rapidly. The present study define this combustion stage as the post-smoldering phase, in which only a small amount of gases is emitted as the temperature decreases.

In case 2 (Figs. 8.3 and 8.6), the combustion was entirely inefficient except during the first 30 s, judging from the $ER_{CO2}(CO)$ values. The period from 0 to 30 s could be considered as the weak flaming phase. The terminology "weak" was used because $[CO_2]$ in the combustion plume was smaller than in case 1 and because $ER_{CO2}(CO)$ was about 0.1, which was twice that in the flaming phase of case 1. In the weak flaming phase, a peak of C_3H_6 was observed. This is consistent with the present view that the decomposition process is weak when the flaming phase is weak.

The period between 45 and 210 s is regarded as the smoldering phase because the temperature gradually decreased and $ER_{CO2}(CO) > 0.15$. When $ER_{CO2}(CO)$ was greater than 0.20 during 45 to 120 s, the carbon may have been partitioned to other, heavier hydrocarbons and particulates because the relative contribution of light hydrocarbons was low and because THC showed high values. $ER_{CO2}(CH_4)$ was < 0.002 at 75 sec; the emission of C_2H_2 was weak in case 2 due to the weak fire intensity.

This pattern of gas phase transition corresponded to that of smoke emission. In inefficient combustion, the carbon is expected to be partitioned to other/heavier compounds or particles. The THC peak at 150 s (Fig. 8.3d) was also delayed in comparison with those of C_2-C_5 hydrocarbons detected at 75 s. It is likely that other hydrocarbons were emitted to the air during these stages of combustion (Andreae et al., 1996). The present study define this combustion stage as the heavy-smoldering phase, in which the rate of both synthesis and degradation of light hydrocarbons is considered to be low under lower temperature (Baulch et al., 1992).

The emission of normal-chain C_4 and C_5 species was 3 times greater than that of iso-chain C_4 and C_5 species, which may be produced from degradation of other organic material or recombination of radicals. The dead plant is made of various organic materials, predominantly cellulose $(C_6H_{10}O_5)_n$. The monomer of cellulose is glucose, which is combined by ß-1,4-glucosido chains. Glucose is a 6-carbon chain structure. As well as the concentration trends with increasing carbon number ($<C_5$) in the present experiments, the slightly lower concentration of n-C_6H_{14} to n-C_5H_{12} in Bonsang et al. (1995) may reflect this structure. The emission of further heavy normal-chain alkanes > C_7 has rarely been reported so far, but they may occur in much smaller concentrations than those of C_5 and C_6 species (for atmospheric concentrations, see Koppmann et al., 1998).

8.4.3. Relationship between the results of the closed-chamber experiments and the time-series of gas concentrations

The total emission of gas "X" integrated over the combustion event, $E(X)$, is linked to the time-series of gas concentrations in the fire plume, $C(X,t)$ as follows:

$$E(X) = \int f(t)C(X,t)dt \tag{8.4}$$

where t is time, $f(t)$ is the time-series of emission (mass flow) rates of the fire plume (molecules s^{-1}). The $f(t)$ is higher in the flaming phase due to intense fire and strong convection.

The time-series of gas concentrations were found to be related to gas phases as described above. However, eq. (8.4) shows that the time-series of gas concentrations were not equivalent to the time-series of gas emissions. The latter are the product of gas concentration and mass flow rate. Hence, simple summing up of concentrations does not reflect the total emission ratios during combustion.

We used $ER_{CO}(X)$ as the base to integrate the results of the closed-chamber experiment and time-series of gas concentrations. The overall gas concentration ratio to CO_2 is expressed as follows:

$$\frac{E(X)}{E(CO_2)} = \frac{\int f(t)[X]dt}{\int f(t)[CO_2]dt} \tag{8.5}$$

Although $\frac{E(X)}{E(CO_2)}$ is not the mean value of $\frac{[X]}{[CO_2]}$ at each sampling time, $ER_{CO2}(X)$ was taken into consideration because $ER_{CO2}(CO)$ can qualitatively describe the variation in

$\frac{E(X)}{E(CO_2)}$. The relationship between $ER_{CO2}(X)$ and $ER_{CO2}(CO)$ is shown in Fig. 8.8 (case 1) and Fig. 8.9 (case 2). In case 1 (Fig. 8.8), the data in the flaming and smoldering phases were largely linear except C_2H_2 which was produced mostly in the flaming phase. This result is similar to Fig. 36.5 of Lobert et al. (1991).

The slopes of linear regressions in the smoldering phase in case 1 were approximately 0.12 for CH_4 (Fig. 8.8a), 0.01 for C_2H_6 (Fig. 8.8b), 0.0025 for C_3H_8 and C_3H_6 (Fig. 8.8c), 0.0007 for n-C_4H_{10} (Fig. 8.8d), 0.000125 for i-C_4H_{10} (Fig. 8.8d), 0.00025 for n-C_5H_{12} (Fig. 8.8e), and 0.00006 for i-C_5H_{12} (Fig. 8.8e). These values were in the range of the results of the closed-chamber experiments (Table 8.5) and, except for CH_4, were close to the minimum values in Table 8.5. Slope values for overall emission should be a little lower than these values because the data points in the post-smoldering phase lower the slope even if the contribution of the post-smoldering phase is small. The data points in the flaming phase can lower the slope more than can those in the post-smoldering phase, especially for heavier C_3-C_5 species because the mass flow rate should be larger in the flaming phase.

In case 2 (Fig. 8.9), the data were scattered even in the smoldering phase. The slopes of linear regressions in the smoldering phase in case 2 were approximately 0.2 for CH_4 (Fig. 8.9a), 0.03 for C_2H_6 (Fig. 8.9b), 0.0125 for C_3H_8 and C_3H_6 (Fig. 8.9c), 0.003 for n-C_4H_{10} (Fig. 8.9d), 0.0006 for i-C_4H_{10} (Fig. 8.9d), 0.0015 for n-C_5H_{12} (Fig. 8.9e), and 0.0006 for i-C_5H_{12} (Fig. 8.9e). The slope values in case 2 were far higher than those in case 1 as well as the maximum values in Table 8.5. The ratios of the slopes in Figs. 8.9 to those in Fig. 8.8 for each gas species became higher with increasing carbon number. There are two likely explanations for this: either the decomposition process is weaker in case 2 under the lower temperature; or the gas species of high carbon number can be easily destroyed in chemical reactions with radicals. Hence, gases easily decomposed in the chemical reactions can survive at lower temperatures.

The carbon in the heavy-smoldering phase should not be partitioned to light hydrocarbons. This is consistent with the results of Bonsang et al. (1995), who showed that the ratio of heavy hydrocarbon concentrations to [CO] is higher under lower combustion efficiency.

8.5 Summary

To investigate the emission processes from CO and related gases from biomass burning, production and degradation of CO and related carbon gases, CO_2, light hydrocarbons and THC, during combustion processes were investigated using a furnace, of dead plant material mainly consisting of Imperata. The closed chamber experiments showed results similar to those reported so far in lighter hydrocarbons.

Previous studies (e.g. Crutzen and Andreae, 1990; Lobert et al., 1991) proposed the flaming and smoldering phases. Analysis of the time-series of gas concentrations at 15-s intervals showed that several additional phases exist: they are a pre-flaming phase, transition phase from the flaming to the smoldering phases, a heavy-smoldering phase and post-smoldering phase. The transition time from flaming to smoldering phases could be defined as the time when $0.07<ER_{CO2}(CO)< 0.1$ after the peak of $[CO_2]$. The pre-flaming phase was brief, before the flaming phase, and was characterized by emission of low concentrations of some hydrocarbons, particularly C_3 and C_4 species. The transition phase, between the flaming and smoldering phases when $0.07<ER_{CO2}(CO)<0.1$, was characterized by an increase in emission of C_3H_6, which is mostly decomposed in the flaming phase. The heavy-smoldering phase appeared when $ER_{CO2}(CO) > 0.20$, and was characterized by emission of low concentrations of light hydrocarbons and probably by the emission of high concentrations of other/heavier hydrocarbons. The post-smoldering phase was characterized by lower $ER_{CO2}(CO)$ values after the smoldering phase, when only a low concentration of gases was emitted in the decreasing temperature conditions.

The results of the closed chamber experiments and of the time-series of gas concentrations were discussed by relating to the phase diagrams of $ER_{CO2}(CO)$ and $ER_{CO2}(X)$ (Figs. 4.8 and 4.9). Emissions of most of hydrocarbons were well correlated with $ER_{CO2}(CO)$ and the correlation coefficients were lower in heavier gas species. However, emission of C_2H_2 was well correlated with $[CO_2]$. For C_3 and C_4 species, normal-chain species had approximately 3 times larger emissions than iso-chain species.

The phase diagrams obtained by the time-series experiments well illustrated the variation of the overall emission rates of the closed chamber experiments. In the efficient combustion case, high emission rates of C_4 species and the emission of C_3 species in the pre-flaming

phase were observed although they were not observed for C_5 species. This finding supports the result of closed chamber experiments and pyrolysis of cellulose. From the time-series experiments, it is deduced that the delays of the peaks of gas concentration depend on the molecular weight because the net balance of synthetic and decomposition chemical reactions are functions of temperature.

Table 8.1 The C-N contents of samples. They were averages of three analyses and are based on mass.

Experiment	Sample no.	Class	Amount g	Moisture content % dry weight	C % dry weight	N % dry weight	Total C g	Total N g	Emitted C g	Emitted N g
Closed chamber experiment	1	fuel	25.6	4.0	33.2	1.3	1.7	0.06	1.5	0.06
		ash	4.8	3.4	16.4	1.2	0.2	0.01		
	2*	fuel	27.4	4.6	41.7	2.4	2.0	0.12	1.9	0.11
		ash	3.9	4.8	16.7	1.2	0.1	0.01		
	3*	fuel	37.2	4.6	41.7	2.4	2.8	0.16	2.5	0.13
		ash	7.5	2.6	14.3	1.1	0.3	0.02		
	4*	fuel	61.5	4.6	41.7	2.4	4.6	0.26	4.2	0.23
		ash	9.3	2.8	15.6	1.2	0.4	0.03		
	5*	fuel	58.0	4.6	41.7	2.4	4.3	0.24	3.7	0.20
		ash	14.7	3.4	19.1	1.3	0.6	0.04		
Tim series experiment	Case 1	fuel	130.0	4.7	44.4	1.8	10.1	0.42	9.2	0.35
		ash	20.2	1.8	12.0	0.9	0.9	0.06		
	Case 2	fuel	97.6	5.5	44.4	1.8	6.7	0.28	5.8	0.20
		ash	16.4	2.2	18.2	1.5	0.9	0.08		

* Fuel samples of Nos.2 to 5 in the closed chamber experiments were taken from the same mass of fuel.

Table 8.2 continues to next page.

Table 8.2-1 (Carbon partitioning)

No.*	Residual	$ER_{CO2}(CO)$	CE (%)	CO	CH_4	C_2H_6	C_2H_4	C_2H_2	C_3H_8	C_3H_6	i-C_4H_{10}	n-C_4H_{10}	i-C_5H_{12}	n-C_5H_{12}
2	-77.097	0.0464	78.1	0.0363	0.0022	1.6E-04	3.7E-04	8.2E-05	3.6E-05	1.0E-04	n.a.	1.6E-05	5.6E-06	4.2E-06
3	0.503	0.1308	31.7	0.0415	0.0061	1.3E-03	2.0E-03	6.7E-05	6.1E-04	1.1E-03	2.7E-05	2.2E-04	2.8E-05	1.1E-04
4	0.482	0.1309	34.1	0.0447	0.0070	1.4E-03	1.2E-03	5.7E-05	6.3E-04	6.8E-04	3.8E-05	1.9E-04	3.7E-05	9.7E-05
5	0.403	0.0687	48.6	0.0334	0.0032	3.3E-04	5.4E-04	1.1E-04	1.1E-04	1.5E-04	2.8E-05	1.2E-04	2.5E-06	1.3E-05

* estimate of no.1 was not possible due to the large leakage of the chamber system.

n.a. means that analysis was not possible due to the low concentration or analytical problem.

Table 8.2 Carbon partitioning of trace gases, gas concentration ratio to CO_2 and gas concentration ratio to CO.

Table 8.2-2 ($ER_{CO_2}(X)$)

No.	CO_2	CO	HCs*	CH_4	C_2H_6	C_2H_4	C_2H_2	C_3H_8	C_3H_6	i-C_4H_{10}	n-C_4H_{10}	i-C_5H_{12}	n-C_5H_{12}
1	1	0.0441	0.0051	0.0024	2.6E-04	3.2E-04	7.7E-05	2.0E-04	1.6E-04	5.4E-05	7.7E-06	n.a.	n.a.
2	1	0.0464	0.0046	0.0024	2.0E-04	4.7E-04	1.1E-04	4.7E-05	1.3E-04	n.a.	2.1E-05	7.2E-06	5.4E-06
3	1	0.1308	0.0608	0.0186	4.0E-03	6.4E-03	2.1E-04	1.9E-03	3.3E-03	8.6E-05	7.0E-04	8.8E-05	3.3E-04
4	1	0.1309	0.0510	0.0197	4.0E-03	3.5E-03	1.7E-04	1.8E-03	2.0E-03	1.1E-04	5.7E-04	1.1E-04	2.8E-04
5	1	0.0687	0.0131	0.0061	6.8E-04	1.1E-03	2.2E-04	2.3E-04	3.1E-04	5.7E-05	2.4E-04	5.1E-06	2.6E-05

*HCs is the sum of hydrocarbons with multipying carbon numbers.

n.a. means that analysis was not possible due to the low concentration or analytical problem.

Table 8.2-3 ($ER_{CO}(X)$)

No.	CO_2	CO	HCs*	CH_4	C_2H_6	C_2H_4	C_2H_2	C_3H_8	C_3H_6	i-C_4H_{10}	n-C_4H_{10}	i-C_5H_{12}	n-C_5H_{12}
1	22.7	1	0.1148	0.055	5.8E-03	7.2E-03	1.7E-03	4.4E-03	3.7E-03	1.2E-03	1.7E-04	n.a.	n.a.
2	21.5	1	0.0992	0.051	4.4E-03	1.0E-02	2.3E-03	1.0E-03	2.9E-03	n.a.	4.5E-04	1.6E-04	1.2E-04
3	7.6	1	0.465	0.142	3.1E-02	4.9E-02	1.6E-03	1.5E-02	2.6E-02	6.6E-04	5.3E-03	6.7E-04	2.5E-03
4	7.6	1	0.3899	0.150	3.0E-02	2.6E-02	1.3E-03	1.4E-02	1.5E-02	8.6E-04	4.4E-03	8.2E-04	2.2E-03
5	14.6	1	0.1907	0.089	9.9E-03	1.6E-02	3.2E-03	3.3E-03	4.5E-03	8.3E-04	3.6E-03	7.5E-05	3.8E-04

*HCs is the sum of hydrocarbons with multipying carbon numbers.

n.a. means that analysis was not possible due to the low concentration or analytical problem.

Table 8.3 Correlation between CO, CO_2 and HCs concentrations in the closed-chamber experiment.

Table 8.3-1 (CO_2)

CO_2	CO	CH_4	C_2H_6	C_2H_4	C_2H_2	C_3H_8	C_3H_6	i-C_4H_{10}	n-C_4H_{10}	i-C_5H_{12}	n-C_5H_{12}
n	5	5	5	5	5	5	5	4	5	4	4
slope	0.132	0.0481	0.0571	0.0256	0.000265	-0.0656	0.0913	0.00019	0.00156	-0.00012	-0.00054
R^2	0.437	0.079	0.003	0.030	0.824	-0.001	0.001	0.185	0.114	-0.668	-0.423

Table 8.3-2 (CO)

CO	CO_2	CH_4	C_2H_6	C_2H_4	C_2H_2	C_3H_8	C_3H_6	i-C_4H_{10}	n-C_4H_{10}	i-C_5H_{12}	n-C_5H_{12}
n	5	5	5	5	5	5	5	4	5	4	4
slope	7.55	0.170	0.0450	0.0632	0.00347	0.0238	0.0388	0.0011	0.0065	0.0028	0.0072
R^2	0.437	0.819	0.602	0.634	0.626	0.521	0.510	0.762	0.848	0.228	0.418

Table 8.4 Correlation between $ER_{CO2}(CO)$ and $ER_{CO2}(HCs)$ in the closed-chamber experiment.

		CH_4	C_2H_6	C_2H_4	C_2H_2	C_3H_8	C_3H_6	i-C_4H_{10}	n-C_4H_{10}	i-C_5H_{12}	n-C_5H_{12}
	n	5	5	5	5	5	5	4	5	4	4
	average	0.098	0.0162	0.0217	0.0020	0.0075	0.0104	0.0009	0.0028	0.0004	0.0013
Fitting											
y=p x	p (slope)	0.131	0.0259	0.0327	0.0017	0.0119	0.0169	0.0008	0.0043	0.0006	0.002
	R^2	0.860	0.764	0.674	0.065	0.745	0.662	0.659	0.782	0.693	0.706

Table 8.5 Comparison of variations in $ER_{CO2}(X)$. Values from Bonsang et al. (1991) were edited from their Table 20.1.

X	Present closed chamber experiments					Bonsang et al. (1991) Ground Savanna(Ivory Coast, Africa)				Lobert et al. (1991) Laboratory			
	mean	fitting	min	max	max/min	mean	min	max	max/min	mean	min	max	max/min
CH_4	0.098	0.131	0.051	0.15	3.0	0.049	0.025	0.068	2.7	0.091	0.052	0.122	2.3
C_2H_6	1.6E-02	2.6E-02	4.4E-03	3.1E-02	7.0	3.5E-03	8.1E-04	5.4E-03	6.6	6.8E-03	1.6E-03	1.1E-02	6.6
C_2H_4	2.2E-02	3.3E-02	7.2E-03	4.9E-02	6.7	1.7E-02	3.6E-03	2.9E-02	8.2	1.2E-02	4.0E-03	2.1E-02	5.2
C_2H_2	2.0E-03	1.7E-03	1.3E-03	3.2E-03	2.5	6.2E-03	5.7E-04	1.4E-02	25.3				
C_3H_8	7.5E-03	1.2E-02	1.0E-03	1.5E-02	14.7	5.4E-04	1.8E-04	1.3E-03	7.3	1.5E-03	2.1E-04	3.2E-03	15.2
C_3H_6	1.0E-02	1.7E-02	2.9E-03	2.6E-02	8.9	2.8E-03	5.2E-04	4.0E-03	7.8	4.9E-03	1.3E-03	7.0E-03	5.3
i-C_4H_{10}	8.9E-04	7.8E-04	6.6E-04	1.2E-03	1.9	3.6E-05	9.4E-06	1.2E-04	12.2				
n-C_4H_{10}	2.8E-03	4.3E-03	1.7E-04	5.3E-03	30.6	1.2E-04	4.0E-05	3.1E-04	7.9	3.0E-04	6.0E-05	7.8E-04	13.0
i-C_5H_{12}	4.3E-04	6.5E-04	7.5E-05	8.2E-04	11.0	3.8E-04	6.9E-05	7.8E-04	11.3				
n-C_5H_{12}	1.3E-03	2.0E-03	1.2E-04	2.5E-03	21.7	1.1E-04	1.8E-05	5.8E-04	31.8	3.0E-04	8.0E-05	6.4E-04	8.0
$ER_{CO2}(CO)$	0.084		0.044	0.137	3.1	0.115	0.057	0.179	3.1	0.073	0.032	0.160	5.0

Table 8.6 Comparison of $ER_{CO2}(X)$ from the present closed-chamber experiments with those in other reports. The values of Bonsang et al. (1995) were converted from their data Table. The values of Hao et al. (1996) were obtained from $ER_{CH4}(X)$ and $ER_{CO2}(CO)$. The C_4 and C_5 ratios mean $ER_{CO}(i\text{-}C_4H10)/ERCO(n\text{-}C_4H_{10})$ and $ER_{CO}(i\text{-}C_4H_{10})/ER_{CO}(n\text{-}C_4H_{10})$, respectively.

X	Present closed chamber experiment	Bonsang et al. (1995) Ground Savanna (Africa)		Lobert et al. (1991)	Nance et al. (1993)	Blake et al. (1996)			Hao et al. (1996)
				Laboratory	Airborne Alaska	Airborne Brazil BFA	Brazil TraceA	Africa TraceA	Ground Zambia(Africa)
	mean	High CE	Low CE						
CH_4	0.098	0.064	0.053	0.091	0.057	0.107	0.094	0.078	0.065
C_2H_6	1.6E-02	5.6E-03	4.9E-03	6.8E-03	7.3E-03	8.5E-03	8.3E-03	5.2E-03	5.8E-03
C_2H_4	2.2E-02	2.8E-02	1.2E-02	1.2E-02		1.7E-02	6.1E-03	8.3E-03	1.8E-02
C_2H_2	2.0E-03	1.1E-02	4.1E-03		3.5E-03	4.6E-03	3.3E-03	4.5E-03	5.5E-03
C_3H_8	7.5E-03	5.0E-04	8.8E-04	1.5E-03	1.7E-03	1.6E-03	1.6E-03	9.7E-04	1.4E-03
C_3H_6	1.0E-02			4.9E-03	4.2E-03	4.9E-03	4.0E-04	1.0E-03	4.8E-03
i-C_4H_{10}	8.9E-04	3.2E-05	6.1E-05			6.7E-05	5.5E-05	4.3E-05	
n-C_4H_{10}	2.8E-03	7.0E-05	2.1E-04	3.0E-04		2.1E-04	2.1E-04	1.6E-04	
i-C_5H_{12}	4.3E-04								
n-C_5H_{12}	1.3E-03			3.0E-04		4.3E-05	5.1E-05	5.3E-05	
C_4 ratio	3.2E-03	4.6E-03	2.9E-03			3.2E-03	2.6E-03	2.7E-03	
C_5 ratio	3.3E-03								
$ER_{CO2}(CO)$	0.084	0.062	0.147	0.073	0.078	0.081	0.037	0.085	

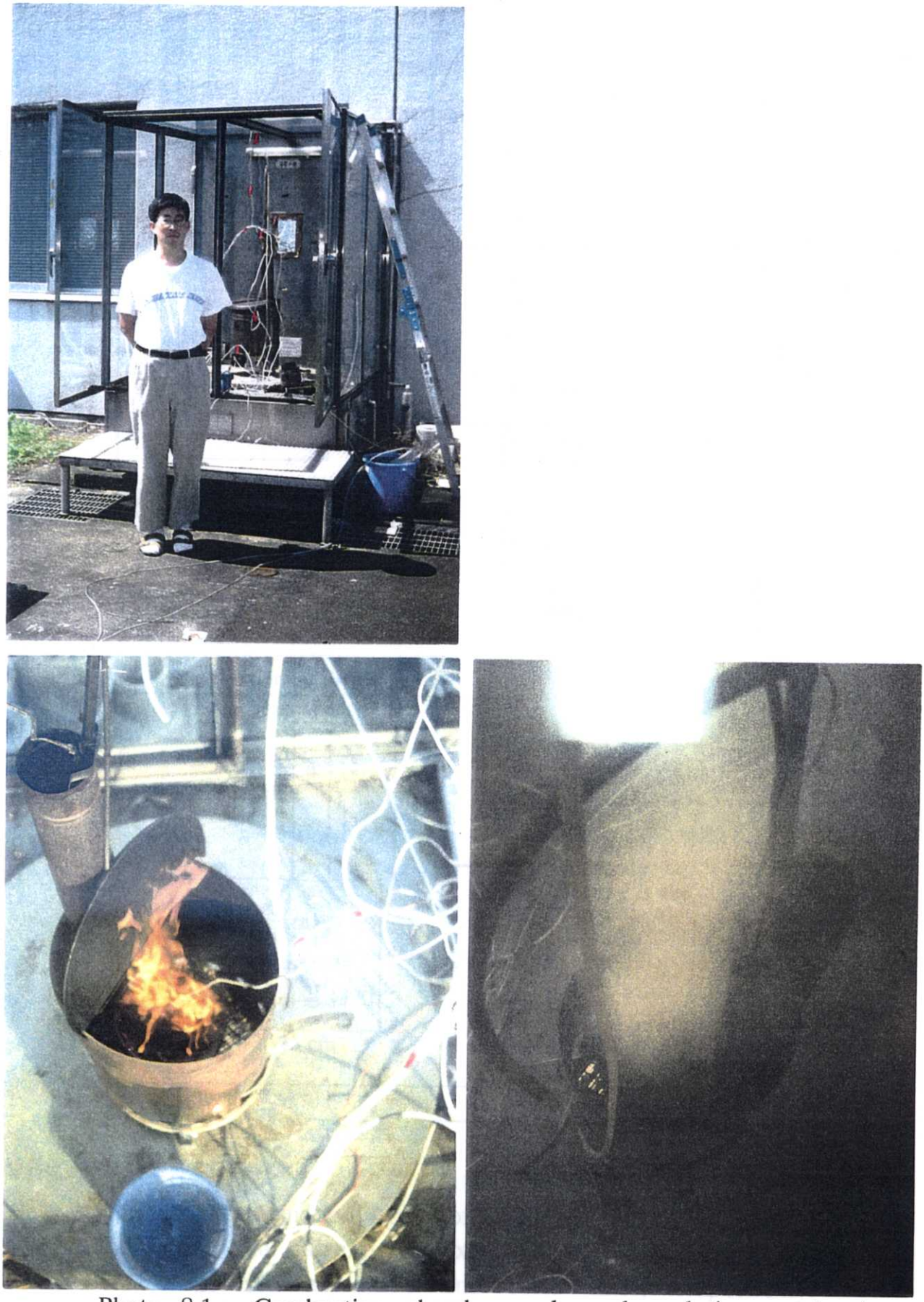

Photo 8.1 Combustion chamber and smokes during combustion experiments.

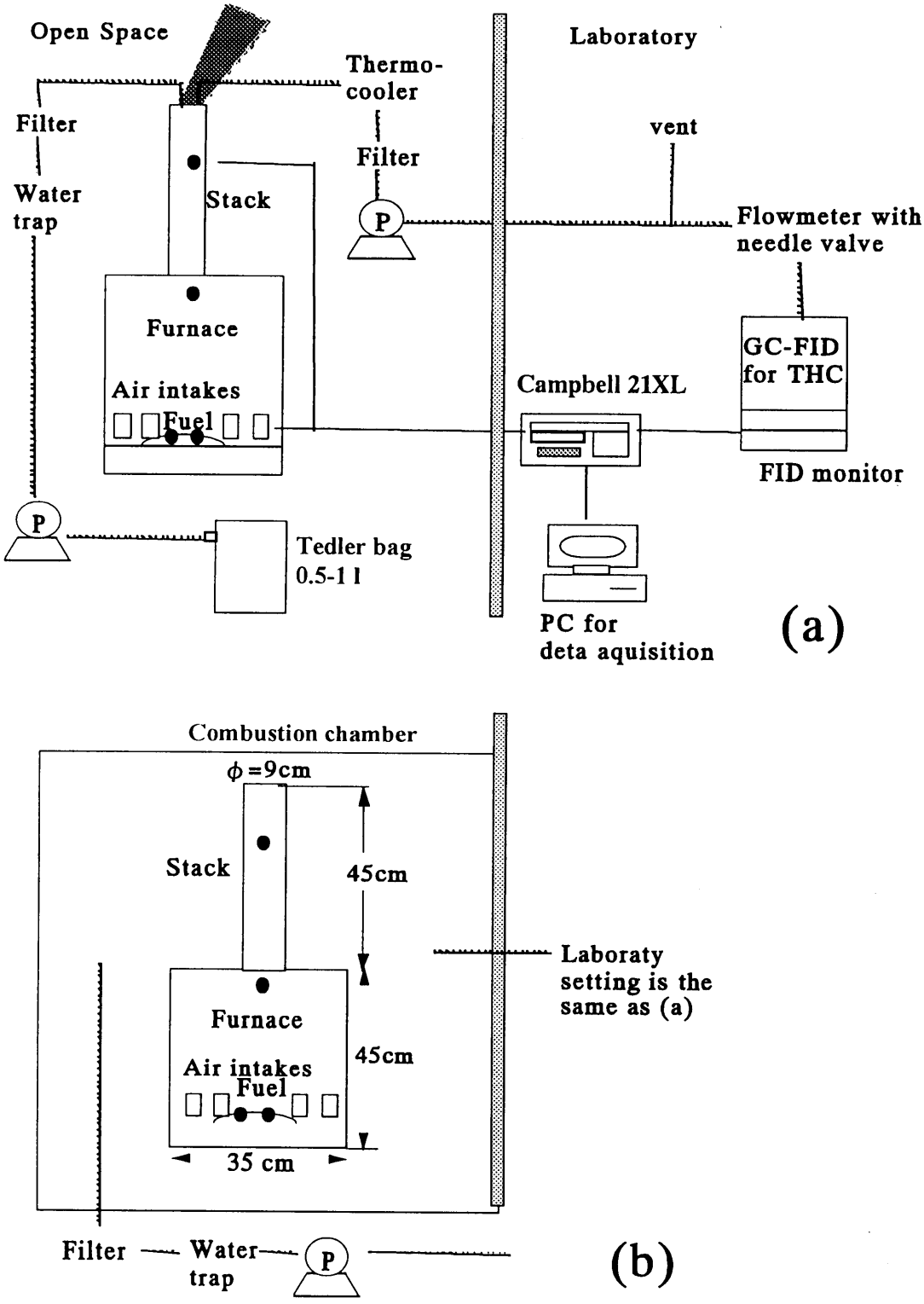

Figure 8.1 Schematic diagram of (a) the time-series experiment and (b) the total gas emission experiment. Gas and data flows were expressed as wavy and solid lines, respectively. Thermocouple thermometers were installed at sites shown by black circles ●. In (a), gas sampling was conducted in the stack whereas in (b), gas sampling was conducted in the mid-level of the chamber.

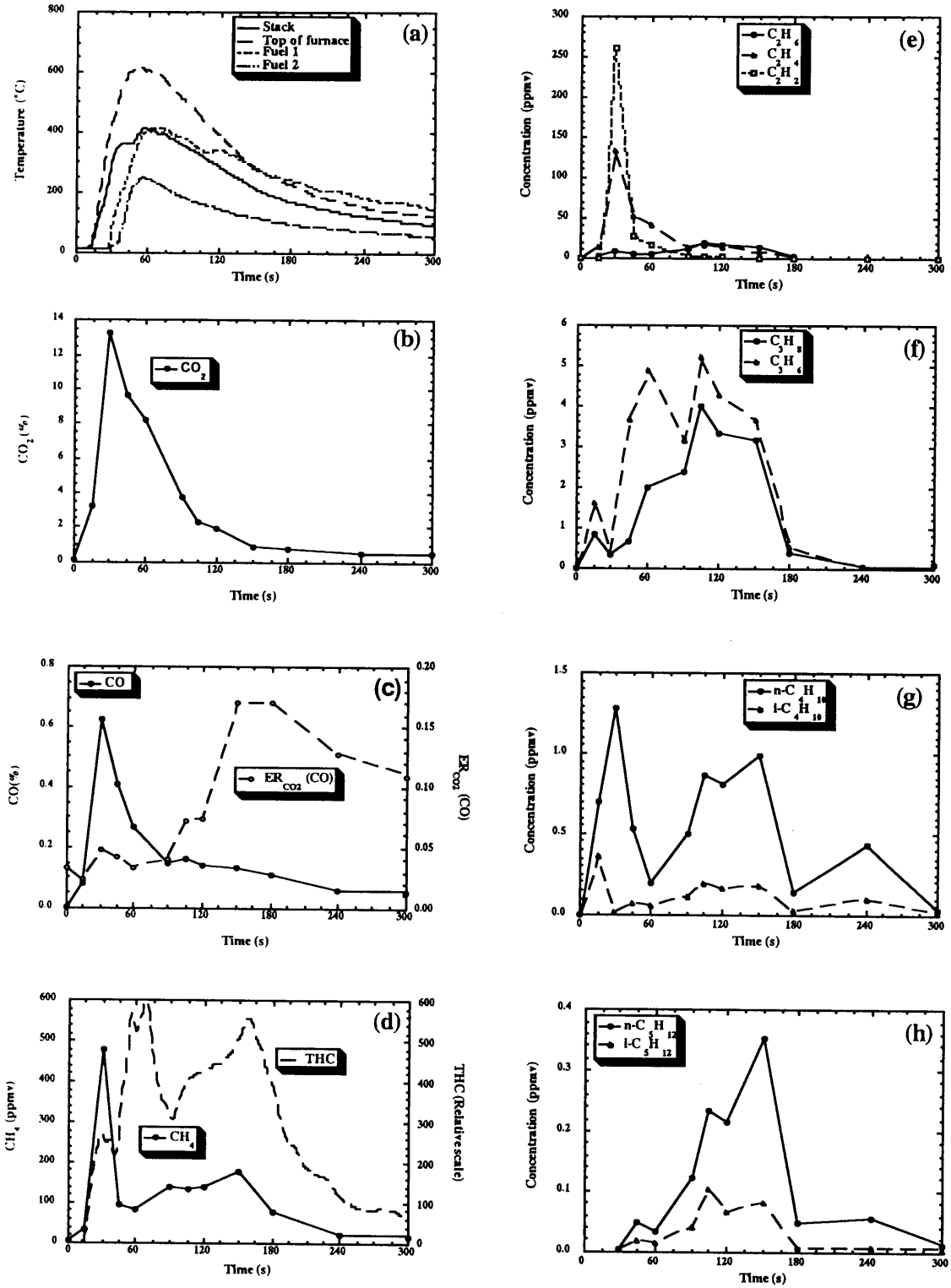

Figure 8.2 Time-series of combustion experiments in case 1 for (a) temperature, (b) CO_2, (c) CO and $ER_{CO2}(CO)$, (d) CH_4 and THC, (e) C_2 gas species, (f) C_3 gas species, (g) C_4 gas species, and (h) C_5 gas species. Time = 0 means time of ignition. Time of gas concentration means time of initial gas sampling.

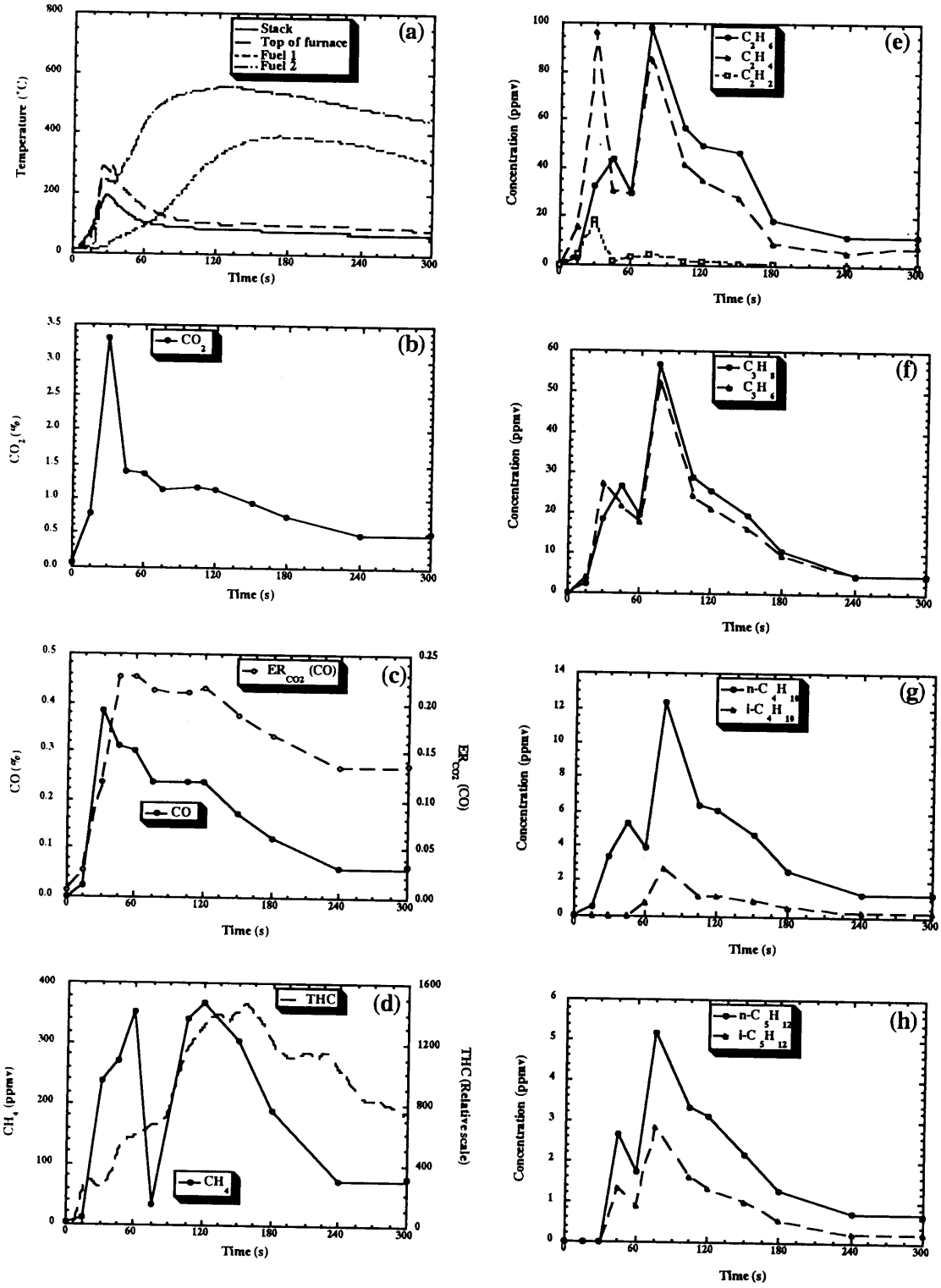

Figure 8.3 Time-series of combustion experiments in case 2 for (a) temperatures, (b) CO_2, (c) CO and $ER_{CO2}(CO)$, (d) CH_4 and THC, (e) C_2 gas species, (f) C_3 gas species, (g) C_4 gas species, and (h) C_5 gas species. Time = 0 means time of ignition.

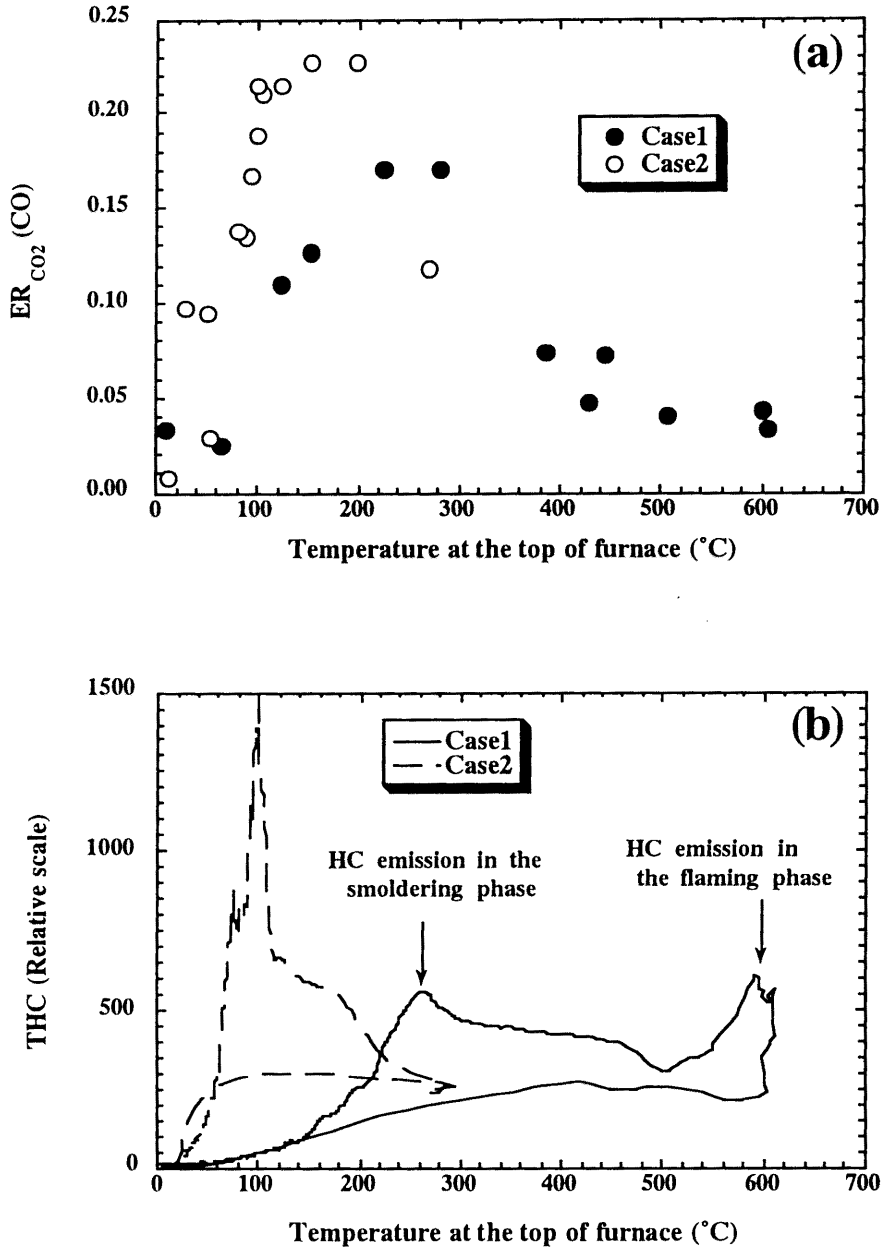

Figure 8.4 Relationship between the temperature at the top of the furnace and (a) $ER_{CO2}(CO)$ and (b) THC. The temperature at this site was chosen because it was considered to represent the variation in average temperature in the furnace. Hence, temperature is a proxy for relative combustion condition.

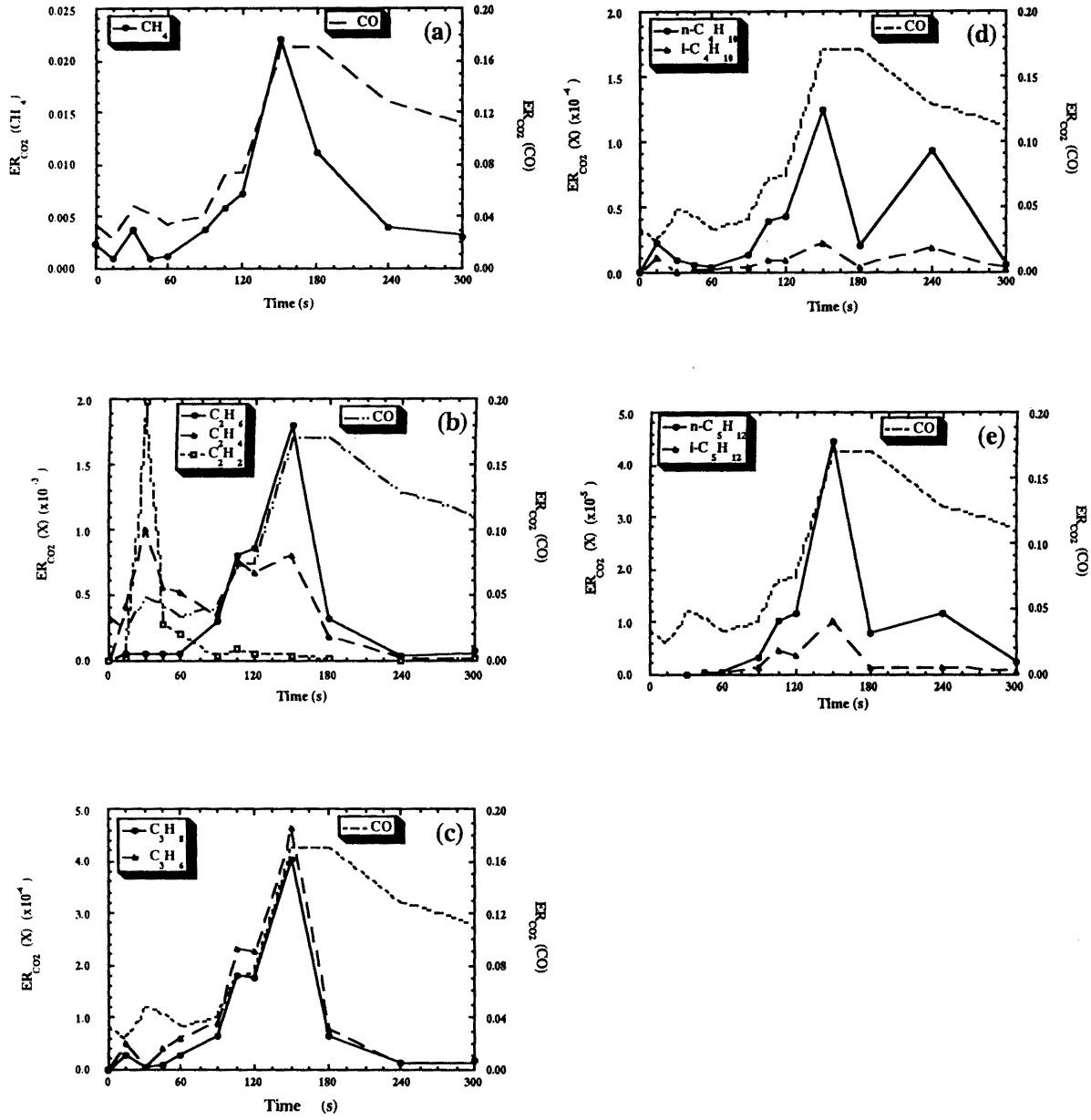

Figure 8.5 Time-series of the ratio of gases to ΔCO_2 in case 1 for (a) CH_4, (b) C_2 gas species, (c) C_3 gas species, (d) C_4 gas species, and (e) C_5 gas species. For reference, $ER_{CO2}(CO)$ is shown in all graphs.

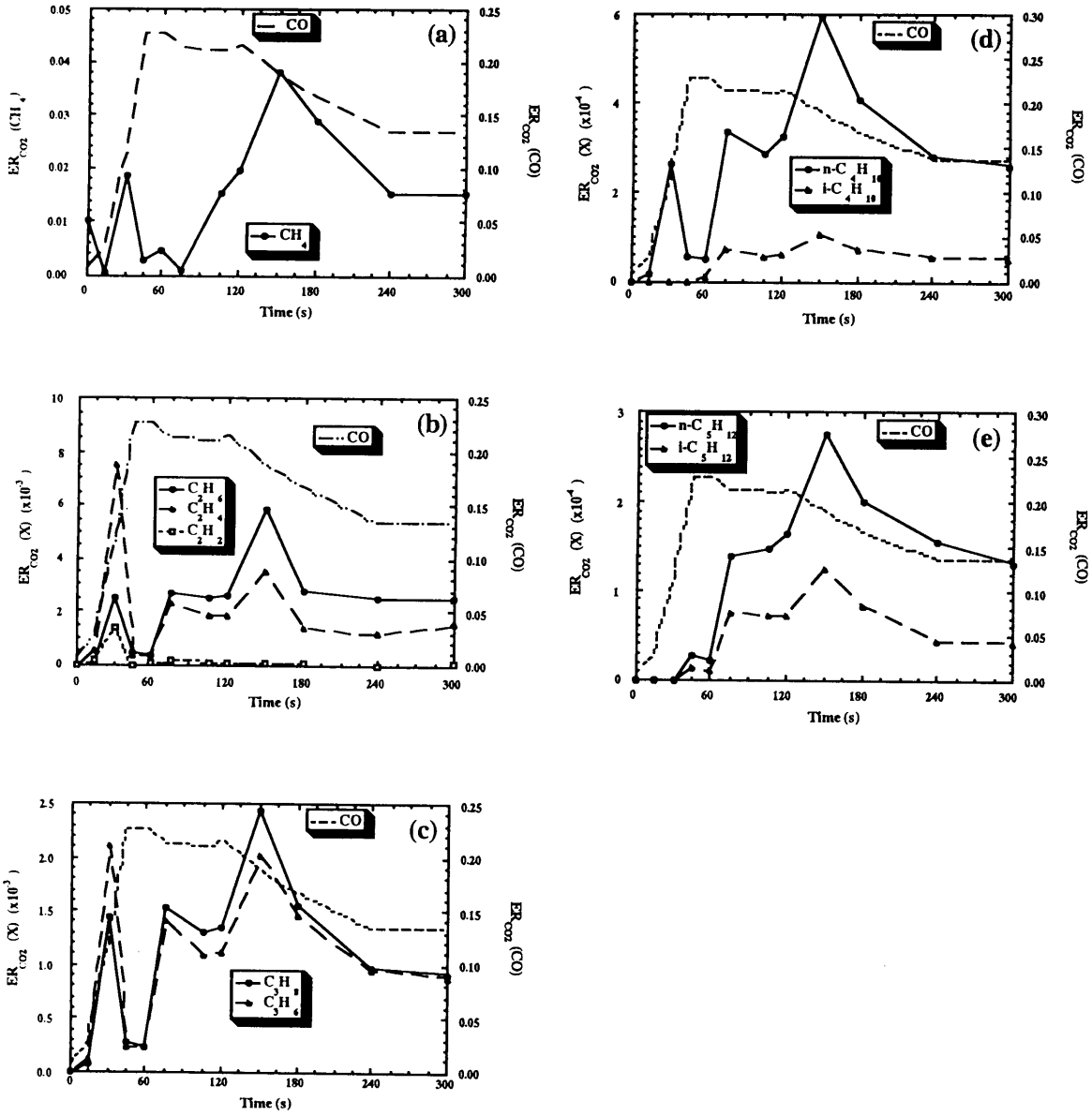

Figure 8.6 Time-series of the ratio of gases to ΔCO_2 in case 2 for (a) CH_4, (b) C_2 gas species, (c) C_3 gas species, (d) C_4 gas species, and (e) C_5 gas species. For reference, $ER_{CO2}(CO)$ is shown in all graphs.

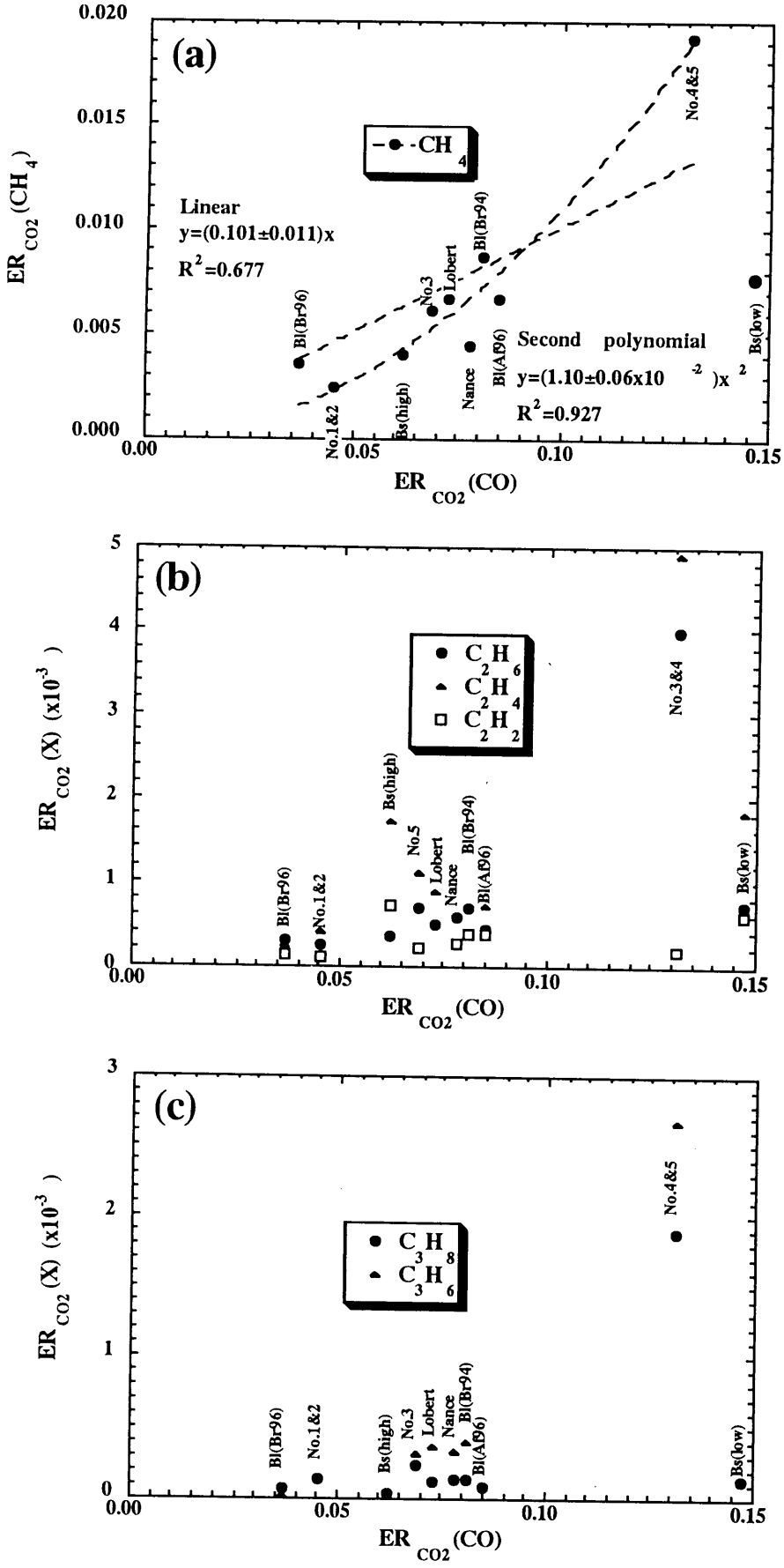

Figure 8.7 continues to next page.

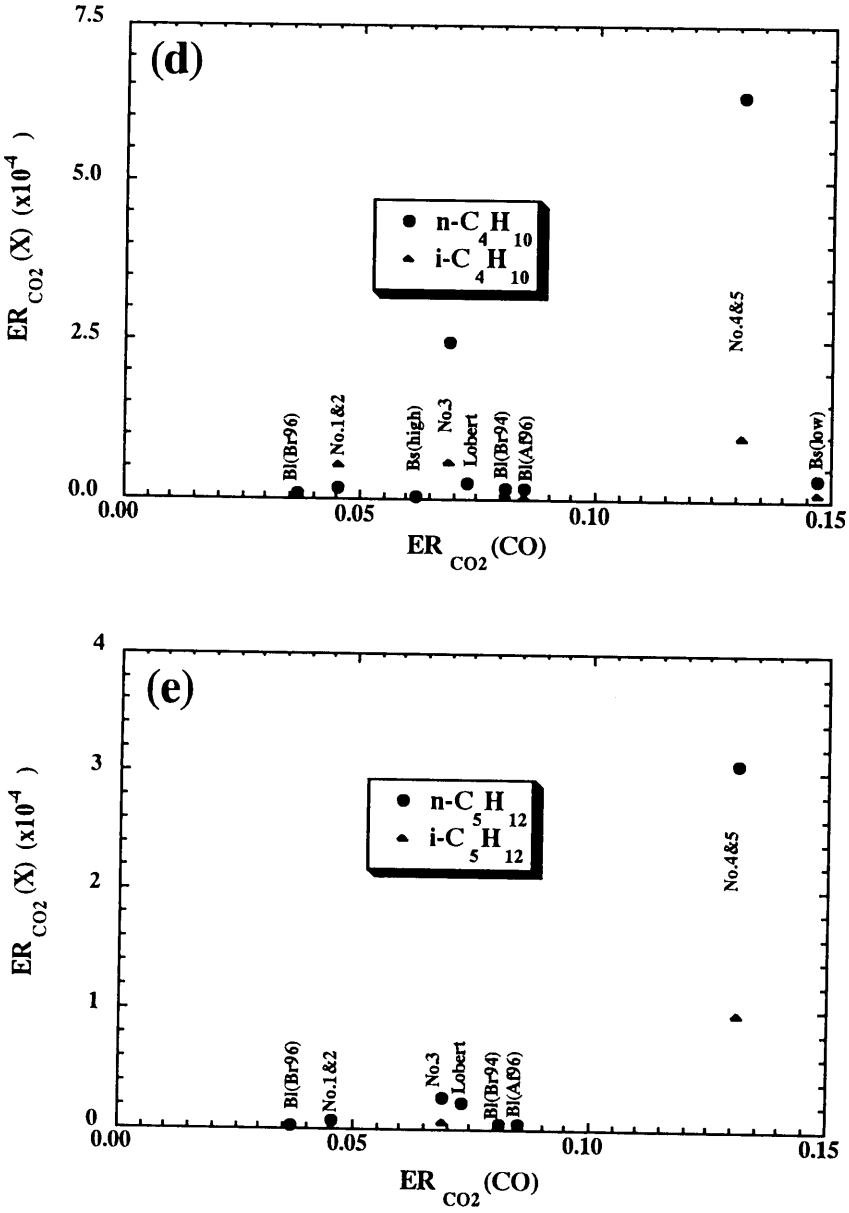

Figure 8.7 Relationship between $ER_{CO2}(CO)$ and $ER_{CO2}(X)$ of our experimental results and other reports for (a) CH_4, (b) C_2 gas species, (c) C_3 gas species, (d) C_4 gas species, and (e) C_5 gas species. Numbers correspond to those in Table 8.1. Bl = Blake et al. (1996) where Br and Af are Brazilian and African results, respectively, and 94 and 96 mean BFA and TRACE-A results, respectively; Bs = Bonsang et al. (1995); Lobert = Lobert et al. (1991); and Nance = Nance et al. (1993).

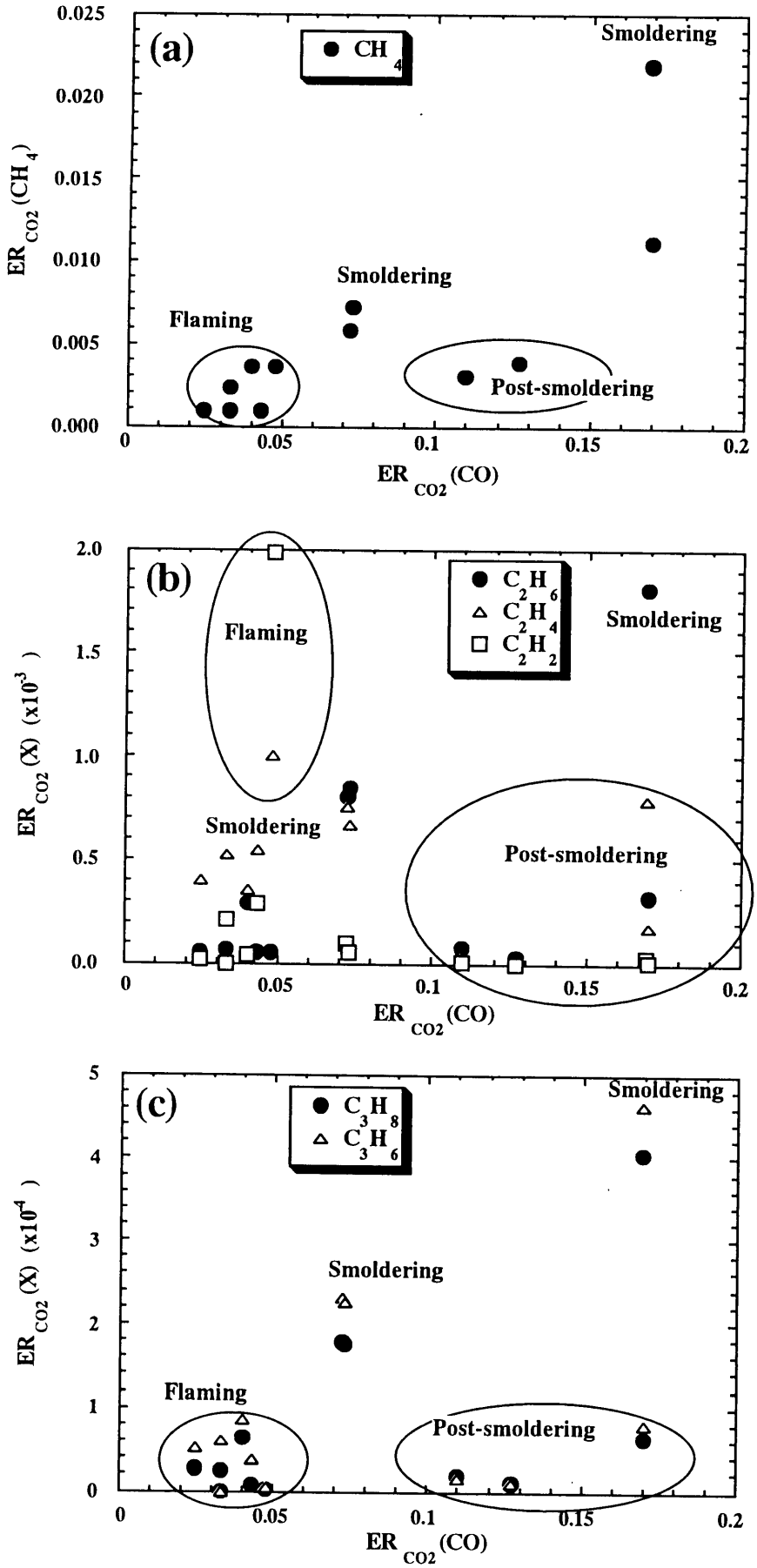

Figure 8.8 continues to next page.

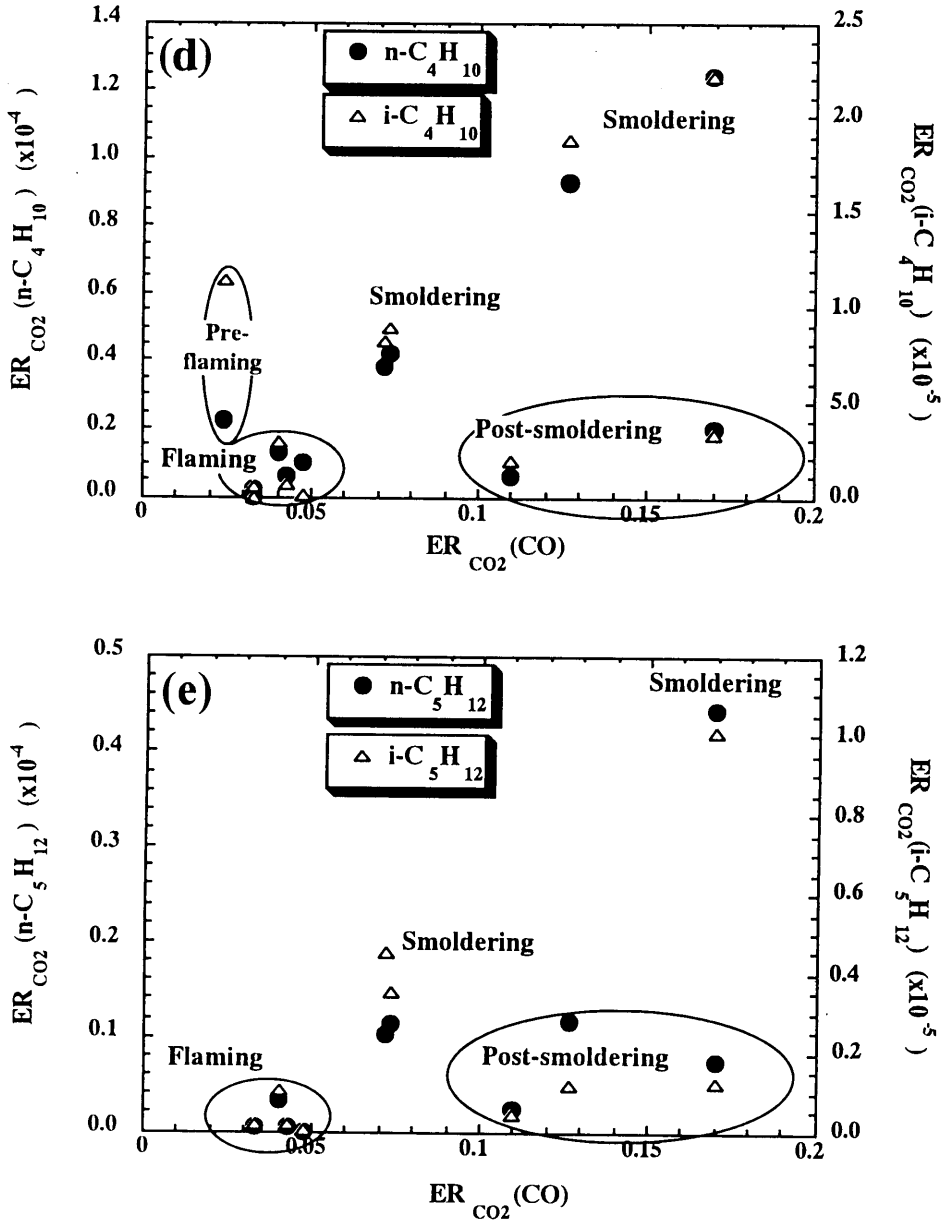

Figure 8.8 Phase diagrams of case 1 in relation to $ER_{CO2}(CO)$ for (a) CH_4, (b) C_2 gas species, (c) C_3 gas species, (d) C_4 gas species, and (e) C_5 gas species.

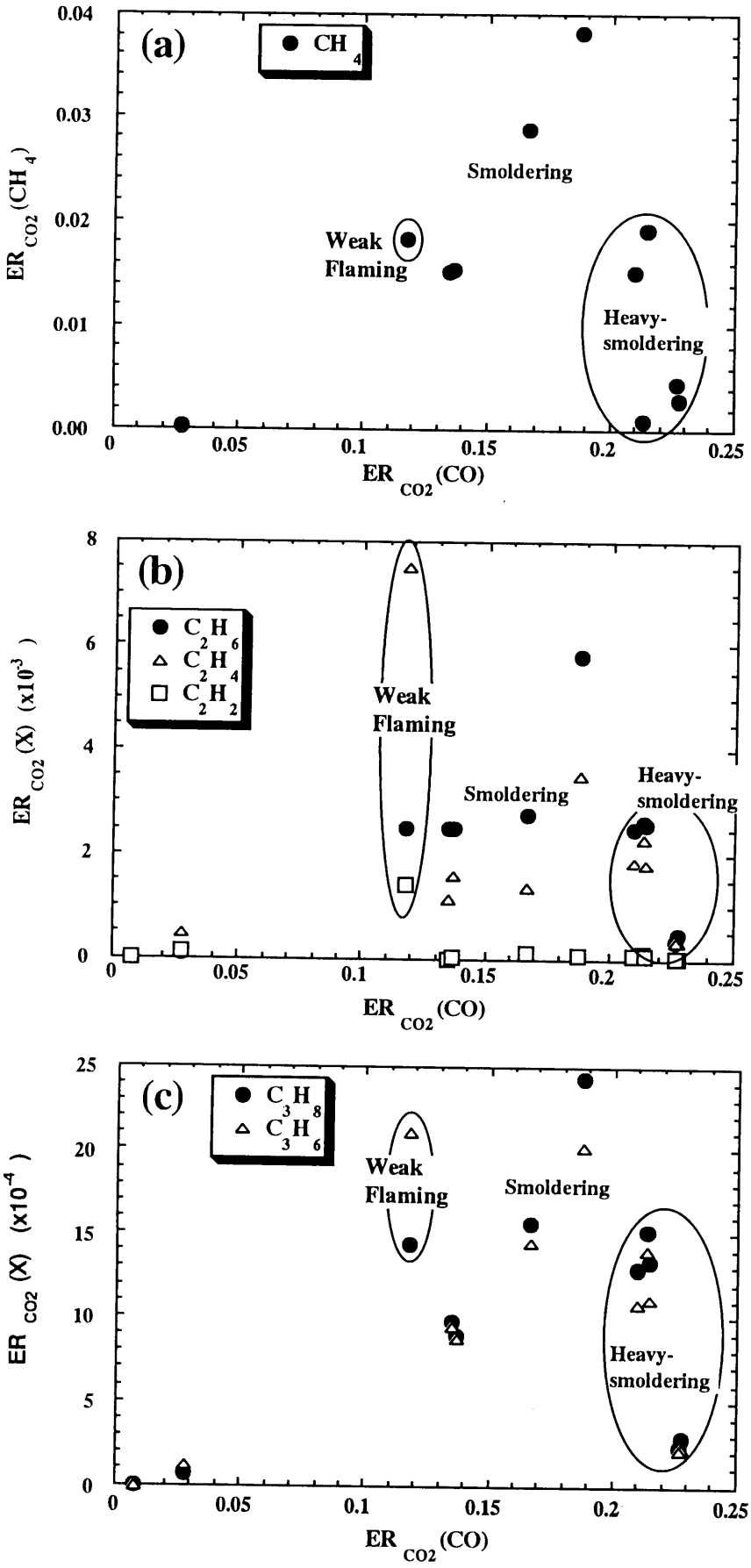

Figure 8.9 continues to next page.

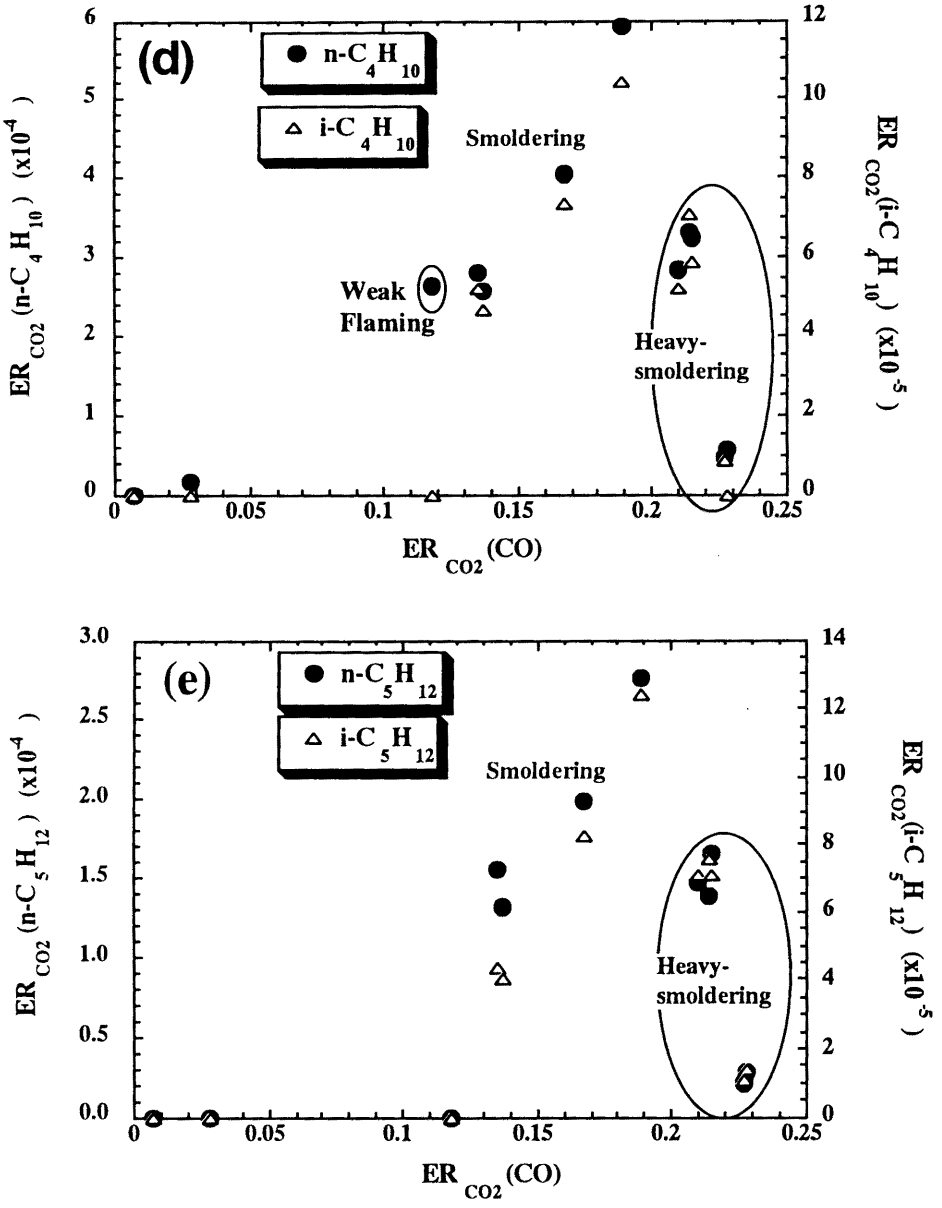

Figure 8.9 Phase diagrams of case 2 in relation to $ER_{CO2}(CO)$ for (a) CH_4, (b) C_2 gas species, (c) C_3 gas species, (d) C_4 gas species, and (e) C_5 gas species.

Chapter 9

Summary and Further Studies

9.1 Summary

The present study improved our understanding of CO and H_2 exchange between the atmosphere and the biosphere (CO and H_2 uptake by soils, CO photoproduction from plant leaves, and CO emission through biomass burning). The study also clarified that the exchange of CO and H_2 exchange is closely related to that of other gases such as CH_4 and other hydrocarbons.

The points accomplished in this study are summarized as follows:

(1) In Chapter 2, it was shown by a field experiment that CO and H_2 concentrations above a grassland were influenced by ground absorption, namely soil uptake. Deposition velocities of CO and H_2 estimated by micrometeorological techniques were generally comparable to those of previous studies. Therefore, soil uptake is a significant sink of CO and H_2.

(2) In Chapters 4 and 5, CO and H_2 uptake by soil was investigated by field measurements and model analysis. Field measurements showed that the deposition velocities of CO and H_2 were positively correlated each other both in the arable field and in the forest, indicating that CO and H_2 deposition velocities are both controlled by soil moisture. Model analysis as well as the field measurements showed that the gas diffusion from the atmosphere to soil is a rate-determining process for CO and H_2 uptake by soil (at least by soils in temperate climate), although CO and H_2 are biologically absorbed by soil.

(3) In Chapter 6, CO and H_2 soil uptake strengths were estimated globally over 1.0° latitude by 1.0° longitude grids using a model incorporating diffusion and biological processes in the soil that were investigated in Chapters 4 and 5. H_2 uptake by soil is found to be very important to explain spatial distribution and seasonal variation of H_2 concentrations in the atmosphere.

(4) In Chapter 7, laboratory experiments were conducted to understand CO emission from vegetation. The results of the experiments showed that CO photoproduction from leaves is a photooxidation process, that the CO photoproduction rate is dependent on O_2 concentration and increases linearly with light intensity, and that CO photoproduction from senescent leaves is about 10 times as large as that from live leaves.

(5) In Chapter 8, combustion experiments were conducted to understand CO emission from combustion processes. The CO emission rate was closely related to duration of inefficient combustion and those of CH_4 and other light hydrocarbons.

9.2 Further studies

Although this study gave light on exchange processes of CO and H_2 between the atmosphere and the biosphere, there still remains further studies.

9.2.1 Soil uptake

Data of deposition velocities from different ecosystems are limited as yet. In the arable field, soil conditions vary with agricultural management practices. Extensive studies are needed to analyze effects of various factors, including agricultural management practices, on deposition velocities of these gases. In the forest, laminar structures such as leaf, humic, and mineral soil layers should be investigated more mechanically, and the variation in deposition velocities of these gases resulting from the ecological transition caused by land use change should be investigated.

Because CO and H_2 are oxidized in the soil layer very close to the surface, it is important to investigate the effect of soil moisture and fertilization, as well as temperature, on the activity of oxidizers. Top soil moisture, which was determined by the balance of evaporation and the upward transport of water from deeper soil, should be extremely important to the deposition process because of its influence on soil diffusivity and in-situ uptake ability of oxidizers. In-situ measurements of soil diffusivity in the top soil (Ball et al., 1997a) , may be useful to understand more about the deposition process onto soil because diffusivity of the

very top soil can be measured in the field. In addition, note that gas exchange in near-surface soil may be driven not only by molecular diffusion but also by the mixing due to wind (Ishihara et al., 1992); this may considerably enhance the CO and H_2 uptake by soil.

The model shown in Chapter 5 revealed the gas transport aspect of CO and H_2 uptake by soil, but it is conceptual and tentative one at this stage. There are many aspects to be improved. In particular, the water transport process in near-surface soil should be incorporated into the model.

The model shown in Chapter 6 qualitatively describes the global uptake strengths of CO, H_2, and CH_4 well. However, the model includes many assumptions to be validated by the measurements in various ecosystems. More fundamental understanding of soil uptake properties in relation to soil moisture is required because soil moisture in arid regions is an important factor regulating global uptake of CO, H_2, and CH_4. The vertical distribution of in-situ uptake activities should be explicitly incorporated into the model as well.

There exists large gap between H_2 uptake strength by a simulation using process-based model in this study and those by hydrogen isotope study (Chapter 6). To reduce the gap between the two methods, it is necessary to obtain much more reliable values of deuterium contents from various sources as well as to improve our model. For example, no data is available on the deuterium contents of hydrogen molecules emitted from biomass burning.

The estimate of CO concentration in the boundary layer, namely ambient concentration for soil uptake is desired to estimate global uptake strengths of CO because the uncertainty in the CO concentration directly lead to be an ambiguous estimation of global CO uptake strengths.

9.2.2 CO photoproduction from vegetation

The production of CO within the leaf remains a matter for discussion. Abiological CO production is common in all natural organic sources and are poorly understood. Systematic explanation of CO dark (thermal) production and photoproduction from plants under various conditions is needed to estimate the production of CO by vegetation.

It is noteworthy that oxygenated hydrocarbons such as acetone are also photoproduced from dead plant matters (Warneke et al., 1999). Systematic understanding of emission of oxygenated hydrocarbon is needed. CO is probably a key gas in the photoproduction of other

carbon gases from dead plant matters as well as from the combustion processes.

For further detailed and exact global estimation of CO emission from vegetation, the distribution of dead biomass, for example, by remote sensing, is also necessary.

9.2.3 Biomass burning

As shown by this study, CO emission from biomass burning should be regarded as an intermediate product in the oxidation process from organic matters. Hence, to understand CO emission from biomass burning more mechanically, the analysis of hydrocarbons are essential. The light hydrocarbons we investigated are basic, but they are only a subset of the hydrocarbons. Biomass burning emits many other compounds as gases or particles. The emissions of these compounds also should be investigated in view of the combustion phases.

Few studies have stressed on the combustion processes so far. The combustion phases we propose may not appear under different conditions of combustion and fuels. Furthermore, time-series of mass flow rate as well as gas concentrations should be incorporated to consider net emission of trace gases both in laboratory and field experiments. Experiments under controlled gas concentrations and temperature have not yet been done thoroughly. Further studies on the complex reactions are desirable, including radical reactions, to reveal the mechanism of trace gas emissions from biomass burning. In the process of biomass burning, CO is a critically important key parameter. It may be a prospective approach to incorporate technological understanding and modeling approach of combustion processes.

At the same time, investigations on amount of burnt biomass are much more necessary to synthetically estimate the influence of biomass burning on global atmospheric environment.

References

Adamsen, A.P.S. and King, G.M. 1993. Methane consumption in temperate and subarctic forest soils: Rates, vertical zonation, and responses to water and nitrogen. *Appl. Environ. Microb.* **59**, 485-490.

Andreae, M.O., Atlas, E., Cachier, H., Cofer, W.R., Harris, G.W., Helas, G., Koppmann, R., Lacaux, J.P. and Ward, D.E. 1996. Trace gas and aerosol emissions from Savanna fires. In *Global Biomass Burning* edited by J.S. Levine, Cambridge, MA, MIT Press, pp. 278-295.

Arif, M.A.S., Houwen, F. and Verstraete, W. 1996. Agricultural factors affecting methane oxidation in arable soil. *Biol. Fertil. Soils* **21**, 95-102.

Badr, O. and Probert, S.D. 1995a. Sources of atmospheric carbon monoxide. *Applied Energy* **49**, 145-195.

Badr, O. and Probert, S.D. 1995b. Sinks and environmental impacts for atmospheric carbon monoxide. *Applied Energy* **50**, 339-372.

Ball, B.C., Dobbie, K.E., Parker, J.P. and Smith, K.A. 1997a. The influence of gas transport and porosity on methane oxidation in soils. *J. Geophys. Res.* **102**, 23301-23308.

Ball, B.C., Smith, K.A., Klemedtsson, L., Brumme, R., Sitaula, B.K., Hansen, S., Priemé, A., MacDonald, J. and Horgan, G.W. 1997b. The influence of soil gas transport properties on methane oxidation in a selection of northern european soils. *J. Geophys. Res.* **102**, 23309-23317.

Bakwin, P.S., Tans, P.P., Zhao, C., Ussler III, W., and Quesnell, E. 1995. Measurements of carbon dioxide on a very tall tower. *Tellus* **47B**, 535-549.

Barlett, K.B., Sachse, G.W., Collins Jr., J.E., and Harriss, R.C. 1996. Methane in the tropical South Atlantic: Sources and distribution during the late dry season. *J. Geophys. Res.* **101**, 24139-24150.

Bartholomew, G.W. and Alexander, M. 1982. Microorganisms responsible for the oxidation of carbon monoxide in soil. *Environ. Sci. Technol.* **16**, 300-301.

Bates, T.S., Kelly, K.C., Johnson, J.E. and Gammon, R.H. 1995. Regional and seasonal variations in the flux of oceanic carbon monoxide to the atmosphere. *J. Geophys. Res.* **100**, 23093-23101.

Batschauer A., 1993. A plant gene for photolyase, an enzyme catalyzing the repair of UV-light-induced DNA damage. *Plant Journal* **4**, 705-709.

Bauer, K., Conrad, R. and Seiler, W. 1980. Photooxidative production of carbon monoxide by phototrophic microorganisms. *Biochimica et Biophysica Acta* **589**, 46-55.

Baulch, D.L., Cobos, C.J., Cox, R.A., Esser, C., Frank, P., Just, Th., Kerr, J.A., Pilling, M.J., Troe, J., Walker, R.W. and Warnatz, J. 1992. Evaluated kinetic data for combustion modelling. *J. Phys. Chem. Ref. Data* **21**, 411-734.

Bédard, C. and Knowles, R. 1989. Physiology, biochemistry, and specific inhibitors of CH_4, NH_4^+, and CO oxidation by methanotrophs and nitrifiers. *Microbiol. Rev.* **53**, 68-84.

Bekku, Y., Koizumi, H., Nakadai, T. and Iwaki, 1995. Measurement of soil respiration using closed chamber method: An IRGA technique. *Ecological Research* **10**, 369-373.

Bender, M. and Conrad, R. 1993. Kinetics of methane oxidation in oxic soils. *Chemosphere* **26**, 687-696.

Bender , M. and Conrad, R. 1994a. Microbial oxidation of methane, ammonium and carbon monoxide, and turnover of nitrous oxide and nitric oxide in soils. *Biogeochemistry* **27**, 97-112.

Bender, M. and Conrad, R. 1994b. Methane oxidation activity in various soils and freshwater sediments: occurrence, characteristics, vertical profiles, and distribution on grain size fractions. *J. Geophys. Res.* **99**, 16531-16540.

Bidwell, R. G. S. and Fraser, D. E. 1972. Carbon monoxide uptake and metabolism by leaves. *Canadian Journal of Botany* **50**, 1435-1439.

Blake, N.J., Blake, D.R., Collins, J.E., Sachse, G.W., Anderson, B.E., Brass, J.A., Riggan, P.J. and Rowland, F.S. 1996. Biomass burning emissions of atmospheric methyl halide and hydrocarbon gases in the south Atlantic region. In *Global Biomass Burning* edited by J.S. Levine, Cambridge, MA, MIT Press, pp. 575-594.

Blake, D.R., Smith, T.W., Chen, T.Y., Whipple, W.J. and Rowland, F.S. 1994. Effects of biomass burning on summertime nonmethane hydrocarbon concentrations in the Canadian welands. *J. Geophys. Res.* **99**, 1699-1719.

Bonsang, B., Lambert, G. and Boissard, C.C. 1991. Light hydrocarbons emissions from africa savanna burnings. In *Global Biomass Burning* edited by J.S. Levine, Cambridge, MA, MIT Press, pp. 155-161.

Bonsang, B., Boissard, C.C., Cloarec, M.F.L., Rudolph, J. and Lacaux, J.P. 1995. Methane, carbon monoxide and light non-methane hydrocarbon emissions from african savanna burnings during the FOS/DECAFE experiment. *J. Atmos. Chem.* **22**, 149-162.

Born, M., Dörr, H. and Levin, I. 1990. Methane consumption in aerated soils of the temperate zone. *Tellus* **42B**, 2-8.

Bouwman, A.F. 1990. Exchange of greenhouse gases between terrestrial ecosystems and the atmosphere. In *Soils and the Greenhouse Effect* edited by A.F. Bouwman, Wiley. Chichester, U.K., pp.61-127.

Castro, M.S., Steudler, P.A., Melillo, J.M., Aber, J.D., and Bowden, R.D. 1995. Factors controlling atmospheric methane consumption by temperate forest soils. *Global Biogeochem. Cycles* **9**, 1-10,.

Cofer III, W.R., Levine, J.S., Sebacher, D.I., Winstead, E.L., Riggan, P.J., Stocks, B.J., Brass, J.A., Ambrosia, V.G. and Boston, P.J. 1989. Trace gas emissions from chaparral and boreal forest fires. *J. Geophys. Res.* **94**, 2255-2259.

Conrad, R. 1988. Biogeochemistry and ecophysiology of atmospheric CO and H_2. *Adv. Microb. Ecol.* **10**, 231-283.

Conrad, R. 1996. Soil microorganisms as controllers of atmospheric trace gases (H_2, CO, CH_4, OCS, N_2O, and NO). *Microbiol. Rev.* **60**, 609-640.

Conrad, R. and Seiler, W. 1980a. Contribution of hydrogen production by biological nitrogen fixation to the global hydrogen budget. *J. Geophys. Res.* **85**, 5493-5498.

Conrad, R. and Seiler, W. 1980b. Role of microorganisms in the consumption and production of atmospheric carbon monoxide by soil. *Appl. Environ. Microb.* **40**, 437-445.

Conrad, R. and Seiler, W. 1982. Arid soils as a source of atmospheric carbon monoxide. *Geophys. Res. Lett.* **9**, 1353-1356.

Conrad, R., Weber, M. and Seiler, W. 1983. Kinetics and electron transport of soil hydrogenases catalyzing the oxidation of atmospheric hydrogen. *Soil Boil. Biochem.*. **15**, 167-173.

Conrad, R. and Seiler ,W. 1984. Destruction and production rates of carbon monoxide in arid soils under field conditions. In *Planetary Ecology* edited by D.E. Caldwell, C.L. Brieler and J.A. Brierley, Van Nostrand Reinhold, pp. 112-119.

Conrad, R. and Seiler, W. 1985a. Influence of temperature, moisture, and organic carbon on the flux of H_2 and CO between soil and atmosphere: field studies in subtropical regions. *J. Geophys.Res.* **90**, 5699-5709.

Conrad, R. and Seiler ,W. 1985b. Characteristics of abiological carbon monoxide formation from soil organic matter, humic acids, and phenolic compounds. *Envir. Sci. Technol.* **19**, 1165-1169.

Conrad, R., Seiler ,W., Bunse, G. and Giehl, H. 1982. Carbon monoxide in seawater (Atlantic ocean). *J. Geophys. Res.* **87**, 8839-8852.

Crill, P.M. 1991. Seasonal patterns of methane uptake and carbon dioxide release by a temperate woodland soil. *Global Biogeochem. Cycles* **4**, 319-334.

Crill, P.M., Butler, J.H., Cooper, D.J. and Novelli, P.C. 1995. Standard analytical methods for measuring trace gases in the environment. In *Biogenic trace gases: Measuring emissions from soil and water* edited by P.A. Matson and R.C. Harris, Blackwell Science, Cambridge MA, pp. 164-205.

Crutzen, P.J. and Andreae, M.O. 1990. Biomass burning in the tropics: Impact on atmospheric chemistry and biogeochemical cycles. *Science* **250**, 1669-1678.

Crutzen, P.J., Delany, A.C., Greenberg, J., Haagenson, P., Heidt, L., Lueb, R., Pollock, W., Seiler, W., Wartburg, A. and Zimmerman, P. 1985. Tropospheric chemical composition measurements in Brazil during the dry season. *J. Atmos. Chem.* **2**, 233-256.

Crutzen, P.J. and Zimmermann, P.H. 1991. The changing photochemistry of the troposphere. *Tellus* **43**, 136-151.

Czepiel, P.M., Crill, P.M. and R.C. Harris, R.C. 1995. Environmental factors influencing the variability of methane oxidation in temperate zone soils. *J. Geophys. Res.* **100**, 9359-9364.

Delmas, R.A., Marenco, A., Tathy, J.P., Cros, B. and Baudet, J.G.R. 1991. Sources and sinks of methane in the african savanna. CH_4 emissions from biomass burning. *J. Geophys. Res.* **20**, 7287-7299.

Denmead, O.T., 1994. Measuring fluxes of greenhouse gases between rice fields and the atmosphere. In *Climate Change and Rice*. edited by Peng, S. et al., Springer-Verlag, Berlin, pp. 15-29.

Dlugokencky, E.J., Steel, L.P., Lang, P.M. and Masarie, K.A. 1994. The growth rate and distribution of atmospheric methane. *J. Geophys. Res.* **99**, 17021-17043.

Dobbie, K.E. and Smith, K.A. 1996. Comparison of CH_4 oxidation rates in woodland, arable and set aside soils. *Soil Biol. Biochem.* **28**, 1357-1365.

Dong, Y., Scharffe, D., Lobert, J.M., Crutzen, P.J. and Sanhueza, E. 1998. Fluxes of CO_2, CH_4 and N_2O from a temperate forest soil: the effects of leaves and humus layers. *Tellus* **50B**, 243-252.

Dörr, H., Katruff, L., and Levin, I. 1993. Soil texture parameterization of the methane uptake in aerated soils. *Chemosphere* **26**, 697-713.

Duggin, J. A. and Cataldo, D. A. 1985. The rapid oxidation of atmospheric CO to CO_2 by soils. *Soil. Biol. Biochem.* **17**, 469-474.

Dyre, A.J., Hicks, B.B. 1970. Flux-gradient relationships in the constant flux layer. *Quart. J. Roy. Meteorol. Soc.* **96**, 715-721.

Ehhalt, D.H. 1999. Gas phase chemistry of the troposphere. In *Global aspects of atmospheric chemistry* edited by R. Zellner, Springer, New York, pp.21-109.

Ehhalt, D.H., Davidson, J.A., Cantrell, C.A., Frieman, I. and Tyler, S. 1989. The kinetic isotope effect in the reaction of H_2 with OH. *J. Geophys. Res.* **94**, 9831-9836.

Ehhalt, D.H. and Schmidt, U. 1977. Vertical profiles of molecular hydrogen in the troposphere and stratosphere. *J. Geophys.Res.* **82**, 5907-5911.

Ehhalt, D.H. and Volz, A. 1976. Coupling of the CH_4 with the H_2 and CO cycle: Isotopic evidence. In *Microbial producrion and utilization of gases* edited by H.G. Schlegel, G. Gottschalk, and N. Pfenning, Goltze, Götingen, Germany, 23-33.

EPA (US Environmental Protection Agency) 1992. Global Ecosystems Database, United States Department of Commerce, Boulder.

Fehsenfeld, F. 1995. Measurement of chemically reactive trace gases at ambient concentrations. In *Biogenic trace gases: Measuring emissions from soil and water* edited by P.A. Matson and R.C. Harris, Blackwell Science, Cambridge MA, pp. 206-258.

Fischer, K. and Lüttge, U. 1978. Light-dependent net production of carbon monoxide by plants. *Nature* **275**, 740-741.

Fishman, J. and Crutzen, P. J. 1978. The origin of ozone in the troposphere. *Nature* **274**, 855-858.

Freyer, H.-D. 1979. Atmospheric cycles of trace gases containing carbon. In *The Global Carbon Cycle* edited by B. Bolin, E.T. Degens, S. Kempe and P. Ketner. Wiley, Chichester, UK, pp.101-28.

Fukumoto, M. 1999. Study of evaporation from bare soil surfaces and surface soil moisture. *Res. Bull. Hokkaido Natl. Agric. Exp. Stn.* **169**, 15 (In Japanese with Englsigh summary).

Fung, I. and Prather, M. 1990. Greenhouse gas trends. In *Policy Options for Stabilizing Global Climate* edited by D.A. Lashof and D.A. Tirpak, Hemisphere Publishing Corporation, New York, pp.32-99.

Gammon, R., Wofsy, S.C., Cicerone, R.J., Delany, A.C., Harris, R.T., Khalil, M.A.K., Logan, J.A., Midgley, P. and Prather, M. 1986. Tropospheric trace gases: sources, distributions and trends. In *Atmospheric Ozone 1985: Assessment of our Understanding of the Processes Controlling its Present Distribution and Change*, Report No16, Vol. 1. WMO, Geneva, pp.57-116.

Gerstle, R.W. and Kemnitz , D.A. 1967. Atmospheric emissions from open burning, *Journal of the air pollution control association* **17**, 324-327.

Goldman, M.B., Groffman, P.M., Pouyat, R.V., McDonnell, M.J. and Pickett, S.T. 1995. CH_4 uptake and N availability in forest soils along an urban to rural gradient. *Soil Biol. Biochem.* **27**, 281-286.

Hao, W.M. and Ward, D.E. 1993. Methane production from global biomass burning. *J. Geophys Res.* **20**, 20657-20661.

Hao, W.M., Ward, D.E., Olbu, G., Baker, S.P. and Plummer, R. 1996. Emissions of trace gases from fallow forests and woodland savannas. In *Global Biomass Burning* edited by J.S. Levine, Cambridge, MA, MIT Press, pp. 361-369.

Harriss, R.C., Sachse, G.W., Collins Jr., J.E., Wade, L., Bartlett, K.B., Talbot, R.W., Browell, E.V., Barrie, L.A., Hill, G.F., and Burney, L.G. 1994. Carbon monoxide and methane over Canada: July-August 1990. *J. Geophys. Res.* **99**, 1659-1669.

Hatano, R., Hasegawa, S. and Sakuma, T. 1995. Calibration for the measurement of soil water content using time domain reflectrometry. *Nihon Dojohiryo Kagaku Zasshi* **66**, 678-680 (in Japanese).

Heichel, G. H. 1973. Removal of carbon monoxide by field and forest soils. *Environ.Qual.* **2**, 419-423.

Hendrickson, O.Q., and Kubiseski, T., 1991. Soil microbial activity at high levels of carbon monoxide. *J. Environ, Qual.* **20**, 675-678.

Hütsch, B.W. 1996. Methane oxidation in soils of two long-term fertilization experiments in Germany. *Soil Biol. Biochem.* **28**, 773-782.

Hütsch, B.W., Webster, C.P. and Powlson, D.S. 1993. Long-term effects of nitrogen fertilization on methane oxidation in soil of the Broadbalk wheat experiment. *Soil Biol. Biochem.* **25**, 1307-1315.

Ingersoll, R.B., Inman, R.E. and Fischer, W.R. 1974. Soil's potential as a sink for atmospheric carbon monoxide. *Tellus* **26**, 151-159.

Ishihara, Y., Shimojima, E. and Harada, H. 1992. Water vapor transfer beneath bare soil where evaporation is influenced by a turbulent surface wind. *Journal of Hydrology* **131**, 63-204.

Johnson, J.E. and Bates, T.S. 1996. SOurces and sinks of carbon monoxide in the mixed layer of the tropical South Pacific Ocean. *Global Biogeochm. Cycles* **10**, 347-359.

Jones, H. G. 1992. Stomatal response to environment. In: *Plants and Microclimate* Cambridge, London, pp145-161.

Jones, R.D. and Morita, R.Y. 1983. Carbon monoxide oxidation by chemolithotrophic ammonium oxidizers. *Can. J. Microbiol.* **29**, 1545-1551.

Kaimal, J.C. and Finnigan, J.J. 1992. *Atmospheric Boundary Layer Flows-Their Structure and Measurement*, Oxford University Press, Oxford.

Keller, M., Mitre, M.E., and R.F. Stallard, R.F. 1990. Consumption of atmospheric methane in soils of Central Panama: Effects of agricultural development. *Global. Biogeochem. Cycles* **4**, 21-27.

Keller, M., Veldkamp, E., Weitz, A,M., and Reiners, W.A. 1993. Effect of pasture age on soil trace-gas emissions from a deforested area of Costa Rica. *Nature* **365**, 244-246.

Khalil, M. A. K. and Rasmussen, R. A. 1988. Carbon monoxide in the earth's atmosphere : Indications of global increase. *Nature* **332**, 242-245.

Khalil, M. A. K. and Rasmussen, R. A. 1990a. The global cycle of carbon monoxide: Trends and mass balance. *Chemosphere* **20**, 227-242.

Khalil, M. A. K. and Rasmussen, R. A. 1990b. Global increase of atmospheric molecular hydrogen. *Nature* **347**, 743-745.

Khalil, M. A. K. and Rasmussen, R. A. 1994. Global decrease in atmospheric carbon monoxide concentration. *Nature* **370**, 639-641.

King, G.M. 1992. Ecological aspects of methane oxidation, a key determination of global methane dynamics. In *Advances in Microbial Ecology* Vol 12., edited by K.C. Marshall, Plenum, New York, pp.431-468.

King, G.M. and Adamsen, A.P.S. 1992. Effects of temperature on methane consumption in a forest soil and in pure cultures of the Methanotroph *Methylomonas rubra*. *Appl. Environ. Microbiol.* **58**, 2758-2763.

Kirchhoff, V.W.J.H., Marinho, E.V.A., Dias, P.L.S., Pereira, E.B., Calheiros, R., Andre, R. and Volpe, C. 1991. Enhancemments of CO and O_3 from burnings in sufar cane fields. *J. Atmos. Chem.* **12**, 87-102.

Kolb, C.E., Wormhoudt, J.C. and Zahniser, M.S. 1995. Recent advaces in spectroscopic instrumentation for measuring stable gases in the natural environment. In *Biogenic trace gases: Measuring emissions from soil and water* edited by P.A. Matson and R.C. Harris, Blackwell Science, Cambridge MA, pp. 259-290.

Koppmann, R., Dülmer, C.P., Bamacher, B., Rudolph, J., Kunz, H., Melzer, D. and Speth, P. 1998. Measurements of carbon monoxide and nonmethane hydrocarbons during POPCORN, *J. Atmos. Chem.* **31**, 53-72.

Koschorreck, M. and Conrad, R. 1993. Oxidation of atmospheric methane in soil: measurements in the field, in soil cores and in soil samples. *Global Biogeochem. Cycle* **7**, 109-121.

Kuhlbusch, T.A.J. and Crutzen, P.J. 1996. Black carbon, the global carbon cycle, and atmospheric carbon dioxide. In *Global Biomass Burning* edited by J.S. Levine, Cambridge, MA, MIT Press, pp. 160-169.

Kuhlbusch, T.A.J., Zepp, R.G., Miller, W.L., Burke, Jr R.A. 1998. Carbon monoxide fluxes of different soil layers in upland canadian boreal forests. *Tellus* **50B**, 353-365.

Laursen, K.K., Hobbs, P.V. and Radke, L.F. 1992: Some trace gas emissions from north american biomass fires with an assessment of regional and global fluxes from biomass burning. *J. Geophys. Res.* **18**, 20687-20701.

Leemans, R. 1990. Possible changes in natural vegetation patterns due to a global warming, WP-08. International Institute for Applied Systems Analysis, Laxenburg Working Paper, IIASA, Laxenberg Austria, pp. 22.

Lenschow, D.H. 1995. Micrometeorological techniques for measuring biosphere-atmosphere trace gas exchange. In *Biogenic trace gases: Measuring emissions from soil and water* edited by P.A. Matson and R.C. Harris, Blackwell Science, Cambridge MA, pp. 126-163.

Lessard, R., Rochette, P., Topp, E., Pattey, E., Desjardins, R.L., and Beaumont, G. 1994. Methane and carbon dioxide fluxes from poorly drained adjacent cultivated and forest sites. *Can. J. Soil Sci.* **74**, 139-146.

Leuning, R. snf Moncrieff, J. 1990. Eddy-covariance CO_2 flux measurements using open- and closed-path CO_2 analyzers: Corrections for analyzer water vapor sensitivity and damping of fluctuations in air sampling tubes. *Boundary-Layer Meteorol.* **53**, 63-76.

Liebl, K.H. and Seiler, W. 1976. CO and H_2 destruction at the soil surface. In *Microbial producrion and utilization of gases* edited by H.G. Schlegel, G. Gottschalk, and N. Pfenning, Goltze, Götingen, Germany, pp. 215-229.

Livingstone, G.P. and Hutchinson, G.L. 1995. Enclosure-based measurement of trace gas exchange: applications and sources of error. In *Biogenic trace gases: Measuring emissions from soil and water* edited by P.A. Matson and R.C. Harris, Blackwell Science, Cambridge MA, pp. 14-51.

Lobert, J.M., Scharffe, D.H., Hao, W.M., Kuhlbusch, T.A., Seuwen, R., Warneck, P. and Crutzen, P.J., 1991: Experimental evaluation of biomass burning emissions: nitrogen and carbon containing compounds. In *Global Biomass Burning* edited by J.S. Levine, Cambridge, MA, MIT Press, pp. 289-304.

Logan, J. A., Prather, M. J., Wofsy, S. C. and McEltoy, M. B. 1981. Tropospheric chemistry:A global perspective. *J. Geophys. Res.* **86**, 7210-7254.

Lüttge, U. and Fischer, K. 1980. Light-dependent net CO evolution by C3 and C4 plants. *Planta* **149**, 59-63.

Marrero, T.R. and Mason, E.A. 1972. Gaseous diffusion coefficients. *J. Phys Chem. Ref. Data* **1**, 3-118.

Matsueda, H., Inoue, H.Y., Asanuma, I., Aoyama, M. and Ishii, M. 1997. Carbon monoxide and methane in surface seawater of the tropical Pacific ocean. In *Dynamics and Characterization of marine organic matter* edited by N. Handa, E. tanoue and T. Hama, Terra Scientific, Tokyo, pp. 209-231.

Matsueda, H., Inoue, H.Y., Sawa, Y., Tsutsumi, Y. and Ishii, M. 1998. Carbon monoxide in the upper troposphere over the western Pacific between 1993 and 1996. NOAA/CMDL and MRI/GRL. *J. Geophy. Res.* **103**, 19093-19110.

McElroy, M.B. and Wofsy, S.C. 1986. Tropical forests: interactions with the atmosphere. In *Tropical Rain Forests and the World Atmosphere*edited by G.T. Prance, Westview Press, Boulder, CO, pp.33-60.

McMahon, T.A. and P.J. Denison, P.J. 1979. Empirical atmospheric deposition parameters-a survey. *Atmos. Envir.* **13**, 571-585.

Migeotte, M.V. 1949. The fundamental band of carbon monoside at 4.7 microns in the solar spectrum. *Phys. Rev.* **75**, 1108-1109.

Millington, R.J. and Quirk, J.M. 1961. Permeability of porous solids. *Trans. Faraday Soc.* **57**, 1200-1207.

Minami, K., Goudriaan, J., Lantinga, E.A., and Kimura, T. 1993. Significance of grasslands in emission and absorption of greenhouse gases. In *Proceedings of the 17th International Grassland Congress*, pp. 1231-1238.

Miyata, A. 1998. Methane exchange between the land and the atmosphere. *A dissertation for the degree of Doctor of Science*, Graduate School of the University of Tokyo.

Miyata, A. Leuning, R., Denmead, O.T., Kim, J., and Harazono, Y. 2000. Carbon dioxide and methane fluxes from an intermittently flooded paddy field. *Agric. and Forest Meteorol.*, in press.

Miyoshi, A., Hatakeyama, S. and Washida, N. 1994. OH radical- initiated photooxidation of isoprene: An estimate of global CO production. *J. Geophys. Res.* **99**, 18779-18787.

Moore, C.J. 1986. Frequency response corrections for eddy correlation systems. *Boundary-Layer Meteorol.* **37**, 17-35.

Morison J. I. and Gifford R. M. 1983: Stomatal sensitivity to carbon dioxide and humidity. *Plant Physiology* **71**, 789-796.

Mosier, A., Schimel, D., Valentine, D., Bronson, L., and Parton, W. 1991. Methane and nitrous oxide fluxes in native, fertilized and cultivated grasslands. *Nature* **350**, 330-332.

Mosier, A., Parton, W.J., Valentine, D.W., Ojima, D.S., Schimel, D.S., and Delgado, J.A. 1996. CH_4 and N_2O fluxes in the Colorado shortgrass steppe: 1. Impact of landscape and nitrogen addition. *Global Biogeochem. Cycles* **10**, 387-399.

Mosier, A.R., Parton, W.J., Valentine, D.W., Ojima, D.S., Schimel, D.S. and Heinemeyer, O. 1997. CH_4 and N_2O fluxes in the Colorado shortgrass steppe 2. Long-term impact of land use change. *Global Biogeochem. Cycles* **11**, 29-42.

Moxley, J.M. and Smith, K.A. 1998a. Factors affecting utilisation of atmospheric CO by soils. *Soil Biol. Biochem.* **30**, 65-79.

Moxley, J.M. and Smith, K.A. 1998b. Carbon monoxide production and emission by some scottish soils. *Tellus* **50B**, 151-162.

Nance, J.D., Hobbs, P.V.and Radke, L.F. 1993. Airborne measurements of gases and particles from alaskan wildfire. *J. Geophys Res.* **98**, 14873-14882.

National Astronomical Observatory 1994. Science table., Maruzen, Tokyo, pp. 454. (in Japanese)

New, M., Hulme, M. and Jones, P. 1999. Representing twentieth century space-time climate variability II: development of 1901-1996 monthly grids of terrestrial surface climate. *J. Climate* , in press.

Nguyen, B.C., Mihalopoulos, N. and Putaud, J.P. 1994. Rice straw burning in southeast asia as a source of CO and COS to the atmospere. *J. Geophys. Res.* **20**, 16435-16439.

Nouchi I. and Kobayashi K. 1995. Effects of enhanced ultraviolet-B radiation with a modulated lamp control system on 17 rice cultivars in the field. *J. Agri. Meteor.* **51**, 11-20.

Novelli, P.C., Lang, P.M., Masarie, K.A., Hurst, D.F., Myers, R. and Elkins, J.W. 1999. Molecular hydrogen in the troposphere: Global distributions, trends, and budget. *J. Geophys. Res.* , in press.

Novelli, P.C., Masarie, K.A. and Lang, P.M. 1998. Distribution and recent changes of carbon monoxide in the lower troposphere. *J. Geophys. Res.* **103**, 19015-19033.

Novelli, P. C., Masarie, K. A., Tans, P.P. and Land, P.M. 1994. Recent changes in atmospheric carbon monoxide. *Science* **263**, 1587-1590.

Osozawa, S. and Hasegawa, S. 1995. Diel and seasonal changes in carbon dioxide concentration and flux in an andisol. *Soil Sci.* **160**, 117-124.

Peiser, G.D., Lizada, M.C.C. and Yang, S.F. 1982. Dark metabolism of carbon monoxide in lettuce disks. *Plant Physiol.* **70**, 397-400.

Pochanart, P., Hirokawa, J., Kajii, Y., Akimoto, H. and Nakao, M. 1999. Influence of regional-scale anthropogenic activity in northeast Asia on seasonal variations of surface ozone and carbon monoxide observed at Oki, Japan. *J. Geophys. Res.* **104**, 3621-3631.

Post, W.M., Pastor, J., Zinke, P.J. and Stangenberger, A.G. 1985. Global patterns of soil nitrogen storage. *Nature* **317**, 613-616.

Potter, C.S. and Klooster, S.A. 1997. Global model estimates of carbon and nitrogen storage in litter and soil pools: response to changes in vegetation quality and biomass allocation. *Tellus* **49B**, 1-17.

Potter, C.S.,Klooster, S.A. and Chatfield, R.B. 1996a. Consumption and production of carbon monoxide in soils: a global model analysis of spatial and seasonal variation. *Chemosphere* **33**, 1175-1193.

Potter, C.S., Davidson, E.A. and Verchot, L.V. 1996b. Estimation of global biogeochemical controls and seasonality in soil methane consumption. *Chemosphere* **32**, 2219-2246.

Priemé, A., and Christensen, S. 1997. Seasonal and spatial variation of methane oxidation in a Danish spruce forest. *Soil Biol. Biochem.* **29**, 1165-1172.

Priemé, A., Christensen, S., Dobbie, K.E. and Smith, K.A. 1997. Slow increase in rate of methane oxidation in soils with time following land use change from arable agriculture to woodland. *Soil Biol. Biochem.* **29**, 1269-1273.

Reichle., JR. G.R., Connors, V.S., Holland, J.A., Sherrill, R.T., Wallio, H.A., Casas, J.C., Condon, E.P., Gormsen, B.B. and Seiler, W. 1990. The distribution of middle tropospheric carbon monoxide during early October 1984. *J. Geophys. Res.* **95**, 9857-9871.

Ridgwell, A.J., Marshall, S.J. and Gregson, K. 1999. Consumption of atmospheric methane by soils: A process-based model. *Global Biogeochem. Cycles* **13**, 59-70.

Rust , R. H., Klute A. and Gieseking ,J. E. 1957. Diffusion-porosity measurements using a non-steady state system. *Soil Sci.* **84**, 453-463.

Sallam, A., Jury, W.A. and Jetey, J. 1984. Measurement of gas diffusion coefficient under relatively low air-filled porosity. *Soil Sci. Soc. Am. J.* **48**, 3-6.

Sanhueza, E., Donoso, L., Scarffe, D. and Crutzen, P.J. 1994a. Carbon monoxide fluxes from natural, managed, or cultivated savannah grasslands. *J. Geophys. Res.* **99**, 16421-16427.

Sanhueza, E., Cardenas, L., Donoso, L. and Santana, M. 1994b. Effect of plowing on CO_2, CO, CH_4, and NO fluxes from tropical savannah soils. *J. Geophys. Res.* **99**, 16429-16434.

Sanhueza, E., Dong, Y., Scharffe, D., Lobert, J.M. and Crutzen, P.J. 1998. Carbon monoxide uptake by temperate forest soils: effects of leaves and humus layers. *Tellus* **50B**, 51-58.

Savage, K., Moore, T.R. and Crill, P.M. 1997. Methane and carbon dioxide exchanges between the atmosphere and northern boreal forest soils. *J. Geophys. Res.* **102**, 29279-29288.

Saxton, K.E., Rawls, W.J., Romberger, J.S. and Papendick, R.I. 1986. Estimating generalized soil-water characteristics from texture. *Soil Sci. Soc. Am. J.* **50**, 1031-1036.

Scharffe, D., Hao ,W.M., Donoso, L., Crutzen, P.J. and Sanhueza, E. 1990. Soil fluxes and atmospheric concentration of CO and CH_4 in the northern part of the guayana shield, Venezuela. *J.Geophys. Res.* **95**, 22475-22480.

Schmidt, U. 1974. Molecular hydrogen in the atmosphere. *Tellus* **16**, 78-90.

Schmidt, U. 1978. The latitudinal and vertical distribution of molecular hydrogen in the troposphere. *J. Geophys.Res.* **83**, 941-946.

Schuler, S. and Conrad, R. 1991. Hydrogen oxidation activities in soil as influenced by pH, temperature, moisture, and season. *Biol. Fertil. Soils* **12**, 127-130.

Seiler, W. 1974. The cycle of atmospheric CO. *Tellus* **26**, 116-135.

Seiler, W. 1976. The cycle of carbon monoxide in the atmosphere. In *Proc. Joint International Conference on Environmental Sensing and Assessment*, Las Vegas, Vol.2., Section35-4, pp.1-9.

Seiler, W. and Conrad, R. 1987. Contribution of tropical ecosystems to the global budgets of trace gases, especially CH_4, H_2, CO and N_2O. In *Geophysiology of Amazonia* edited by R. Dickinson, John Wiley, New York, pp. 133-162.

Seiler, W. and Fishman, J. 1981. The distribution of carbon monoxide and ozone in the free troposphere. *J. Geophys. Res.* **86**, 7255-7265.

Seiler, W. , Giehl, H. and Bunse, G. 1978. The influence of plants on atmospheric carbon monoxide. *Pageoph*. **116**, 439-451.

Seiler, W., Giehl, H. and Roggendorf, P. 1980. Detection of carbon monoxide and hydrogen by conversion of mercury oxide to mercury vapor. *Atmospheric Techniques* **12**, 40-45.

Seiler, W. and Schmidt, U. 1974. New aspects of CO and H_2 cycles in the atmosphere. In *Proc. International Conference on the Structure, Composition and General Circulation of the Upper and Lower Atmospheres and Possible Anthropogenic Perturbations*, Melbourne, pp.192-222.

Seiler, W. and Warneck, P. 1972. Decrease of the carbon monoxide mixing ratio at the tropopause. *J. Geophys. Res.* **77**, 3204-3214.

Smith, K.A., Bremner, J.M. and Tabatabai, M.A. 1973. Sorption of gaseous atmospheric pollutants by soils. *Soil Sci.* **116**, 313-319.

Soil Management Support Services and USDA Soil Conservation Service and Japanese Committee of the Ninth International Soil Classification Workshop, 1987. Tour guide of Ninth international soil classification workshop: properties, classification, and utilization of andisols and paddy soils Kanto, Tohoku, and Hokkaido, Japan., Washington.

Spratt, H.G. and Hubbard, J.S. 1981. Carbon monoxide metabolism in roadside soils. *Appl. Environ. Microbiol.* **41**, 1192-1201.

Steudler, P.A., Bowden, R.D., Mellilo, J.M., and Aber, J.D. 1989. Influence of nitrogen fertilization on methane uptake in temperate forest soil. *Nature* **341**, 314-316.

Striegl, R.G. 1993. Diffusional limits to the consumption of atmospheric methane by soils. *Chemosphere* **26**, 715-720.

Striegl, R.G., McConnaughey, T.A., Thorstenson, D.C., Weeks, E.P. and J.C. Woodward, J.C. 1992. Consumption of atmospheric methane by desert soils. *Nature* **357**, 145-147.

Sudo, S., Yonemura, S., Tsututa, H., and Kawashima, S. 2000. Methyl halide emissions by biomass burning in a rural agricultural field. *J. Atmos. Chem.*, submitted.

Swinnerton, J.W. and Lamontagne, R.A. 1974. Carbon monoxide in the south Pacific ocean. *Tellus* **16**, 136-142.

Tanner, C. B. and Thurtell, G.W. 1969. Anemoclinometer measurements of Reynolds stress and heat transport in the atmospheric surface layer, final report. TR ECOM 66-G22-F, Univ. Wisconsin, Madison, WI. U.S.A.

Tarr, M.A., Miller, W.L. and Zepp, R.G. 1995. Direct carbon monoxide photoproduction from plant matter. *J. Geophys. Res.* **100**, 11403-11413.

Tate, C.M. and Striegl, R.G. 1993. Methane consumption and carbon dioxide emission in tallgrass prairie: Effects of biomass burning and conversion to agriculture. *Global Biogeochem. Cycles* **7**, 735-748.

Thompson, A.M., 1992. The oxidizing capacity of the Earthe's atmosphere: Probable past and future changes. *Science* **256**, 1157-1165.

Tie, X.X., Kao, C.-Y. J., and Mroz, E.J., 1992. Net yield of OH, CO, and O_3 from the oxidation of atmospheric methane. *Atmos. Envir.* **26A**, 125-136.

Topp, G.C., Davis, J.L. and Anman, A.P. 1982. Electromagnetic determination of soil water content using TDR: 1. Application to wetting fronts and steep gradients. *Soil Sci. Soc. Am. J.* **46**, 672-678.

Troxler, R. F., Dokos, J. M. 1973. Formation of carbon monoxide and bile pigment in red and blue-green algae. *Plant Physiology* **51**, 72-75.

United States Department of Agriculture, Soil Conservation Service 1994. Keys to Soil Taxonomy. 6th edition, Pocahontas, Blacksburg Virginia.

Volz, A., Ehhalt, D. H., and Derwent, R. G. 1981. Seasonal and latitudinal variation of ^{14}CO and the tropospheric concentration of OH radicals. *J. Geophys. Res.*, **86**, 5163-5171.

Warneck, P. 1988. *Chemistry of the Natural Atmosphere*, Academic press, San Diego CA.

Warneke, C., Karl, T., Judmaier, H., Hansel, A., Jordan, A., Lindinger, W. and Crutzen, P.J. 1999. Acetone, methanol, and other partially oxidized volatile organic emissions from plant dead matter by abiological processes: Significance for atmospheric HO_x chemistry. *Global Biogeochem. Cycles* **13**, 9-17.

Webb, E.K. 1970. Profile relationships: The log-linear range, and extension to strong stability. Quart. J. Roy. Meteorological. Soc. **106**, 85-100.

Webb, E.K, Pearman, G.I., and Leuning, R. 1980. Correction of flux measurements for density effects due to heat and water vapor transfer. *Quart. J. Roy.Meteorol. Soc.* **106**, 85-100.

Whalen, S.C. and Reeburgh, W.S. 1990. Consumption of atmospheric CH_4 by tundra soils. *Nature* **346**, 160-162.

Whalen, S.C. and Reeburgh, W.S. 1996. Moisture and temperature sensitivity of CH_4 oxidation in boreal soils. *Soil Biol. Biochem.* **28**, 1271-1281.

Whalen, S.C., Reeburgh, W.S. and Barber, V. 1992. Oxidation in boreal forest soils: A comparison of seven measures. *Biogeochemistry* **16**, 181-211.

World Meteorological Organization (WMO) 1995. *Scientific Assessment of Ozone Depletion:1994*, Global Ozone Research and Monitoring Project - Report No.37, World Meteorological Organization, Geneva.

Yonemura, S. and Iwagami, N. 1996. Infrared absorption measurement of carbon monoxide column abundance over Tokyo. *Atmos. Envir.* **30**, 3697-3703.

Yonemura, S. , Kawashima, S., and Tsuruta, H. 1999b. Continuous measurements of CO and H_2 deposition velocities onto an andisol: Uptake control by soil moisture. *Tellus* **51B**, 688-700.

Yonemura, S., Kawashima, S., and Tsuruta, H. 2000a. Carbon monoxide, hydrogen, and methane uptake by soils in a temperate arable field and a forest. *J. Geophys. Res.*, in press.

Yonemura, S., Miyata, A., and Yokozawa, M. 2000b. Concentrations of carbon monoxide and methane at two heights above a grass field and their deposition onto the field. *Atmos. Envir.*, submitted.

Yonemura, S., Morokuma, M., Kawashima, S., and Tsuruta, H. 1999a. Carbon monoxide photoproduction from rice and maize leaves. *Atmos. Envir.* **33**, 2915-2920.

Yonemura, S. and Yokozawa, M. 1999. A process-based model for the globa estimation of CH_4 and CO uptake strengths by soils. *World Resource Rev.*, in press.

Yonemura, S., Yokozawa, M, Kawashima, S., and Tsuruta, H. 2000c. Model analysis to the influence of soil gas diffusivity on CO and H_2 uptake by soil. *Tellus*, in press.

Yonemura, S., Yokozawa, M, Kawashima, S., and Tsuruta, H. 2000d. Trace gas absorption by soil. In *Computor methods on Flow and Transport in Porous Media*, in press.

Yonemura, S., Sudo, S., Tsuruta, H., and Kawashima, S. 2000e. Mechanism of carbon monoxide, carbon dioxide and light hydrocarbon emissions from the combustion of plant material. *J. Atmos. Chem.*, submitted.

Zander, R., Demoulin, Ph., Ehhalt, D. H., Shmidt, U., and Rinsland, C. P. 1989. Secular increase of the total vertical column abundance of carbon monoxide above central Europe since 1950. *J. Geophys. Res.* **94,** 11021-11028.

Zepp, R.G., Miller, W.L., Burke, R.A., Parsons, D.A.B. and Scholes, M.C. 1996. Effects moisture and burning on soil-atmosphere exchange of trace carbon gases in southern African savannah. *J. Geophys. Res.* **101**, 23699-23706.

Zepp, R. G., Miller, W. L., Tarr, M. A. and Burke, R. A. 1997. Soil–atmosphere fluxes of carbon monoxide during early stages of postfire succession in upland Canadian boreal forests. *J. Geophys. Res.* **102**, 29301-29311.

Zhang, C., Zalich, D.A. and Randall, D.A. 1999. Simulations of soil moisture and surface water balance using the simple bisphere model 2. *J. Meteor. Soc. Japan* **77**, 217-234.

Zimmermann, P.R., Chatfield, R.B., Fishman, J., Crutzen, P.J. and Hanst, P.L. 1978. Estimates on the production of CO and H_2 from the oxidation of hydrocarbon emission from vegetation. *Geophys. Res. Lett.* **5**, 679-682.

Zobler, L. 1986. A world soil file for global climate modeling. *NASA Technical Memorandum* **87802**, pp.32.

Appendix A List of symbols often used

C	ppbv	the concentration of the gas in gas-phase
C_M	g cm^{-3}	the concentration of the gas per mass per unit volume of soil
C_{atm}	ppbv	atmospheric concentration of the gas
C_{eq}	ppbv	equillibrium (compensation) concentration of the gas
$[CO]_{eq}$	ppbv	equillibrium (compensation) concentration of CO
D_A	cm^2s^{-1}	molecular diffusivity
D_s	cm^2s^{-1}	diffusivity in soil driven by molecular diffusion
		(Diffusion in soil is assumed to be driven by molecular diffusion)
d	cm	the depth of inactive layer
d_p	g cm^{-3}	soil particle density
E_A	kJ mol^{-1}	Activation energy by Ahhrenius plots
F	arbitrary	the flux of the gas
F_0	arbitrary	the flux of the gas at soil surface
$P_{in\text{-}situ}$	s^{-1}	in-situ (abiological) production rate in soil based on space
P_s	cm^3s^{-1} g^{-1}	in-situ (abiological) production rate in soil based on
		unit mass of soil
R_{SMOW}		the ratio of deuterium in the Standard Mean Ocean Water
u_{insitu}	s^{-1}	in-situ (bacterial/enzymatic) uptake rate in soil based on space
u_s	cm^3s^{-1} g^{-1}	in-situ (bacterial/enzymatic) uptake rate in soil based on unit
		mass of soil
V_a		volume of gas per unit volume of soil (air-filled porosity)
V_l		volume of liquids (water) per unit volume of soil
V_s		volume of solids per unit volume of soil
v_d	cm s^{-1}	(net or gross) deposition velocity at the soil surface
v_{nd}	cm s^{-1}	net deposition velocity at the soil surface
v_{gd}	cm s^{-1}	gross deposition velocity at the soil surface
ρ	arbitrary	density of air

Appendix B List of abbreviations

n	number of samples
p	p value (statistics)
s.d	standard deviation
CCT	Closed-Chamber Technique or experiments by CCT
CRU	Climate Research Unit
ECD	Electron Capture Detector
FAO	Food and Agriculture Organization
FID	Flame Ionization Detector
HC(s)	Hydrocarbon(s)
IPCC	International Panel on Climate Change
NIAES	National Institute of Agro-Environemental Sciences
NMHC(s)	Non-Methane Hydrocarbon(s)
NOAA/CMDL	National Oceanic and Atmospheric Administration/ Climate Monitoring and Diagnosis Laboratory
OFT	Open-Flow (chamber) Technique or experiments by OFT
R^{2*}	the coefficient of determination adjusted by degrees of freedom
RGA3	Reduction Gas Analyzer 3 (Trace Analytical)
RGD	Reduction Gas Detector
SWI	Soil wetness index
TCD	Thermal Conductivity Detector
TDR	Time domain reflectometry
THC	Total Hydrocarbon
TSM	Top soil moisture
WFPS	Water-Filled Pore Space (e.g., Saxton et al., 1986)
WMO	World Meteorological Organization

Appendix C Global H_2-uptake strength by soil obtained from the balance of HD

Ehhalt (1999) concluded only qualitatively that global H2-uptake strength by soil is similar to the destruction with OH radicals. Ehhalt and Volz (1976) investigated deuterium content in the atmosphere and sources of hydrogen molecule (Table A.1). From this report, it is possible to quantitatively discuss about global balance of hydrogen molecule using deuterium balance. In the atmosphere, most deuterium exists as deuterated hydrogen molecule, HD. The global balance of deuterium can be expressed as:

$$\frac{d}{dt}([\mathrm{H_2}]) = S_{H2} - L_{H2} \tag{A.1}$$

$$S_{H2} = S_{Tech} + S_{BB} + S_{CH4} + S_{NMHC} \tag{A.2}$$

$$L_{H2} = L_{H2\text{-}OH} + L_{H2\text{-}Soil} = k_{H2\text{-}OH}[\mathrm{OH}][\mathrm{H_2}]\frac{m_{H2}}{m_{air}}B_{Trop}{}^2 + k_{H2\text{-}Soil}[\mathrm{H_2}]\frac{m_{H2}}{m_{air}}B_{Trop} \tag{A.3}$$

where, $[H_2]$ and [OH] is the annually- and globally-averaged atmospheric concentration of hydrogen molecule and hydroxyl radical (dimensionless), respectively, S_{H2} is the sum of sources of hydrogen molecule (Tg yr^{-1}), L_{H2} is the sum of sinks of hydrogen molecules (Tg yr^{-1}), S_{Tech} is anthropogenic technological sources, S_{BB} is biomass burning source (Tg yr^{-1}), S_{CH4} is a source from the destruction of CH_4 (Tg yr^{-1}), S_{NMHC} is a source from the destruction of non-methane hydrocarbons (Tg yr^{-1}), B_{trop} is the tropospheric burden of total atmosphere (Tg), m_{air} is the mean molecular weight of air, (g) m_{H2} is the molecular weight of H_2 (=2g), $k_{H2\text{-}OH}$ (Tg yr^{-1}) is the rate constant in the reaction of H_2 with OH, and $k_{H2\text{-}Soil}$ is the rate constant in the reaction of H_2 with soil (Tg yr^{-1}).

When, the fractionation by the soil uptake is expressed by β, the global balance of deuterated hydrogen molecule can be expressed using the numerals in Table A.1 as:

$$\frac{d}{dt}([\mathrm{HD}]) = S_{HD} - L_{HD} \tag{A.4}$$

$$\begin{aligned} S_{HD} &= \left(1-\frac{500}{1000}\right)R_{SMOW}\left(S_{Tech}+S_{BB}\right)+\left(1-\frac{100}{1000}\right)R_{SMOW}\left(S_{CH4}+S_{NMHC}\right) \\ &= 0.5R_{SMOW}\left(S_{Tech}+S_{BB}\right)+0.9R_{SMOW}\left(S_{CH4}+S_{NMHC}\right) \end{aligned} \tag{A.5}$$

$$\begin{aligned} L_{HD} &= L_{HD-OH}+L_{HD-Soil} = k_{HD-OH}[\mathrm{OH}][\mathrm{HD}]\frac{m_{HD}}{m_{air}}B_{Trop}{}^{2}+k_{HD-Soil}[\mathrm{HD}]\frac{m_{HD}}{m_{air}}B_{Trop} \\ &= \left(\frac{k_{H2-OH}}{\alpha}[\mathrm{OH}][\mathrm{HD}]B_{Trop}{}^{2}+\frac{k_{H2-Soil}}{\beta}B_{Trop}[\mathrm{HD}]\right)\frac{m_{HD}}{m_{air}} \\ &= \left\{\frac{k_{H2-OH}}{\alpha}[\mathrm{OH}]\left(1+\frac{100}{1000}\right)R_{SMOW}[\mathrm{H_2}]B_{Trop}{}^{2}+\frac{k_{H2-Soil}}{\beta}B_{Trop}\left(1+\frac{100}{1000}\right)R_{SMOW}[\mathrm{H_2}]\right\} \\ &\times\frac{m_{HD}}{m_{air}} \\ &= \left(\frac{1.1L_{H2-OH}R_{SMOW}}{\alpha}+\frac{1.1L_{H2-soil}R_{SMOW}}{\beta}\right)\frac{m_{HD}}{m_{H2}} \end{aligned} \tag{A.6}$$

where m_{HD} is the molecular weight of HD (=3g), [HD] is the yearly- and globally-averaged

atmospheric concentration of deuterated hydrogen molecule (dimensionless), S_{HD} is the total sources of deuterated hydrogen molecule, L_{HD} is the total sink of deuterated hydrogen molecule, R_{SMOW} is the ratio of deuterium in the Standard Mean Ocean Water depicted in Ehhalt and Volz (1976) (=roughly 1/6000), $L_{HD\text{-}OH}$ is a sink of HD by the reaction with OH radicals, $L_{HD\text{-}Soil}$ is a sink of HD by soil uptake , $k_{HD\text{-}OH}$ is the, $k_{HD\text{-}Soil}$ is the, α is the fractionation factor by the reaction with OH, β is the fractionation factor by the soil uptake. In eq. (A.6), the present study assumed that the fractionation of deuterium in the source of biomass burning was the same as that in the source of technological source, and the fractionation of the reaction from non-methane hydrocarbons was the same as that of the reaction from CH_4.

Under the equilibrium condition, time derivative in eq. (A.4) is zero and :

$$0.5R_{SMOW}\left(S_{Tech}+S_{BB}\right)+0.9R_{SMOW}\left(S_{CH4}+S_{NMHC}\right) = \left(\frac{1.1L_{H2-OH}\alpha R_{SMOW}}{\alpha}+\frac{1.1L_{H2-soil}R_{SMOW}}{\beta}\right)\frac{m_{HD}}{m_{H2}} \quad \text{(A.7)}$$

Dividing this eq (A.7) by R_{SMOW}:

$$0.5\left(S_{Tech}+S_{BB}\right)+0.9\left(S_{CH4}+S_{NMHC}\right) = \left(\frac{1.1L_{H2-OH}}{\alpha}+\frac{1.1L_{H2-soil}}{\beta}\right)\frac{m_{HD}}{m_{H2}} \quad \text{(A.8)}$$

Ehhalt et al. (1989) obtained , α , as 1.65±0.05 from laboratory experiments.

The β can be determined by the difference of molecular diffusivity because the driving force of soil uptake is firstly molecular diffusion (Chapter 5). Molecular diffusivity is roughly proportional to the square root of molecular weight. If the exponential model (eq.

5.20) is applied, the fractionation by the soil uptake is proportional to the square root of molecular diffusivity, which is proportional to the biquadratic root of molecular weight. Then,

$$\beta = \left(\frac{M(HD)}{M(H2)}\right)^{1/4} = \left(\frac{3}{2}\right)^{1/4} = 1.11. \qquad \text{(A.9)}$$

This value is larger when non-exponential model is applied. This value is larger than 1.06 of Ehhalt et al. (1989). This might be due to their experimental design.

Global H_2-uptake strength by soil can be calculated using eq. (A.8) and previous estimated value of Table 1.2. If the global balance of Ehhalt (1999) is applied, global soil uptake is calculated as 11.7 Tg yr^{-1} while if that of Novelli et al. (1999) is applied, it is as 16.4 Tg yr^{-1}. Both of these values are far smaller than the estimation of 70 Tg yr^{-1} obtained from the simulation using a process-based model.

Table A.1 Deuterium content in the atmosphere and some of its sources

	Deuterium content δ ‰	
H_2 source	Ehhalt et al. (1989)	Value used in this study
Uncontaminated troposphere	>+70	100
CH4 oxidation	-100	-100
Internal combustion engines	-290 to -690	-500